SHAPE MEMORY POLYMER SYSTEMS WITH ADVANCED PROCESSING

CAPABILITIES AND TUNABLE MECHANICAL PROPERTIES

A Dissertation

by

MICHAEL KEITH HEARON II

Submitted to the Office of Graduate and Professional Studies of
Texas A&M University
in partial fulfillment of the requirements for the degree of

DOCTOR OF PHILOSOPHY

Chair of Committee,	Duncan J. Maitland
Co-Chair of Committee,	Elizabeth Cosgriff-Hernandez
Committee Members,	Melissa A. Grunlan
	Thomas S. Wilson
	Karen L. Wooley
Head of Department,	Gerard L. Cote

December 2014

Major Subject: Biomedical Engineering

ABSTRACT

The ability of shape memory polymers (SMPs) to undergo geometric transformations upon exposure to stimuli has inspired application-driven research in a diverse array of scientific fields. The shape memory effect has been demonstrated in a number of polymeric systems, and recently the scientific community has shown a growing interest in developing shape memory polymer systems that exhibit other advanced material properties in combination with shape memory. High performance shape memory polymer (SMP) systems with tunable thermomechanical properties and good biocompatibility that can be processed using conventional thermoplastic processing techniques are of importance for a variety of industrial applications. For SMP-based medical devices in particular, the functional utility that arises from a clinician's ability to trigger geometric transformations after device implantation in the body is both multi-dimensional in nature and complex in conceptualization. The materials science of human physiology constitutes tremendous variations in tissue modulus and architecture, and consequently implantable devices may require SMPs that both exhibit highly tunable material properties and possess the ability to be processed into desired geometries using conventional thermoplastic processing techniques such as 3D printing, injection molding, extrusion or dip-coating. The tunability of material properties, toughness and processability of many SMP systems has been shown to be highly dependent on the nature and extent of crosslinking in the SMPs. This dissertation introduces a series of new amorphous, thermally actuated shape memory polymer systems that exhibit highly tunable material properties and advanced processing capabilities and to demonstrate

these SMP systems viability as platform systems for medical device design. A special

focus is also given to the development of new shape memory polymer systems derived

from novel green formulations to stress the importance of building for a sustainable

future from a materials engineering standpoint.

DEDICATION

To my parents, Mike and Sandra Hearon, who inspire me to dream

To the faculty at Westminster Schools of Augusta, who taught me how to learn

To refinement through failure and the pursuit of perfection

ACKNOWLEGEMENTS

I would first like to thank my Ph.D. adviser, Professor Duncan J. Maitland, for giving me the opportunity to come to Texas A&M University and help drive the development of new materials for use in medical device applications in the Biomedical Device Laboratory. His support, guidance and willingness to provide me with freedom to operate both enabled this dissertation and allowed me to grow tremendously as a scientist. By allowing me to work independently, he provided me with an environment that fostered creative thinking and championed diverse research strategies. I would also like to thank Dr. Thomas S. Wilson, whose continued support and guidance since summer 2008, when the work reported in this dissertation first began while I was an undergraduate summer intern at Lawrence Livermore National Laboratory, helped shape my development as a researcher. Additionally, I want to express my most sincere gratitude to Professor Karen L. Wooley, who in spring 2011 agreed to join my Ph.D. dissertation committee and provided much needed guidance and direction for my Ph.D. project from a chemical synthetic standpoint. After joining my dissertation committee, Professor Wooley repeatedly provided invaluable insight and support both from collaborative research and professional development standpoints. She welcomed me into her group as a collaborator, and as a result of her open-mindedness and collaborative spirit, I was provided with numerous opportunities to expand my technical skill set. I also want to thank Professors Elizabeth Cosgriff-Hernandez and Melissa A. Grunlan for their time and energy investments in me over the course of my time at Texas

A&M University, especially during the 2009-2010 academic year when I first began my Ph.D. work. During this time, both Profs. Cosgriff-Hernandez and Grunlan generously volunteered a significant amount of their time to help me become established as a synthetic polymers researcher in Biomedical Engineering department. In particular, I thank Professor Cosgriff-Hernandez for her willingness to provide me with access to her laboratory in 2009 and 2010 so that I could jumpstart my Ph.D. research.

Additionally, I am grateful for the time, suggestions and shared memories with my co-workers in the Biomedical Device Laboratory at Texas A&M University and collaborators in the Advanced Polymer Research Laboratory at The University of Texas at Dallas, in the Wooley group at Texas A&M University, in the Additive Manufacturing working group at Lawrence Livermore National Laboratory, and in the Advanced Materials Laboratory at Georgia Tech, where my research career first began.

In the Biomedical Device Laboratory at TAMU, Landon Nash time and time again served as a dependable and highly competent collaborator, and I owe the completion of a number of projects reported in this dissertation to his open-mindedness to collaboration. Cameron Maher progressed tremendously as a researcher while working under my direction as an undergraduate research assistant, and I am also grateful for the support that I received from undergraduate researchers Justin Calk, Sarah E. Smith, Christine Laramy, Casey Collins and Andrew Torres. Wonjun Hwang selflessly volunteered his time to me on numerous occasions to support the mechanical engineering and device fabrication aspects of my Ph.D. work, and Brent Volk, Jennifer Rodriguez and Andrea Muschenborn also served as great resources to me from shape memory characterization,

In the Additive Manufacturing working group at Lawrence Livermore National Laboratory, I want to thank Eric Duoss and Chris Spadaccini for modeling to me what a highly efficient and well-delegated research team looks like. I also thank John Vericella for his technical support in the areas of resin formulation and rheological characterization.

NOMENCLATURE

D_0	Minimum Dose to Gelation (Charlesby-Pinner Parameter)
DMA	Dynamic Mechanical Analysis
DSC	Differential Scanning Calorimetry
ε	Strain
E'	Storage Modulus
E''	Loss Modulus
E_r	Rubbery Modulus
EWG	Electron Withdrawing Group
G'	Shear Storage Modulus
G''	Shear Loss Modulus
p_0	Degradation Density (Charlesby-Pinner Parameter)
PU	Polyurethane
q_0	Crosslinking Density (Charlesby-Pinner Parameter)
σ	Stress
SMP	Shape Memory Polymer
Tan δ	Tangent Delta
T_g	Glass Transition Temperature
T_m	Crystalline Melt Transition Temperature
T_{trans}	Thermal Transition Temperature
μ_1	Thermoplastic Molecular Weight (Charlesby-Pinner Parameter)

TABLE OF CONTENTS

LIST OF TABLES

LIST OF SCHEMES

LIST OF FIGURES

CHAPTER I

INTRODUCTION AND LITERATURE REVIEW*

Complex engineering challenges often require advanced solutions, and the emergence of smart materials has inspired innovation in a diverse array of scientific fields. Shape memory polymers (SMPs) offer novel materials-based avenues to solving scientific challenges because of their demonstrated ability to actively undergo geometric transformations upon exposure to environmental stimuli such as heat, light, and solvents or moisture.[1-3] The shape memory effect, first reported for polymers in crosslinked polyethylene for heat-shrink applications in the 1950s, has been reported for numerous polymer systems and is well-characterized in the literature.[4, 5] The ability of materials to store a temporary geometry and then actuate to a primary geometry has driven SMP-based research in fields ranging from biomedical engineering and aerospace engineering to the fashion and culinary industries. Applications ranging from aircraft wings with self-deploying components[6] to automotive bodies with heat-erasable deformities[7] have been proposed, and a significant faction of SMP-based research has been directed at biomedical engineering applications.[2]

The potential clinical impacts of medical devices capable of changing geometries after insertion into the body to perform pre-programmed therapeutic functions appear to be very promising, and one device, an SMP-based suture anchor called Morphix®, received FDA clearance in 2009 and has since been implanted into humans.[8] Numerous other devices, such as cardiovascular stents, embolectomy devices, and catheters are also currently being investigated.[1]

One major drawback surrounding many shape memory polymer systems is an inherent limitation in industrial relevance. The advantages that SMPs offer: namely, the ability to change geometries or exert forces on surrounding environments in order to perform a specialized function upon exposure to a stimulus, may also limit their use to applications that share such specialized design criteria. Also, the fundamental polymer architecture that enables good shape memory behavior also imposes inherent limitations on the manners in which these SMPs can be processed into geometries for desired applications. Although covalent crosslinking in SMPs enables better cyclic shape memory behavior and greater recoverable strain capacity and affords greater and more tunable recovery stresses than those of thermoplastic analogs, covalently crosslinked polymers are not suitable for processing by a number of thermoplastic processing techniques that have long been established as industry manufacturing standards. For low-cost commodity plastics applications, industrial relevance is often dependent on a material's suitability for subjection to large-scale manufacturing using high throughput processing techniques such as extrusion, injection molding and recently 3D printing, and dip coating or solution casting may be employed for higher-profit applications. This

dissertation addresses these challenges by reporting the development of a series of new high performance shape memory polymer systems that exhibit facile tunability of mechanical and shape memory properties and that possess the ability to be processed using high throughput thermoplastic manufacturing techniques. To produce well-engineered SMPs that excel from both mechanical performance and material processability standpoints, post-polymerization crosslinking synthetic strategies are developed that allow for thermoplastics to be crosslinked after processing to afford network SMPs with highly tunable properties and a potentially broad application range.

A. The Shape Memory Effect: A Fundamental Dichotomy

A discussion of certain key fundamental principles that enable shape memory behavior in polymeric systems is provided in this section for the purpose of establishing links between these concepts and the materials-related challenges that this work seeks to overcome.

1. The Role of Thermal Transitions in the Shape Memory Effect

The shape memory cycle for a one-way, thermally actuated SMP is illustrated in terms of stress/temperature, stress/strain, and strain/temperature planes in Figure 1(a). Step 1 is isothermal loading of a polymer at a temperature above a thermal transition, T_{trans}, Step 2 is cooling at a constant load, Step 3 is isothermal unloading, and Step 4 is shape recovery under load free conditions. When a polymer is first formed as the result

of an initial polymerization, its chains assume a conformational state of highest entropy, as shown in Figure 1(b).

When a polymer is heated to a temperature at which sufficient kinetic energy is present to enable chain mobility, the polymer chains are driven to states of lower conformational entropy. Such a temperature, T_{trans}, can be a glass transition temperature (T_g), a crystalline melt temperature (T_m), or another thermal transition, and the polymer chain segments that exhibit T_{trans} are referred to as "switching segments". Upon cooling below T_{trans} and unloading, switching segment chain mobility is inhibited, and a thermodynamic barrier enables the deformed polymer chains to maintain this state of lowered conformational entropy. Heating above T_{trans} under load-free conditions provides switching segment chains with sufficient kinetic energy to regain mobility, and an entropic driving force causes the chains return to their highest-entropy conformations, enabling shape recovery. Since T_{trans} is effectively the temperature at which a pre-programmed thermally actuated SMP undergoes actuation to primary geometry, the ability to manipulate T_{trans} allows for SMPs to be designed for applications requiring various actuation temperatures. Achieving tailorable actuation temperatures in the SMP systems reported in this work is a key material design objective for each SMP system and a main motivating factor for the synthetic strategies and experimental characterization techniques employed.

2. The Role of Crosslinking in the Shape Memory Effect

Associative interactions that prevent polymer chains from permanently sliding past

one another during deformation enable shape recovery under load-free conditions by effectively acting as anchors for chains as they return to high-entropy conformations.[9] Such interactions, often called "netpoints" in SMP literature, include covalent crosslinks,[10] physical crosslinks such as thermoplastic chain entanglements and dispersed glassy or crystalline phases,[11] supramolecular[12] or ionomeric[13] moieties that exhibit stimuli-responsive dissociative transitions, and other associations.[14] The extent to which an associative interaction enables shape recovery varies with the extent and nature of the interaction. Covalent crosslinks provide permanent tethering sites for deformed polymer chains and enable high percentages of applied deformations to be recovered over multiple deformation cycles,[15] while physical interactions such as chain entanglements have sometimes been shown be less effective netpoints, especially during large deformations and over multiple deformation cycles.[16]
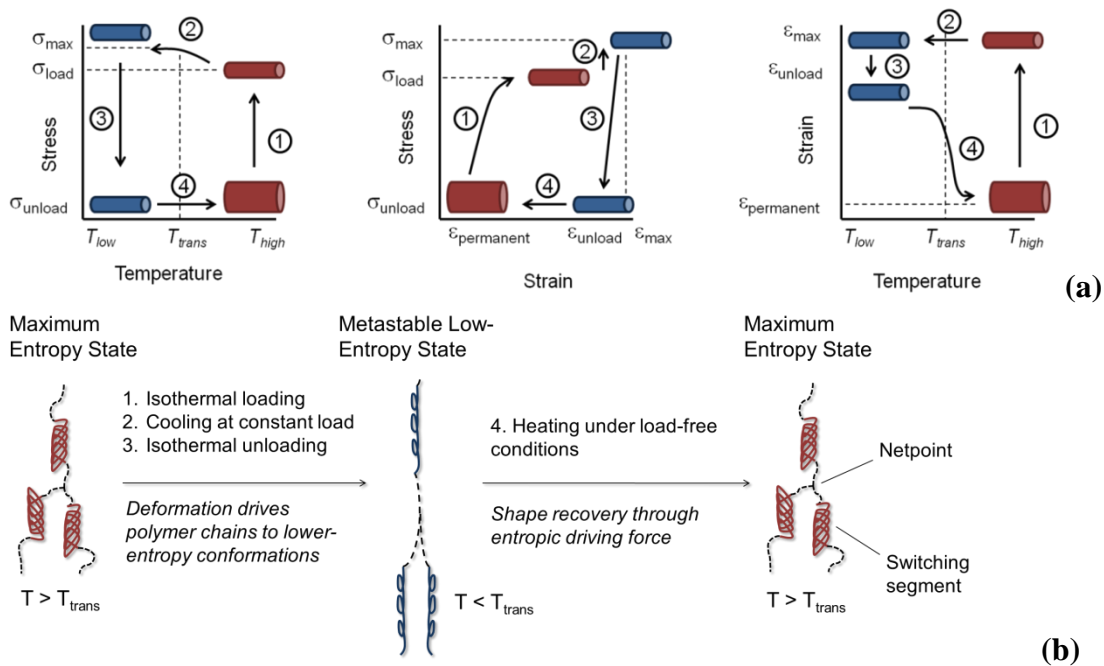
Figure 1- (a) Illustration of the shape memory cycle in stress/temperature, stress/strain, and strain/temperature planes; (b) illustration of the entropy-driven mechanism shape memory effect in a one-way, thermally actuated SMP. Reprinted with permission from "Porous Shape-Memory Polymers" by Keith Hearon, Pooja Singhal, John Horn, Ward Small IV, Corey Olsovsky, Kristen C. Maitland, Thomas S. Wilson and Duncan J. Maitland, *Polymer Reviews* 2013 *53* (1) 41-42, Copyright © 2013 Taylor & Francis

In addition to influencing recoverable strain capacity for SMPs during recovery in load-free conditions, associative interactions also influence the force that an SMP exerts on its surroundings if actuation occurs under constrained environmental conditions. The theory of rubber elasticity, which some attribute as having origins that date back to Gough's 1805 observations that rubber reversibly gives off heat when stretched and that it reversibly contracts upon heating, defines ideal rubber behavior as that in which the stress response, σ, during an applied deformation, ε, is proportional to the difference between the deformation and its inverse square, as shown in Equation (1). The constant

6

of proportionality that relates stress and strain in Equation 1 is modulus, E, which is also defined by the elastic theory of rubber as being inversely proportional to the average molecular weight between crosslinking sites M_c, as shown in Equation (2), in which ρ is density, R is the ideal-gas constant, and T is absolute temperature. Substituting the right side of Equation (2) for the E variable in Equation (1) yields Equation (3).

$$\sigma = E(\varepsilon - \frac{1}{\varepsilon^2}) \tag{1}$$

$$E = \frac{3\rho RT}{M_c} \tag{2}$$

$$\sigma = \frac{3\rho RT}{M_c}(\varepsilon - \frac{1}{\varepsilon^2}) \tag{3}$$

The relationship in Equation 3 predicts the internal stress response of an ideal rubber to be inversely proportional to the average molecular weight between crosslink sites in that polymer, or to increase with increasing crosslink density. When a shape memory polymer is heated above its actuation temperature, its stress response to applied deformation is thus predicted to increase with increasing crosslink density, and cooling below T_{trans} to fix the applied deformation allows the internal stress response to be stored as potential energy. If an SMP storing a temporary secondary geometry is constrained during actuation and prevented from freely recovering its original geometry, it will exert a recovery stress on its environment. This recovery stress will be proportional to that of the initial internal stress response and, consequently, proportional to crosslink density. The ability of SMPs to exert stimuli-responsive stresses on their environments offers a material capability of great potential value, and applications such as biomedical sutures for graft fixation have been proposed that utilize the recovery stress of SMPs in constrained conditions as a functional behavior to improve device functionality. Since

7

the optimal recovery stress for an SMP may vary in magnitude for different applications, the ability to tune the recovery stress in SMPs is also an important aspect of material design for SMP systems. Yakacki and others have demonstrated that recovery stress can be tailored in SMP systems by varying crosslink density.

B. An Assessment of Shape Memory Polymer Systems

1. The Material Attributes of Well-Engineered SMP Systems

The term "SMP system" is used in this study to refer to a series of formulations built around a core chemical foundation that have been reported together for the purpose of enabling tailorable material properties. As discussed in Sections 1 and 2, achieving control of actuation temperature (for thermally actuated SMPs) and of recovery stress via controlling crosslink density are of primary importance. As reported by Yakacki and others, the ability to control crosslink density independently of T_{trans} is an important aspect of designing SMP systems for biomedical device and other applications because doing so enables the fabrication of SMP devices with varying recovery stresses that actuate at the same temperature. Achieving independent control of T_{trans} and crosslink density is often a synthetic challenge because of the influence that crosslinking often has on thermal transitions and on the glass transition in particular. The ability to control T_{trans} independently of crosslink density is also a key objective when designing a new SMP system. Such synthetic control allows for the fabrication of SMP-based devices that actuate at varying temperatures while exerting equivalent recovery stresses on their

8

surroundings. Also, concerning the issue of the breadth of T_{trans}, the more narrow the

breadth of a thermal transition in an SMP, the more precise its shape actuation will be

with respect to temperature and the more rapid the shape recovery time will be.

Additional design criteria for material properties of SMP systems include the selection

of SMP formulations that enable as high toughness, and in the case of biomedical

applications, that the SMPs exhibit good biocompatibility and tunable modulus at body

temperature. As progress in polymer science continues consideration should also be

given to the investigative development of new polymeric materials that are derived from

sustainable formulations, and such a consideration is provided in Chapter IX of this

work.

2. The Role of SMP Chemical Class

The shape memory effect has been demonstrated in polymer systems with

numerous chemistries and varying morphologies, including epoxy resins,[17] acrylics,[18]

polyesters,[19] polyurethanes,[20] polysiloxanes,[21] poly(thioether) SMPs[22] and even

supramolecular polymers.[23] Each SMP chemistry and morphology has certain

advantages and disadvantages, which largely determine the application range of the

SMP. For example, acrylic SMPs made by uncontrolled free radical polymerization are

generally easier to synthesize than polyurethane SMPs because the acrylic

polymerization process is much less moisture sensitive; however, polyurethane SMPs

generally have higher toughness than acrylics because of interchain hydrogen bonding

between carbamate groups. Semicrystalline SMPs with T_m switching segments

9

generally have faster actuation times than amorphous SMPs with T_g-based switching segments; however, the optical clarity of amorphous SMPs makes T_g-based SMPs potentially useful in applications where turbid or opaque materials cannot be used, such as laser-actuated biomedical implant devices.[24] The advantages of aliphatic, amorphous polyurethanes, which include moderate to high toughness, good biocompatibility and potential bioresorbablility, high optical clarity, and demonstrated production success in industry make amorphous polyurethane SMPs excellent candidate materials for biomedical device applications.[25] Consequently, aliphatic, amorphous polyurethanes are the focus of a significant portion of this dissertation.

3. Processing Challenges Associated with Covalent Crosslinking

While covalent crosslinking offers certain material advantages for SMPs in that it enables efficient and tunable shape memory behavior, these advantages are often accompanied by tradeoffs in processing capability.   Many proposed SMP-based applications require components with complex geometries or require manufacturing by high-throughput thermoplastic processing techniques to be produced in an economically advantageous manner. Thermoplastic processing techniques such as 3D printing, extrusion, injection molding and solution casting are especially useful when high-throughput processing and/or complex prototype fabrication are desired. Thermoset polymers do not flow at elevated temperatures and consequently cannot be processed by traditional thermoplastic processing methods, and alternative thermoset processing methods are sometimes costly and time-consuming.[26] For example, reaction injection

molding allows for the curing of thermosets in complex geometries but requires that polymers be inside molds during the time of curing.[27] Post-cure thermoset machining allows thermosets to be mass-produced into simple geometries but afterwards requires individual machining of each device.[28]

4. Post-Polymerization Crosslinking

One method of improving the processability of covalently crosslinked polymers is the development of thermoplastics that are capable of undergoing subsequent crosslinking reactions after processing. Post-polymerization crosslinking potentially offers the processing advantages associated with thermoplastics and mechanical behavioral advantages associated with thermosets. Vulcanization, the process of crosslinking natural rubber in the presence of sulfur at high temperatures, was first developed by Charles Goodyear in the 19th Century.[29] A number of industrially produced adhesives, coatings and resins utilize post-polymerization crosslinking through the curing of oligomeric species end-capped or otherwise functionalized with reactive groups. Late 20th Century studies such as those of Le Roy[30] and Goyert[31] have reported successful crosslinking of thermoplastic polyurethanes and acrylates using ionizing irradiation, and Bezuidenhout, et al. were awarded U.S. Patent 7538163 in 2009 for the development of other chemical mechanisms of post-polymerization polyurethane crosslinking.[32] In the shape memory polymers field, Voit, et al. have reported a thermoplastic acrylic SMP system that can be crosslinked after blending with reactive additives using electron beam irradiation. This acrylic SMP system exhibits a tunable

11

glass transition range of approximately 25 to 60°C and a tunable crosslink density range that corresponds to rubbery moduli between 1 and 13 MPa.[33] Recently, researchers from the Bowman group have reported the development of two-stage reactive polymer network forming systems, which exhibit innovative processing capabilities. These dual cure polymers are prepared by mixing a stoichiometrically limited quantity of polythiol monomers with an excess of polyacrylate monomers and allowing a self-limiting thiol-Michael addition "stage 1" polymerization to occur in the presence of base. The resulting lightly-crosslinked networks are elastomeric in nature, exhibit moduli in the range of 0.5 to 15 MPa and can be easily deformed into new geometries. After deformation into desired shapes, the remaining acrylate groups can be cured using UV polymerization, and the fully cured networks exhibit increases in moduli that can span several orders of magnitude. Applications ranging from lithographic micropatterning to biomedical suture anchors have been proposed from this system, and a shape memory effect was demonstrated for certain formulations.[34]

C. Summary of the Dissertation

This dissertation builds upon recent momentum in the shape memory polymers literature base and seeks to employ post-polymerization crosslinking as a means of improving the processing capability of covalently crosslinked SMP systems. The primary motivation behind the studies reported herein is to establish one or more new SMP systems in the literature as potential platform systems for the design of medical devices and other applications. Despite the fact that improving processing capability is

an objective of this work, accomplishing this objective must not be done at the expense of controlling or maintaining integrity of mechanical behavior. The materials that this work seeks to introduce, when fully optimized, must be completely processable by thermoplastic processing techniques, must exhibit tunable glass transitions between approximately 40 and 80°C and tunable rubbery moduli between 1 and 30 MPa, must exhibit toughnesses between 50 and 100 MJ/m^3, must exhibit good biocompatibility, and must be fabricated into medical devices to demonstrate their viability as candidate materials for medical device design. Additionally, an investigative development also should seek to formulate post-polymerization crosslinkable SMP systems through green synthetic processes and/or from naturally-derived precursors to demonstrate the importance of including environmental sustainability initiatives in the design objectives of materials engineering studies moving forward.

In Chapter III, a thermally crosslinkable aliphatic polyurethane SMP system is reported that undergoes post-polymerization crosslinking upon exposure to elevated temperatures under evacuated environmental conditions. A tunable glass transition range from approximately 40 to 78°C, a toughness greater than 50 MJ/M^3 at T = T$_g$ for a select formulation, and cyclic recoverable strains approaching 100% for a sample subjected to 0.50 mm/mm prestrain were observed. However, control of crosslink density was limited to a rubbery shear modulus range of 1 to 2.5 MPa, and the industrial viability of this thermally crosslinkable SMP system may also be limited because of the requirement of a mold and evacuated atmospheric conditions during high-temperature post-polymerization curing processes.

In Chapters IV, V, and VI, the focus in this work shifts to the development of electron beam crosslinkable polyurethane shape memory polymer systems. Materials in these systems can be molded into complex geometries and subjected to crosslinking by electron beam irradiation at a later time at ambient temperature so as to maintain molded geometries. To achieve electron beam crosslinking in thermoplastic polymers over a desirable range, a new synthetic strategy is employed that is based on a hypothesis that certain structural moieties enable enhanced thermoplastic susceptibility to e-beam crosslinking. In Chapter IV, crosslink density is tuned over a corresponding rubbery modulus range of 1 to 40 MPa by solution blending acrylic radiation sensitizer additives with thermoplastic polyurethanes prior to e-beam irradiation, and cyclic recoverable strains approaching 100% are observed for sample subject to 0.25 mm/mm prestrain. While this crosslink density range is acceptable in accordance with the material design objectives of this work, the acrylic sensitizer additives present potential problems because of thermal instability during elevated temperature processing. In Chapter V, the thermal stabilization effects of the addition of varying quantities of the free radical inhibitor 1,4-benzoquinone are investigated for the sensitizer-based e-beam crosslinkable PU SMP system reported in Chapter IV, and increased elevated temperature working times of up to 24 h are demonstrated by the addition of select free radical inhibitor compositions. In Chapter VI, new formulations for a sensitizer-free e-beam crosslinkable SMP system are reported. This new SMP system exhibits tunable rubbery moduli from 0.1 to 55 MPa, tunable glass transitions from 40 to 80°C, toughness values greater than 90 MJ/m^3 for select compositions, cyclic recoverable strains approaching

100% for samples subject to 0.25, 0.50 and 1.00 mm/mm prestrains, and 72 h mouse

3T3 fibroblast cell viabilities greater than 90% for select formulations subjected to

biocompatibility testing. The sensitizer-free SMP system reported in Chapter VI

represents the final, optimized version of the e-beam crosslinkable SMP systems

reported in this dissertation.

In Chapter VII, a thermoplastic PU SMP system that can by crosslinked by

solution blending with polyfunctional thiol additives and subsequent subjection to UV

light to afford UV catalyzed thiol-ene free radical addition crosslinking is reported. This

thiol-ene crosslinkable PU SMP system was developed to provide an "all-in-house"

alternative system to the e-beam crosslinkable SMP system reported in Chapter VI,

which requires e-beam irradiations that generally must take place at external facilities.

The thiol-ene crosslinkable PU SMP system reported in Chapter VII exhibits tunable

rubbery moduli from 0.1 to 25 MPa, tunable glass transitions from 35 to 105 °C,

toughness values greater than 90 MJ/m^3 for select formulations, cyclic recoverable

strains approaching 100% for samples subject to 0.25, 0.50 and 1.00 mm/mm prestrains

and 72 h mouse 3T3 fibroblast cell viabilities greater than 91% for select formulations

subjected to biocompatibility testing.

In Chapter VIII, in accordance with the final design criterion established in this

Introduction, SMP systems built from novel green formulations are reported. UV

catalyzed thiol-ene "click" chemistry is utilized as the polymerization mechanism for

these SMP systems. The first green SMP system reported is a poly(thiother-co-

carbonate) SMP system derived from the coffee extract quinic acid, in which glass

transition is tunable over the range of 30 to 75°C, biodegradation rate at physiological

conditions is tunable over the range of 10 days to greater than 60 days, cyclic

recoverable strains approaching 100% for samples subjected to 0.30 mm/mm prestrains

were observed, and 72 h mouse 3T3 fibroblast cell viabilities varying between 80 and 95

% were observed for select formulations subjected to biocompatibility testing. The

second SMP system reported in Chapter VIII is prepared using a direct polymerization

of the citrus fruit extract D-limonene and polythiol co-monomers, and 72 h mouse 3T3

fibroblast cell viabilities greater than 93% were observed for select formulations

subjected to biocompatibility testing. Upon addition of recycled polystyrene additives to

heated limonene/polythiol monomer mixtures, homogeneous solutions result, and

formation of limonene-*co*-polythiol networks upon UV curing results in nanocomposite

polymers with precipitated PS microphases, in which modulus at 25°C is tunable from 1

to 600 MPa as recycled polystyrene composition increases from 0 to 40 weight fraction.

Cyclic free strain recovery showed 5-cycle recoverable strains approaching 100% across

the glass transitions of both the polythioether (~0°C) and polystyrene (~100°C) phases.

CHAPTER II

METHODS

A. Dynamic Mechanical Analysis

Dynamic mechanical analysis is a versatile thermomechanical characterization tool that provides data about the viscoelastic behavior of materials. The strain response of a polymeric substrate to an applied stress is consistent neither with the strain rate independent response characteristic of an elastic solid nor with the strain rate dependent response characteristic of a Newtonian fluid, but is instead considered to be a viscoelastic response that is part elastic and part Newtonian in nature. In DMA, sinusoidal deformations are applied to polymer specimens, and the material response to the deformations are measured and recorded. Provided that applied deformations do not extend past the linear elastic regime of the polymer, elastic responses are recorded by the instrument as being "in phase" with applied deformations (i.e., immediate, without and delay time), while viscous responses are recorded as being "out of phase." The complex modulus, E*, corresponds to the sum of the in-phase and out-of-phase responses and the phase angle (δ) can then be measured. E* and δ can then be used to calculate storage modulus, E', loss modulus, E'', and tangent δ, the ratio of loss modulus to storage modulus, as shown in Equations 4 and 5.

$$E^* = E' + iE'' \tag{4}$$

$$\tan \delta = \frac{E''}{E'} \tag{5}$$

For the purpose of this work, which focuses on the information that provided by DMA

17

related to thermal transitions and crosslinking in polymer systems, the majority of the data are presented in as plots of E' versus temperature, and a significant number of plots of tangent delta versus temperature are also presented. Since the majority of the materials synthesized in this study are amorphous polymers that utilize glass transitions as switching segments to enable the shape memory effect, the general term "T_{trans}" from this point forward will be replaced with the more specific term "T_g." Since glass transitions are by definition regions in which sufficient kinetic energy is present for polymers to undergo long-range molecular segmental motion and are not specific temperature points, there are multiple manners in which glass transition values can be reported.

Once method of reporting T_g values is to report DMA tan delta peak temperatures, which correspond to temperatures of maxim E''/E' ratio and provide a good indicator of a temperature at which a polymer is well into its glass transition. One common method of quantifying the breadth of glass transitions in SMPs is the DMA tangent delta full width half maximum (FWHM) method, which measures the temperature differential between a tangent delta peak's two half-maximum values. SMPs with high network homogeneity generally exhibit narrow T_g breadth.

B. Differential Scanning Calorimetry

Differential scanning calorimetry is a thermal analysis technique in which changes in enthalpy in a sample are measured in comparison with that of a reference are measured and recorded. One major advantage of DSC is that it can be run on small

quantities of sample with very little preparation time. A sample is placed in a DSC pan

and loaded into a DSC furnace along with an identical empty pan. The differential heat

flow required to heat both the sample and reference pans at the same rate is monitored.

DSC is utilized in this work in multiple ways. First, the changes in enthalpy flow that

occur when polymer undergoes a thermal transition are measureable by DSC, and the

onset of the glass transition peak on a plot of differential heat flow versus temperature is

indicative of the onset temperature at which long range segmental motion becomes

favorable in a polymer. For shape memory polymers being subject to programming and

recovery across glass transitions, the DSC peak onset temperature is indicative of the

temperature at which shape recovery will begin during the shape memory cycle. Such

information is very useful in predicting "maximum exposure temperatures" for SMPs

that have been programmed to store secondary geometries. DSC can also be used to

provide indirect evidence of the onset and occurrence of reactions in samples during

heating, and a number of industrial practices employ DSC as a method of determining

appropriate working temperatures and times for thermally curable resins. In Chapter IV,

is used as a method of indirectly evaluating the maximum working temperatures for

polymer blends containing reactive additives.

C. Tensile Testing

Uniaxial tensile testing can be used to characterize the stress/strain response of

polymeric materials. For SMPs, which by definition exhibit significant changes in

stiffness over regions of narrow temperature change, obtaining multi-temperature strain-

to-failure data is of significant importance. Strain-to-failure experiments can be utilized to map out temperature regions for which a material is and is not suitable for various applications. Strain-to-failure experiments extend past the linear elastic regions of deformation. Concerning specific temperatures of deformation relative to glass transitions in polymers, DMA tan delta peak temperatures correspond to temperatures of maxim E''/E' ratio and provide a good indicator of a temperature at which a polymer is well into its glass transition. Tan delta peak temperatures also correspond to temperatures at which theoretical maxim strain occurs for crosslinked polymers. DMA loss modulus peak temperature values provide the temperatures that correspond to the maximum overall contribution of the viscous or damping component of a polymer's strain response. Loss modulus peak temperatures, which occur near glass transition onset, correspond to theoretical maximum energy dissipation regimes and consequently are predicted to represent temperatures that correspond to maximum theoretical toughness of polymers during deformation to failure.

D. Sol/Gel Analysis

Sol/gel analysis experiments are useful for determining what percentage of a polymer's chains are incorporated into a crosslinked network and what percentage of a polymer's chains exist as unincorporated species. Sol/gel analysis experiments are generally used to determine the gel fraction, G, of a polymer. After recording an original mass value, m_0, polymers samples are immersed in a vial or jar in the presence of a significant excess of an appropriate solvent (e.g. 150:) for several days, during

which any thermoplastic chains that were not incorporated in the polymer network are dissolved in the solvent. Removal of the swollen polymer, solvent evaporation, and re-massing the polymer provides a second mass data value, m_f. The gel fraction of a polymers is defined according to Equations (6) and (7), where s is sol fraction, 1- G.

$$G = \frac{m_f}{m_0} \tag{6}$$

$$s = 1 - G \tag{7}$$

Gel fraction data provide information about the extent of network formation do not provide information about crosslink density.

CHAPTER III

A THERMALLY CROSSLINKED POLYURETHANE SHAPE MEMORY

POLYMER SYSTEM*

A discussion of the shape memory effect and an argument supporting the development of new shape memory polymer systems that exhibit both advanced processing capability and tunable thermomechanical properties are provided in Chapter I. This discussion addresses the role that crosslinking plays in enabling shape memory behavior and in influencing polymer processability and mechanical behavior. The development of a series of new SMP systems that are capable of being processed into desired geometries as thermoplastics and subsequently crosslinked using post-polymerization crosslinking techniques is presented as a route to achieving both advanced processing capability and tunable mechanical properties in new SMP systems. Chapter III reports the first method of post-polymerization crosslinking mentioned in Chapter I: the synthesis of thermoplastic polyurethane SMPs that contain backbone C=C motifs and the crosslinking of these SMPs by thermally induced radical chain polymerization of the C=C groups.

A. Materials and Methods

1. Thermally Crosslinked Polyurethane Synthesis and Specimen Preparation

Monomer selection criteria, sample formulations, synthetic protocols, and preparation techniques used to prepare thermally crosslinkable thermoplastic polyurethane SMP specimens for a number of thermomechanical analysis experiments are provided in the following section.
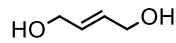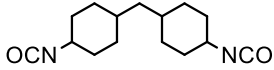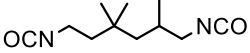
1.1 Monomer Selection and Thermoplastic Polyurethane Synthesis

The alkene diol monomer 2-butene-1,4-diol (TCI America, *cis* and *trans* mixture, >97%) was selected to enable the synthesis of thermoplastic polyurethanes containing backbone C=C functionalities, and thermally induced post-polymerization crosslinking was attempted at these C=C sites. Urethane chemistry was selected because of the high relative thermodynamic stability of the C=C group in 2-butene-1,4-diol relative to the stability of its hydroxyl groups towards reaction with isocyanates. This unsaturated site was expected to remain unreactive during the initial polymerization and thus be preserved in the polymer backbone to allow for subsequent crosslinking, which was predicted to occur at at fairly uniform intervals along the step-growth-prepared thermoplastic polymer chains. The diisocyanate monomers dicyclohexylmethane-4,4'-diisocyanate (DCHMDI, TCI America, >90%) and trimethylhexamethylene diisocyanate (TMHDI, 2,2,4- and 2,4,4- mixture, TCI America, >97%) were selected and used in varying ratios during synthesis provide a mechanism of tuning glass transition

temperatures, with DCHMDI being the higher-T_g monomer. Formulations and

monomer structures for the 2-butene-1,4-diol-*co*-(*x* DCHMDI : *1-x* TMHDI)

thermoplastic polyurethane series synthesized are provided in Table 1. All chemicals

were used as received without further purification.

Table 1- Formulations for thermoplastic polyurethane samples synthesized for thermal crosslinking study. Monomer structures are provided below the table.

Sample ID	Eq. 2-butene-1,4-diol	Eq. DCHMDI	Eq. TMHDI
DCHMDI-0.00	1.00	0.00	1.01
DCHMDI-0.10	1.00	0.10	0.91
DCHMDI-0.20	1.00	0.20	0.81
DCHMDI-0.40	1.00	0.40	0.61
DCHMDI-0.60	1.00	0.60	0.41

Polyurethane polymerizations were carried out in THF (anhydrous, >99.9%) in

0.50 g/mL solutions using stoichiometric diisocyante/diol ratios with a 0.01 molar NCO

excess. The synthetic route and reaction conditions for these polymerization reactions

are provided in Scheme 1. Diisocyanate monomers were stored under dry nitrogen until

use to prevent moisture absorption. 30 g scale immiscible diol and diisocyante monomer

mixtures were prepared in 60 mL glass vials in a glove box under dry nitrogen, after

which approximately 30 mL of anhydrous THF was added, and clear solutions resulted

upon gentle shaking.   The vials were loosely sealed to prevent pressure buildup and

were then placed in a Thermoline furnace at 60°C under a dry nitrogen atmosphere for

24 hours to allow for polymerization. The resulting viscous polymer solutions were then

poured into 15.0 cm × 15.0 cm × 5.0 cm polypropylene dishes and placed into a Yamato

benchtop vacuum drying oven at 80°C for 72 h at 1 torr. After solvent evaporation,

thermoplastic films approximately 1.0 to 2.0 mm in thickness were removed from the

polypropylene dishes, placed in 10 g batches between Teflon-coated stainless steel plates

separated by a 15.0 cm × 15.0 cm × 1.0 mm square stainless steel spacer with a 12.0 cm

× 12.0 cm square opening and pressed at 150°C for 30 s to uniform thicknesses of 1.0

mm using a Carver heated press. All pressed samples were stored under desiccation

until further use.

Scheme 1- Synthetic route for 2-butene-1,4-diol-co-(x DCHMDI : 1-x TMHDI)
thermoplastic polyurethane series whose formulations are shown in Table 1.
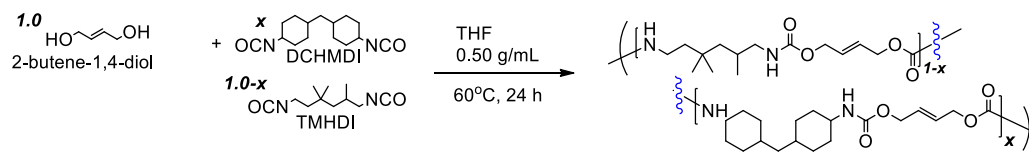
1.2 Attempted Thermal Crosslinking of Thermoplastic Polyurethanes

No thermal initiator was used to induce thermal crosslinking. After the

thermoplastic polyurethane films were prepared, crosslinking was attempted by exposure

to high temperatures. The thermoplastic films prepared for post-polymerization thermal

crosslinking were placed on 15.0 cm × 15.0 cm Teflon-coated stainless steel plates and

heated in a vacuum oven to 200°C at 1 torr until the onset of crosslinking was visible.

The onset of crosslinking was attributed to an observed transformation in polymeric rheology.   Initial heating to 200°C under vacuum resulted in what appeared to be residual solvent or other gases "boiling" out of the heated films. After approximately 1 h, the bubbles no longer appeared to boil, but instead began to slowly swell and fall back onto the film surfaces in a manner characteristic of that of highly viscous liquid. Releasing the vacuum after approximately 1.5 h resulted in the disappearance of any bubble-shaped swells in the films. However, maintaining the vacuum longer than approximately 2 h resulted in permanent bubble-shaped swells protruding from the films. Thus, the onset of crosslinking in the films was attributed to the point in which bubble-shaped swells in the polymer films no longer appeared to fall back to the film surfaces under an evacuated atmosphere. When the onset of crosslinking was observed, vacuum was released, and the samples were left under nitrogen at 200°C for an additional 10 h. Thermal crosslinking yielded films approximately 1.0 mm in thickness.

To provide insight into the effects of time and temperature on thermal crosslinking, the DCHMDI-0.00 sample was subjected to heating at varying temperatures and varying times without the use of evacuated atmospheric conditions. One series of samples was heated to 200°C for 1, 2, 3, 4, 6, 8, 10, and 12 h, and a second series of samples was heated to 225°C for 2.5, 4, 6, and 8 h.

1.3 Preparation Specimens for Thermomechanical Characterization Experiments

Samples in which thermal crosslinking was attempted were prepared using a Universal Laser Systems CO_2 VeraLaser laser machining instrument. 30.0 mm × 10.0

mm × 1.0 mm rectangular specimens were prepared for torsion rectangle DMA

experiments, 30.0 mm × 4.0 mm × 1.0 mm rectangular specimens were prepared for

shape memory characterization experiments, and ½-sized ASTM Type IV dog bone

specimens prepared for tensile testing experiments.

2. Experimental Parameters

The experiments performed in this study were conducted to determine if post-

polymerization crosslinking occurred when thermoplastic polyurethane samples were

subjected to 200°C heating conditions, to provide thermomechanical data pertaining to

the glass transitions and crosslink density of these samples, to determine the effects of

crosslinking on shape memory behavior, and to determine toughness and ultimate tensile

properties to provide a basis for the consideration of these new materials as candidate

materials for various applications.

2.1. Sol/Gel Analysis

To determine the fraction of polymer chains that became incorporated into

crosslinked networks during attempted thermal crosslinking, sol/gel analysis

experiments were performed to determine gel fraction. Since the thermoplastic

urethanes were synthesized in 0.50 g/mL THF solutions and remained in solution after

polymerization, THF was selected as the solvent for sol/gel analysis experiments.

Approximately 0.05 g specimens of each thermally crosslinked varying DCHMDI

formulation in Table 1 were dried at 80°C for 24 h at 1 torr, massed, and placed in 40

mL glass vials, after which approximately 10 g of THF (200:1 mass equivalent) was added to each vial. The vials were then sealed and heated to 50°C on a J-Kem Scientific Max 2000 reaction block at 150 rpm for 24 h. Visibly swollen polymer samples were then removed from the solvent-containing vials, vacuum-dried at 80°C for 24 h at 1 torr, and re-massed to determine the gel fraction of each sample.

2.2. Differential Scanning Calorimetry

Differential scanning calorimetry (DSC) experiments were run on thermally crosslinked samples to determine if any crystallinity was present in the samples and also to determine the glass transition onsets of the materials. DSC experiments were run using a Perkin–Elmer Diamond DSC. 5.0 mg samples were cut from thermally crosslinked samples and placed in standard aluminum DSC pans. The samples were loaded at room temperature. For the DSC experiments, the temperature range was -20 to 200°C, with a ramp rate of 20°C/min and a soak time of 2 min at the end of each heating/cooling cycle. An initial ramp cycle was run for each sample to relieve thermal stress and allow any residual solvent or monomer to evaporate, and a second ramp cycle was run to determine glass transitions. Glass transitions were determined using the Pyris software according to the half-height method.

2.3. Dynamic Mechanical Analysis

Dynamic Mechanical Analysis (DMA) experiments were run in shear on all samples subjected to heating and on the thermoplastic DCHMDI-0.00 sample using a

TA Instruments AR-2000 ARES Rheometer in the Torsion Rectangle instrument mode to provide data showing the effect of temperature on shear modulus for the thermally crosslinked samples. Temperature sweep DMA experiments were run at 1 Hz from 25 to 150°C using a heating rate of 1°C/min.

2.4. Shape Memory Characterization: Cyclic Free Strain Recovery

Cyclic free strain recovery experiments were run using a TA Instruments Q800 dynamic mechanical analyzer to evaluate the difference in percent recoverable strain between the thermoplastic and crosslinked samples. In the "DMA- Strain Rate" mode in tension using a preload force of 0.01 N and a strain of 1.0%, rectangular samples were heated to $T_g + 35$°C (tan delta peak), strained to 0.50 mm/mm prestrain, and were then rapidly quenched to 0° while maintaining the 50% strain and held isothermally for 30 min. For free strain recovery, the instrument force was then set to 0 N, and the temperature was ramped from 0°C to 140°C at 2°C/min. For cyclic testing, the samples were cooled back to $T_g + 35$°C at -10°C/min, held isothermally for 30 min, strained again to 0.50 mm/mm, and then subjected to the same free strain recovery procedures. Percent strain recovered as a function of temperature and time was recorded using TA Instruments QSeries software. For thermoplastic samples, 2-cycle experiments were run, and for thermally crosslinked samples, 3-cycle experiments were run.

2.5. Tensile Testing

To determine toughness, ultimate tensile strength and maximum strain capacity, tensile testing experiments were carried out to failure on thermally crosslinked DCHMDI-0.40 dog bone samples. Strain-to-failure experiments were run on n = 5 dog bone specimens using an MTS Insight 2® universal tensile testing machine equipped with a thermal chamber using a strain rate of 10 mm/min. After allowing specimens to thermally equilibrate for 10 min to T_g, which was determined from the peak of tan delta in the DMA results, strain-to-failure experiments were run.

2.6. Qualitative Shape Recovery Analysis (37°C Actuation)

Shape recovery at 37°C was characterized using qualitative shape recovery analysis to demonstrate the ability of one thermally crosslinked SMP formulation both to store a secondary geometry at 25°C and to actuate to its primary geometry at 37°C to simulate the shape fixity and actuation requirements of a biomedical implant device designed to actuate upon introduction to physiological conditions. The qualitative recovery analysis was performed on a thermally crosslinked DCHMDI-0.00 sample, for which DMA results showed tangent delta peak and tangent delta FWHM values of 41°C and 10°C, respectively, and for which DSC results showed a glass transition onset of approximately 33°C. For qualitative shape recovery analysis, $60.0 \times 4.0 \times 1.0$ mm rectangular strip specimens were immersed in 70°C water, deformed into helical geometries using tweezers, and subsequently quenched while maintaining the secondary helical geometries by immersion in ice water baths. The helical samples were then

removed from the ice water baths, patted dry with paper towels, and allowed to equilibrate at 25°C. The deformed helical samples were then subjected to sustained 25°C conditions for 1 h to provide a qualitative shape fixity analysis. After 1 h, the still-helical samples were then placed in 37°C water baths, and shape recovery was recorded using a high-definition digital video camera. From the shape recovery videos, actuation times at 37°C could be determined.

B. Results and Discussion

Results for experimental techniques used to provide structural and thermomechanical profiles for the thermally crosslinkable polyurethane SMP system prepared in this study are provided in this section. These results can effectively be used to assess the degrees to which this new SMP system exhibits advanced processing capability and/or tunability of material properties.

1. Sol/Gel Analysis Results and Discussion

Each of the thermally crosslinked varying DCHMDI polyurethane samples exhibited a gel fraction greater than 0.90. Gel fractions for each formulation in this series are provided in Table 2. Since the 2-butene-1,4-diol, DCHMDI and TMHDI monomer purities were only 97%, 90%, and 97%, respectively, and since the urethane samples may have absorbed ambient atmospheric moisture during massing, the evaporation of water and other impurities during the THF evaporation process may have contributed to the experimentally observed sol fractions in these thermally crosslinked

samples. Even if the observed sol fractions, which range from 0.06 to 0.09, are entirely

the consequence of inefficient susceptibility in this polymer system to thermal

crosslinking, the sol/gel analysis results nonetheless demonstrate that this polyurethane

can be crosslinked using post-polymerization heating. The observed gel fractions, which

were all greater than 0.90, indicate that a high extent of network formation occurred

during the thermal crosslinking process.[35]

Table 2- Sol/gel analysis results for 2-butene-1,4-diol-co-(x DCHMDI : 1-x TMHDI) samples thermally crosslinked at 200°C for 12 h at 1 torr.

x DCHMDI	Gel Fraction
0.00	0.92
0.10	0.91
0.20	0.91
0.40	0.94
0.60	0.93

2. DSC Results and Discussion

Each formulation in the thermally crosslinked varying DCHMDI series exhibited

a differential heat flow profile characteristic of that of an amorphous polymer, and DSC

results showed glass transitions that increased with increasing DCHMDI composition.

Plots of differential heat flow versus temperature are provided in Figure 2 for each of

these samples, and these results show glass transition onsets that range from

approximately 33°C for the DCHMDI-0.00 formulation to approximately 73°C for the

DCHMDI-0.60 formulation. These results show a single step transition indicative of a

glass transition, with no indication of crystallinity or other secondary phases. Since a

thermally actuated, amorphous SMP that is storing a secondary geometry begins to undergo shape recovery at the onset of its glass transition, it is important that glass transition onset data be determined in order to provide an accurate assessment of the thermal conditions to which such an SMP can be exposed. For example, the DCHMDI-0.00 formulation, which exhibits a T_g onset of approximately 33°C, is predicted to be able to maintain a stored secondary geometry at 25°C but is predicted to undergo shape actuation at 37°C. Consequently, this formulation could be useful in the design of an SMP-medical device that needs to maintain a secondary geometry at room temperature and undergo actuation to a primary geometry at body temperature.
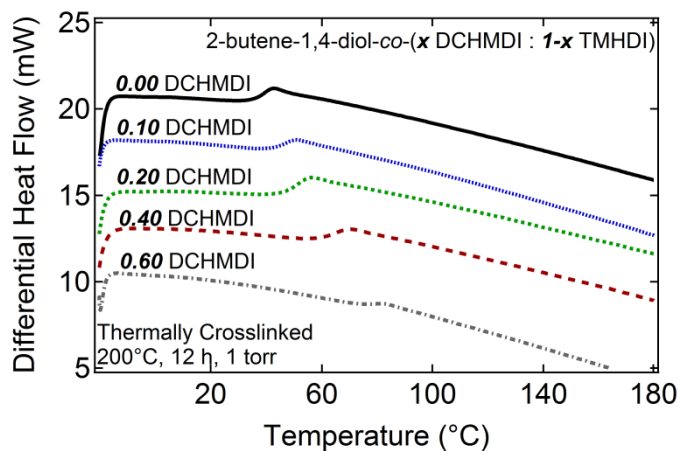
Figure 2- DSC results (endotherm up) for the thermally crosslinked 2-butene-1,4-diol-co-(x DCHMDI : 1-x TMHDI) SMP series. Glass transition onsets increased with increasing DCHMDI composition over the range of approximately 33°C to 73°C.

3. DMA Results and Discussion

DMA results for the thermally crosslinked varying DCHMDI series are provided in Figure 3(a-c). Figure 3(a) shows plots of storage modulus versus temperature for thermoplastic and thermally crosslinked DCHMDI-0.00 samples. The thermally crosslinked sample exhibits thermomechanical behavior characteristic of that of an amorphous, covalently crosslinked polymer, including a region of glassy behavior at lower temperatures, a glass transition region in which storage modulus decreases rapidly with increasing temperature, and a rubbery plateau region at temperatures above its glass transition. This thermomechanical behavior is significantly different from that observed for the same polymer formulation before it is subjected to thermal crosslinking: the thermoplastic DCHMDI-0.00 sample does not exhibit a significant rubbery plateau region, and it begins to flow at approximately 120 °C. At and above this temperature, sufficient energy is present to overcome the interactions associated with linear chain entanglements and other interchain physical interactions. In contrast, such rheological is not observed for covalently crosslinked polymers, which exhibit storage modulus plateau regions at temperatures above their glass transitions and are predicted by the equation for an ideal rubber to exhibit rubbery moduli that increase linearly with increasing temperature. Storage modulus versus temperature and tangent delta versus temperature data for the entire varying DCHMDI series are provided in Figure 3(b) and 3(c) respectively. In correlation with the T_g trends observed in the DSC results, these DMA results show an increase in glass transition with increasing DCHMDI composition, with tangent delta peak temperatures ranging from 41 to 80°C. The sharpness of the glass

34

transition, as seen in the tan delta curves, is evidence of a homogenous network structure. This homogeneity arises from the base polymer's being an alternating copolymer and is indicative that there is a narrow dispersion of molecular weights between crosslink sites.[15, 19, 36] When coupled with the high gel fraction data listed in Table 2, the DMA results in Figure 3 provide decisive evidence that the samples in the varying DCHMDI series are chemically crosslinked.

Concerning the issue of crosslink density in the thermally crosslinked SMP system, Figure 3(b) shows shear rubbery moduli that vary from approximately 0.9 to 2.1 MPa. The equation for an ideal rubber predicts rubbery modulus to be inversely proportional to the average molecular weight between crosslink sites in an elastomeric network, and the recovery stress of shape memory polymers has been shown to increase with increasing crosslink density. While the variation in rubbery moduli observed for the SMP series in Figure 3(b) is significant enough that it should enable some control of recovery stress for a given pre-strain condition, no clear trend relating structure and crosslink density is discernible.
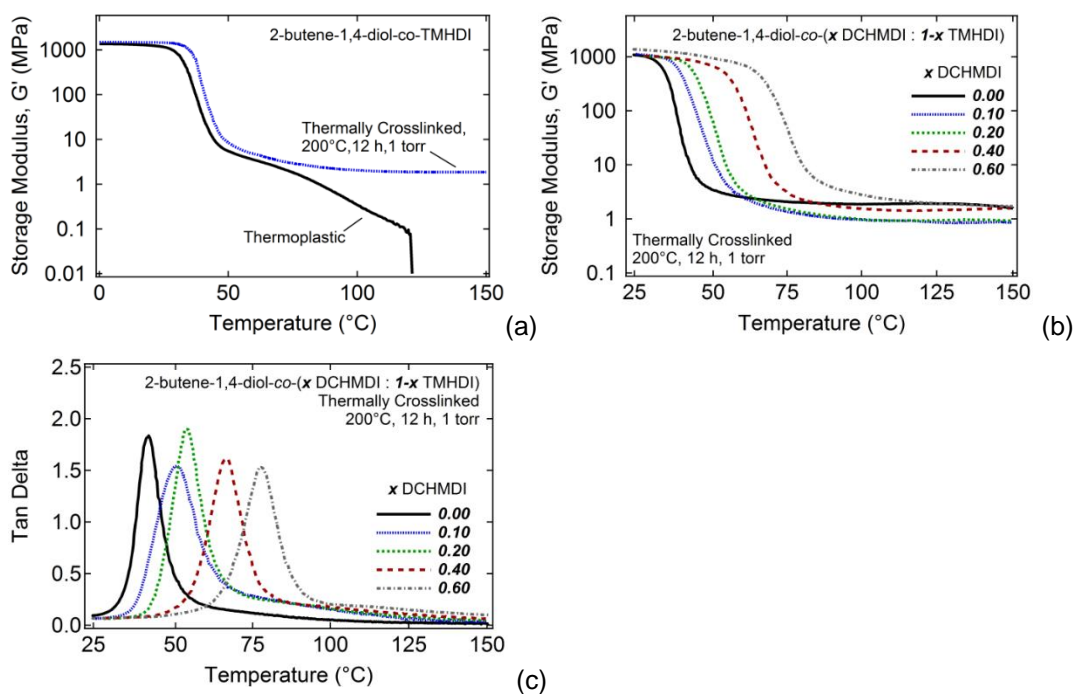
Figure 3- **(a) DMA results showing plots of storage modulus versus temperature for thermoplastic and thermally crosslinked DCHMDI-0.00; (b) DMA results showing storage modulus versus temperature for each formulation in the thermally crosslinked varying DCHMDI series; (c) DMA results showing plots of tangent delta versus temperature**

To provide some fundamental insight into the thermal crosslinking mechanism for this new SMP series, the effects of temperature and heat exposure time in atmospheric conditions on thermal crosslinking for the DCHMDI-0.00 sample were studied. These experiments were carried out under atmospheric conditions instead of in an evacuated environment in order to evaluate this thermally crosslinkable SMP system's viability for use in industrial applications in which the use of evacuated processing conditions might not be feasible (e.g., high throughput manufacturing processes for large molded plastic components). Figure 4 shows the effects of increasing heat exposure time and increasing temperature on network formation for the

36

DCHMDI-0.00 formulation. Increasing 200°C heat exposure time from 0 to 10 h results in increasingly pronounced rubbery plateau modulus regions. Although elastic behavior is seen to increase with heat exposure time for the 200°C samples, none of these samples appears to undergo significant network formation crosslinked in the 10-hr time period shown in Figure 4. However, increasing the heat exposure temperature from 200 to 225°C results in what appears to be a more accelerated and more highly efficient crosslinking process. The 225°C, 2.5 h sample exhibits a positive-sloping rubbery modulus of approximately 0.4 MPa. Since these experiments were conducted in the presence of oxygen, which can both inhibit free radical polymerization reactions by forming peroxy radicals that inhibit propagation and can also significantly increase thermal degradation in a number of polymer systems, the results observed in Figure 4 are not surprising.
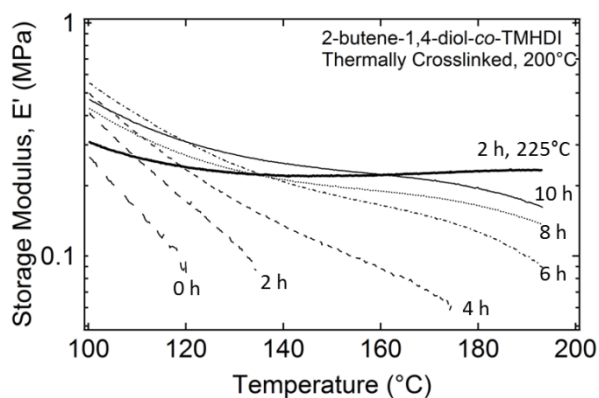
Figure 4- DMA plots of storage modulus versus temperature for DCMHDI-0.00 samples subjected to varying heat exposure times and varying temperatures

4. Cyclic Free Strain Recovery Results and Discussion

Cyclic shape memory behavior was determined using multi-cycle free strain recovery experiments for thermally crosslinked and thermoplastic DCHMDI-0.40 samples subjected to 0.50 mm/mm prestrain, and plots of recoverable strain versus temperature for these two samples are provided in Figure 5(a) and 5(b). After free strain recovery Cycle 1, the thermally crosslinked DCHMDI-0.40 sample recovered 95.5% strain. After the second and third cycles, the sample recovered 94.8% and 94.6% strain, respectively. The thermoplastic samples did not demonstrate high percent recoverable strain. After cycle 1, percent recoverable strain was 46.1%, and after cycle 2, it was 3.1%.
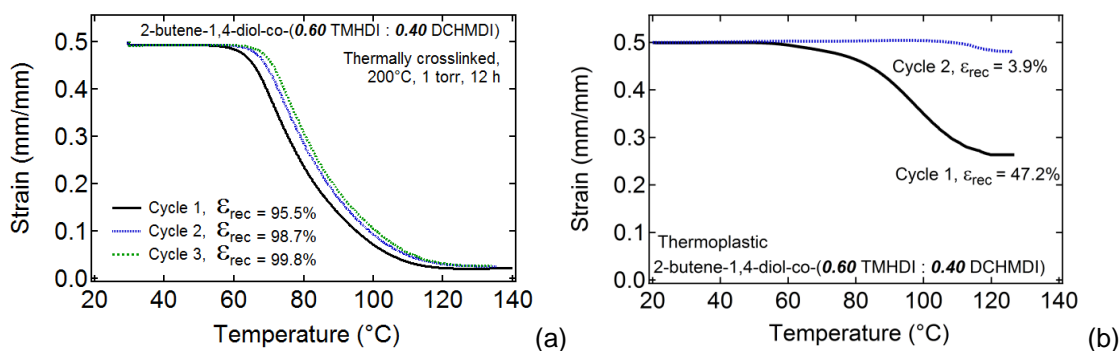
Figure 5- Cyclic free strain recovery data showing plots of recoverable strain versus temperature for (a) thermally crosslinked DCHMDI-0.40 (3 cycles) and (b) thermoplastic DCHMDI-0.40 (2 cycles)

5. Tensile Testing Results and Discussion

Strain to failure results demonstrated that this new class of polyurethane SMPs exhibits moderate to high toughness. Figure 6 shows average strain/strain data for five

strain-to-failure experiments conducted on dog bone specimens prepared from the thermally crosslinked DCHMDI-0.40 sample, which were conducted at DMA tangent delta peak temperature. All five specimens exhibited failure strains greater than 5.0 mm/mm and also exhibited strain hardening that resulted in an ultimate tensile strength at T_g of approximately 25 MPa and a toughness at T_g of approximately 50.2 MJ/m^3.
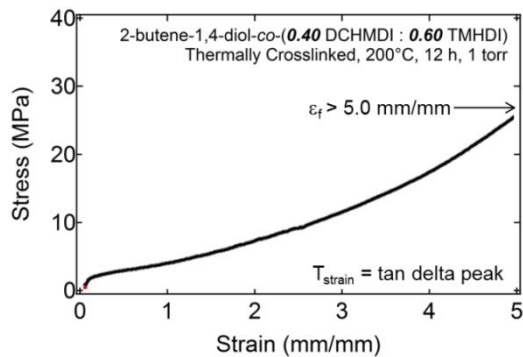
Figure 6- Strain-to-failure results averaged for n=5 specimens of the thermally crosslinked DCMHDI-0.40 formulation. These tensile testing experiments were conducted at Tg as determined by DMA tangent delta peak temperature.

6. Qualitative Shape Recovery Analysis Results and Discussion

DCHMDI-0.00 samples programmed into secondary helical geometries exhibited what appeared to be complete shape fixity at 25°C over the course of 1 h of exposure to ambient conditions. After immersion in 37°C water baths, these samples achieved full shape recovery in 12 seconds at 37°C. Images of the recovery of sample DCHMDI-0.00 from a programmed helical geometry to its primary flat geometry are provided in Figure 7, which were captured at different points during the sample's 12-second recovery

period.

Figure 7 – Images showing shape recovery from a secondary helical geometry to a primary flat geometry in 12 s at 37°C for the DCHMDI-0.00 SMP

C. Summary and Conclusions

The primary objective of this work was the synthesis and characterization of a new shape memory polymer system that exhibits advanced processing capabilities and tunable thermomechanical properties. A series of aliphatic polyurethane SMPs comprised of backbone repeat unit C=C moieties that can be synthesized into thermoplastic precursors, processed into complex geometries using thermoplastic processing techniques, and subsequently crosslinked using heat exposure was developed. The synthetic strategy in this study sought to achieve post-polymerization crosslinking via thermally induced radical chain polymerization through backbone C=C groups. Upon heating this series of thermoplastic polyurethanes to 200°C under an evacuated atmosphere, covalent crosslinking was shown to be achievable, and sol/gel analysis and DMA results provided concrete evidence of the formation of covalent networks during the attempted thermal crosslinking processes. A characterization of the thermal crosslinking mechanism was attempted by examining the relationship between temperature and heat exposure time on crosslinking in ambient atmospheric conditions

(i.e., in the presence of oxygen). Figure 4 shows that both increased heat exposure time and increased temperature increased the thermal crosslinking. However, most of the rubbery modulus values in Figure 4 are too low for the corresponding materials to be considered thermoset SMPs, and further analysis of the thermal crosslinking mechanism is necessary before quantitative conclusions can be drawn about the mechanism.

One limitation of this thermally crosslinkable PU SMP system is limited industrial relevance because of the high temperatures required to achieve crosslinking. A thermoplastic article that has been processed into a complex geometry would have to be kept in a thermally stable mold (most likely made of metal or PTFE) during thermal crosslinking at 200°C in order for it to retain the shape into which it is molded. Without a supporting mold, the thermoplastic would most likely begin to flow and collapse under its own weight. While the preparation of mm-thick films using this thermally crosslinking technique works quite effectively, the fabrication of more complex geometries may be quite more difficult. A second limitation of this thermally crosslinkable SMP system is that crosslink density was observed to be tunable over a quite limited range (a shear rubbery modulus range of only 0.9 to 2.1 was observed). Since the development of a truly versatile SMP system that possesses both advanced processing capabilities and tunable mechanical properties is desired, alternative post-polymerization crosslinking methods will be investigated in subsequent chapters of this work.

D. Acknowledgements

CHAPTER IV

AN ELECTRON BEAM CROSSLINKABLE POLYURETHANE SHAPE MEMORY

POLYMER SYSTEM REQUIRING SENSITIZER ADDITIVES*

The development of a series of new SMP systems that are capable of being processed into desired geometries as thermoplastics and subsequently crosslinked using post-polymerization crosslinking techniques is the focus of this work. In Chapter III, a thermoplastic polyurethane SMP system with tunable glass transitions that can be made to undergo post-polymerization crosslinking upon subjection to heating is reported. Two limitations of this thermally crosslinkable PU SMP system are limited industrial relevance because of the high temperatures required to achieve crosslinking and limited control of crosslink density. The focus of this dissertation now shifts to the development of an electron beam crosslinkable PU SMP system. E-beam crosslinking is particularly attractive because molded thermoplastic articles can be irradiated in the bulk state at ambient temperature and because a number of methods of tuning crosslink density have been reported for e-beam crosslinked polymers. In Chapter IV, control of crosslink density is attempted using radiation sensitizer additives.

A. Introduction and Literature Review

1. Current Shortcomings of Electron Beam Crosslinkable Polymers

The crosslinking of bulk thermoplastic polymers has been achieved in multiple polymeric systems using electron beam irradiation.[37, 38, 39, 40] Many e-beam crosslinkable thermoplastics suffer practically because the synthetic accommodations generally required to achieve desirable crosslink densities in industrial polymeric systems often exceed practical synthetic design requirements. Thermoplastic molecular weights that afford rheological behavior unsuitable for elevated temperature thermoplastic processing are often required for application-sufficient e-beam crosslinking to occur in many thermoplastics.[41, 42] The addition of thermally unstable sensitizer additives has long been shown increase e-beam crosslinking susceptibility in many thermoplastics,[43, 44] and the shelf lives of thermoplastic/sensitizer blended systems are often limited by the addition of such unstable additives.[45] Ultimately, achievable crosslink densities are limited for e-beam crosslinkable polymeric systems in comparison with those achievable by many other conventional polymerization methods.[46] Consequently, electron beam crosslinking in polymer systems has frequently been quantified in terms of extent of network formation (gel fraction) and not in terms of crosslink density (rubbery modulus).[47-49] As discussed in Chapter I, for shape memory polymers, it is important that crosslinking be defined in terms of both gel fraction and crosslink density. In an attempt to enable better thermoplastic processing capability while preserving tunability of thermomechanical properties, an in-depth

structural synthetic strategy is employed in this work that seeks to enhance e-beam

crosslinking susceptibility in thermoplastic polymers.

2. Alpha Hydrogen Theory: A Well-Established Mechanism for E-Beam Crosslinking

As shown in Scheme 2, Alpha Hydrogen Theory of electron beam crosslinking,

which has been supported in numerous studies since the 1950's, states that one of the

dominant mechanisms of electron beam crosslinking may be the free radical

recombination that occurs between e-beam generated radicals after hydrogen atom

abstraction at carbons located in positions alpha to electron withdrawing groups (EWGs)

in polymer backbones or side chains.[50-53]

Scheme 2 – Alpha hydrogen theory for mechanism of e-beam crosslinking in polymers.
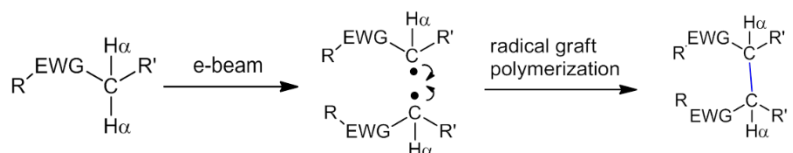
After observing a higher e-beam crosslinking response in poly(methyl acrylate)

than that observed in poly(ethyl-, propyl- and tert-butyl- acrylate), Schultz concluded in

his 1956 article: "The presence of hydrogen atoms alpha to the alcoholic oxygen of the

ester group is believed to contribute strongly to the crosslinking reactions of

polyacrylates under ionizing radiations." In the field of shape memory polymers,

radiation crosslinkable polyester SMPs have been reported,[54, 55] and Voit, et al. have

recently investigated electron beam crosslinking in poly(acrylate) SMP systems in an

attempt to improve thermoplastic processing capability while also maintaining tunability of thermomechanical properties.[33] However, these SMP systems generally suffer from the same practical limitations as those of many other polymer systems, which include rheologically-unfavorable high thermoplastic molecular weight requirements, thermally unstable sensitizer additive requirements and low-to-moderate achievable crosslink densities that do not afford desirable control of recovery stresses.[33, 56]

3. Resonance Stabilization Hypothesis for Enhancing E-Beam Crosslinking

Building upon the literature-supported alpha hydrogen theory for e-beam crosslinking of thermoplastic polymers, we developed the hypothesis that electron beam crosslinking can be further enhanced by the incorporation of C=C functionalities in positions adjacent to alpha-EWG C-H units. Through allylic resonance stabilization of α-EWG C-centered radicals, EWG-CH$_2$$\alpha$-C=C moieties in thermoplastic repeat units are predicted to enable for longer radical life, thereby increasing the probability of crosslinking events occurring by radical recombination, as also shown in Scheme 3. In Chapter III, thermoplastic polyurethanes containing backbone EWG-CH$_2$$\alpha$-C=C motifs are synthetized and subjected to e-beam irradiation, and trifunctional acrylate sensitizer additives are blended with these thermoplastics in varying quantities using solution blending to tailor crosslink density over a desirable range. This "first-generation" e-beam crosslinkable SMP is prepared from aliphatic diisocyanates, various saturated aliphatic diols, and 2-butene-1,4-diol.

Scheme 3- Schematic of hypothesized radiation crosslinking mechanism for polyurethane SMPs made from 2-butene-1,4-diol and TMHDI. 1: Thermoplastic samples are irradiated, radicals form at α-carbamate carbons; 2: If C=C groups are present at α-carbamate sites, resonance may stabilize the radicals; 3: Crosslinking then proceeds by radical graft polymerization, and crosslinking may be enhanced by the resonance stabilization effects described in 2; 4: If mobile, reactive radiation sensitizer molecules are blended with the thermoplastic, these sensitizers can also enhance a polymer susceptibility to radiation crosslinking.
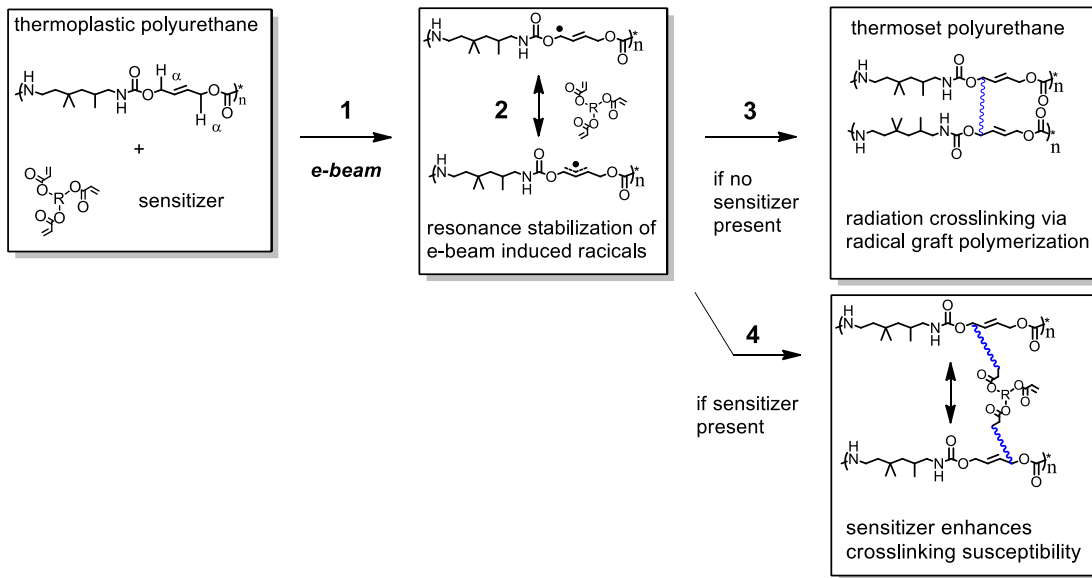
4. Charlesby-Pinner Model for Random Electron Beam Crosslinking

The random radiation crosslinking of thermoplastic polymers is described in the classical Charlesby-Pinner equation, where s is sol fraction, p_0 is degradation density, q_0 is crosslinking density, μ_1 is initial molecular weight (M_n), and d is dose.

$$s + s^{1/2} = \frac{p_0}{q_0} + \frac{1}{q_0 \mu_1 d} \qquad (8)$$

Electron beam irradiation of polymers results in both random chain scission and random inter-chain bond formation (i.e., crosslinking), and the ratio of scission to crosslinking, p_0/q_0, describes the inverse crosslinking efficiency of a given polymer system at a specific dose. In a classical Charlesby-Pinner analysis plot, $s + s^{1/2}$ is plotted against $1/d$, and a linear fit of the data yields a positively-sloping trend line with intercepts at $s + s^{1/2}$ equals two and $1/d$ equals zero. The $s + s^{1/2}$ equals two intercept represents the inverse crosslinking efficiency, represented by the ratio p_0/q_0, and the $1/d$ equals zero intercept represents d_0, the minimum dose to gelation, which corresponds to the theoretical dose that is necessary to achieve crosslinking in 1% of an irradiated polymer's chains.[51, 57] Radiation sensitizers have high mobility in comparison with that of bulky polymer chains and are highly reactive with polymer radicals induced during irradiation. Sensitizers have been shown to reduce the amount of energy required for crosslinking (i.e., d_0) and to decrease the random nature of e-beam crosslinking by making it more favorable. Deviations from linearity in Charlesby-Pinner plots of $s + s^{1/2}$ vs. $1/d$ are indicative of less random and more directed crosslinking events and have been shown to be characteristic of sensitized e-beam crosslinkable polymer systems.[56]

5. Synthetic Strategy

In this study, we seek to develop a polyurethane SMP system with novel processing capabilities that can be crosslinked in the bulk state using electron beam irradiation after thermoplastic processing to afford tunable mechanical properties. This SMP system is formulated based on the resonance stabilization hypothesis proposed in

Scheme 3. Backbone EWG-CH2α-C=C moieties are incorporated into thermoplastic

repeat units. The effects of four independent parameters on electron beam crosslinking

were investigated: radiation sensitizer composition, radiation dose, carbon-carbon

double bond composition, and thermoplastic molecular weight. The ratio of sensitizer to

polymer is varied over the wide range of 2.5 to 25 mole % for the purpose of

maximizing achievable variations in crosslink density. A dose range of 25 to500 kGy is

selected because numerous previous studies have demonstrated successful electron beam

crosslinking of various polymer systems over this dose range.[39, 55] To determine the

effect of carbon-carbon double bond composition on radiation crosslinking, 2-butene-

1,4-diol is co-polymerized with non-olefinic monomers, including its saturated analog

1,4-butanediol, and radiation crosslinking studies are carried out on the resulting co-

polymers. To determine the effects of molecular weight on e-beam crosslinking, M_w is

varied from 3.7 to160 kDa by adding varying amounts of the capping agent methanol to

thermoplastic polymerization mixtures. Crosslinking is quantified using sol/gel analysis

and dynamic mechanical analysis (DMA), and further thermal and thermomechanical

characterizations are performed using differential scanning calorimetry (DSC), strain-to-

failure, and shape memory characterization experiments.

6. Prototype Fabrication

To demonstrate the processability of this SMP system, a neurovascular stent

prototype is fabricated using dip-coating, CO_2 laser machining and subsequent

crosslinking by electron beam irradiation. From a processing proof-of-concept

49

standpoint, an SMP neurovascular stent is selected as the target medical device prototype because the geometry of a small stent is in many ways ideal for fabrication by dip-coating, which is a very effective thermoplastic processing method for producing hollow or thin-walled prototypes.[58] From a medical device standpoint, a stent application falls in line with previous studies reported by our group and our collaborators, in which the developments of neurovascular stents from other polyurethane materials are reported.[59] In these former studies, we investigated the collapse pressure of laser-etched SMP stents and solid tubular stents fabricated using the Mitsubishi MM7520 SMP. The solid tubular stent (expansion ratio ~2.1) was able to withstand the maximum pressure expected to be exerted by an artery, while the laser-etched stent (expansion ratio ~2.7) was possibly susceptible to collapse at temperatures higher than normal body temperature (i.e., a fever). In this materials engineering study, we aim to demonstrate the successful fabrication of a post-polymerization crosslinkable SMP neurovascular stent in order to provide an avenue for future biomedical device engineering studies, including the continuing development of neurovascular SMP stents.

B. Materials and Methods

Thermoplastic polyurethane SMPs are synthesized, and the effects of sensitizer composition, radiation dose, thermoplastic C=C functionalization and thermoplastic molecular weight are quantified using sol/gel analysis and DMA characterization experiments. The effects of crosslinking on tensile and shape memory behavior are determined using tensile testing and shape memory characterization experiments. A

50

neurovascular stent prototype is fabricated via dip-coating to demonstrate the advanced processing capabilities of this post-polymerization crosslinkable SMP system.

1. Synthetic Design and Sample Preparation for Sensitizer Containing Electron Beam Crosslinkable SMP System

The polyurethane shape memory polymers synthesized in this study are generally derived from 2-butene-1,4-diol and trimethylhexamethylene diisocyanate (TMHDI) and consequently share similarities in formulation with those in the thermally crosslinked SMP system reported in Chapter III. Diethylene glycol (DEG) and 1,4-butanediol (1,4-but) are co-polymerized with select samples to investigate the effect of polymer backbone C=C composition on electron beam crosslinking. Methanol (MeOH) is added in varying amounts to select polymerization batches to control molecular weight in order to determine the effects of molecular weight on e-beam crosslinking. Two acrylic sensitizer additives are solution blended with select thermoplastic polymers in varying quantities to determine the effects of sensitizer composition on e-beam crosslinking.

1.1 Monomer Selection and Thermoplastic Polymer Synthesis

All reagents and starting materials were used as received unless otherwise stated. TMHDI (97%), 2-butene-1,4-diol (97%), and diethylene glycol (DEG) (99%) were purchased from TCI America. Anhydrous tetrahydrofuran (THF) (> 99.9%, inhibitor free), anhydrous methanol (> 99.8%), tris[2-(acryloyloxy)ethyl] isocyanurate (TAcIC) (97%, inhibited, 100 ppm monomethyl ether hydroquinone), and 1,4-butanediol (99%)

were purchased from Sigma Aldrich. Pentaerythritol triacrylate (PETA) (97%, inhibited, 400 ppm 4-methoxyphenol) and Zirconium(IV) 2,4-pentanedionate catalyst (Zr Cat) (99%) were purchased from Alfa Aesar. This catalyst was selected because it has been shown to favor urethane formation over urea formation when moisture is present.[60] All starting materials were stored in a LabConco glove box under dry air until use to prevent moisture absorption. The chemical structures of the monomers and sensitizers used in this study are provided in Table 3.

All thermoplastic urethanes were synthesized in 0.33 g/mL solutions in anhydrous THF in 100g-scale reaction batches. To enhance experimental accuracy, the Zr catalyst was first diluted by making 0.100 wt% stock solution in THF. All solvents, alcohol and isocyanate monomers and catalysts were stored, massed, and mixed under dry air in a LabConco glove box. 100g samples (total monomer mass, 1.01 NCO excess) were massed in the glove box in 225 mL glass jars that were previously flame dried, after which the THF and Zr catalyst solution (0.010 total wt %, unless otherwise noted) were added. The jars were sealed, and the polymerizations were carried out in a LabConco RapidVap instrument at 80 °C for 24h at a vortex setting of 150 RPM. The RapidVap was used to heat and mix the monomer solutions. After 24h, the viscous polymer solutions were poured into 12" x 9" rectangular polypropylene (PP) dishes, which were placed under vacuum at 80°C for 72 h to remove solvent.

1.2 Molecular Weight Characterization

Gel permeation chromatography (GPC) characterization was carried out on a Viscotek GPCmax VE-2001 instrument, equipped with twin LT5000L mixed medium organic columns. The detector system was a Viscotek Model 302 Triple Detector Array system, simultaneously operating differential pressure, refractive index and light-scattering detection modes. All GPC analyses were carried out at a constant column temperature of 40°C. The carrier solvent was tetrahydrofuran (THF) and the carrier flow-rate was 1 ml/min. Each polyurethane sample was prepared as a 4 mg/ml solution in spectroscopy grade THF, filtered through a 2 μm PTFE Millipore filter to remove gel/particulate matter, and injected into the GPC system. For each sample, number and weight average molar mass (M_n & M_w) distributions were obtained and the polydispersity index (PDI) was determined. Triplicate analyses were performed for each polyurethane system.

1.3 Radiation Sensitizer Blending, Film Casting, and Irradiation

After the solvent was evaporated, the optically clear thermoplastic films were cut into strips and placed in 40 mL glass vials in masses of 4-5g. All masses were recorded, and amounts of radiation sensitizer (TAcIC and PETA) necessary to make 2.5-25 mole % samples were calculated based on these masses. The thermoplastic strips were then re-dissolved in THF (0.14 g/mL solution) using the heat and vortex features of the RapidVap at 50 °C and 150 RPM for 12 h. The new polymer solutions were allowed to cool to ambient temperature, after which the radiation sensitizers were solution blended

in desired amounts. Each blended polymer solution was then poured out evenly into three 2" x 4" polypropylene dishes to give final films of about 0.30 mm thickness. The PP dishes were placed at ambient temperature in a fume hood for 72 h and then in a vacuum oven at 25°C at 1 torr for an additional 2 weeks. The resulting amorphous thermoplastic films were then placed in 2" x 3" x 2 mil polyethylene bags. The samples were then irradiated at 25, 50, 100, 150, 200, 300, and 500 kGy using a 10 MeV electron accelerator located at the Texas A&M University National Center for Electron Beam Research.

2. Experimental Methods

The experiments conducted in this study were driven by the motivation to achieve control of crosslink density over as great a range as possible. While the sol/gel analysis experiments and Charlesby-Pinner calculations provide insight into the radiation crosslinking mechanisms that occur in these polyurethane systems during e-beam irradiation, the DMA results provide a more SMP-bent characterization approach. The constrained recovery experiments were conducted on samples with varying crosslink density in order to demonstrate the effect of crosslink density on recovery stress and ultimately to provide validation for this work's motivation. A neurovascular stent prototype was also fabricated using dip-coating and subsequent laser machining to demonstrate this SMP system's ablility to be processed using thermoplastic techniques.

2.1 Sol/Gel Analysis

To determine the extent of network formation in irradiated samples, a sol/gel analysis was conducted. Since the thermoplastic urethanes were synthesized in 33% THF solutions and remained in solution after polymerization, THF was chosen as the solvent. 50 mg samples were dried at 80°C for 24 h, massed in triplicate, put in 150:1 THF mixtures in 40 mL glass vials, and heated at 50°C on in a LabConco RapidVap at 150 RPM for 24 h. The solvent was then changed, and the process was repeated for another 24h. The swollen samples were then vacuum-dried at 90°C at 1 torr for 48 hours, after which no further mass change from solvent evaporation was measurable.

2.2 Differential Scanning Calorimetry

To ensure that the irradiated polyurethane samples were amorphous, differential scanning calorimetry (DSC) was run on the irradiated 2-but-160 sample series. Experiments were run using a TA Instruments Q200 DSC under at nitrogen atmosphere. 5.0 mg samples were cut from the irradiated films and placed in standard TA aluminum DSC pans with TA hermetic lids. Two-cycle runs were performed on each sample, in which the temperature range was -20 to 200°C, the ramp rate was 20°C/min, and an isothermal time of 2 min was added to the end of each heating/cooling cycle. The initial ramp cycle was run for each sample to relieve thermal stress and allow any residual solvent, monomer, or sensitizer to evaporate or react.

2.3 Dynamic Mechanical Analysis

All DMA experiments were run using a TA Instruments Q800 Dynamic Mechanical Analyzer. 25 x 4 x 0.3 mm rectangular samples were laser cut using a Gravograph LS100 40W CO2 laser cutter. All plots generated were recorded by QSeries software and analyzed using Universal Analysis graphing software. In the "DMA Multifrequency/Strain" mode, DMA experiments were run to determine the effects of sensitizer content, radiation dose, thermoplastic C=C composition, and molecular weight on the rubbery modulus and T_g of the irradiated urethanes. The frequency was set to 1 Hz, the Preload Force to 0.01 N, the Strain to 0.1%, and the Force Track to 150%. All experiments were run from 0-200 °C with a ramp rate of 2 °C/min in a nitrogen environment. Glass transition temperature (T_g) is measured as the peak of tangent δ, unless otherwise indicated.

2.4 Strain-to-Failure Experiments

ATSM Type V dog bone samples were machined from irradiated polymer films using the Gravograph CO_2 laser cutter and then carefully hand-sanded using 600-grit sandpaper. Strain-to-failure experiments were performed at a displacement rate of 10 mm/min at T_g using an Instron 5965 electromechanical, screw-driven test frame, which was equipped with a 500N load cell, 1kN high temperature pneumatic grips, and a temperature chamber that utilizes forced convection heating. An Instron Advanced Video Extensometer with a 60mm field-of-view lens was used to optically measure the deformation of the samples by tracking parallel lines applied at the ends of the gauge

length. The samples were heated to T_g under zero load (bottom grip unclamped). The temperature was held at T_g for 30 minutes to reach thermal equilibrium, after which the bottom grip was clamped, and the experiments were started thereafter. Data were recorded and processed using Instron Bluehill 3 software.

2.5 Shape Memory Characterization Experiments

Shape memory tests were performed on ASTM Type V dog bone samples using the same Instron 5695 instrument assembly described in the previous experimental section. This assembly also used liquid nitrogen for cooling. The shape memory tests were performed in tension for select compositions according to ASTM D638 standards for Type V dogbone samples. The samples were heated to 80°C under zero load (bottom grip released). The temperature was held at 80°C for 30 minutes to reach thermal equilibrium, and then the bottom grip was closed and the samples were loaded to nominal strains of 0.30 mm/mm (for free strain recovery) or 0.25 mm/mm (for constrained recovery) at a displacement rate of 50mm/min. The crosshead displacement was held constant and the temperature was reduced, at a rate of 1°C/min, to 25°C. The temperature was held at 25°C for 30 minutes to reach thermal equilibrium. After cooling to the glassy phase, the specimen was unloaded at a displacement rate of 5mm/min until zero load was applied to the sample. For the free strain recovery tests, the bottom grip was pneumatically released, and the specimen was allowed to hang freely from the top grip to ensure zero applied load. For the constrained recovery tests, the bottom grip was re-attached to ensure zero displacement.   The temperature was then ramped at a rate of

1°C/min to the original temperature of 80°C while maintaining the zero load or constant displacement conditions for the free or constrained recovery tests, respectively.

3. Neurovascular Stent Prototype Fabrication

In order to demonstrate the novel processing capabilities of the polyurethane SMP system reported in this study, a neurovascular stent prototype was fabricated using a dip-coating procedure. Cylindrical pins were dip-coated in a polymer solution, crosslinked using electron beam irradiation, and then machined into complex stent geometries using CO_2 laser machining.

3.1 Dip-coating

The dip-coating solution was prepared in a 60 mL glass vial by dissolving 22 g of 2-but-160 in 27 g THF. This concentration of polymer and solvent was qualitatively optimized in multiple dip-coating trials to achieve desirable viscosity and volume for dip-coating. Brass rods initially measuring 1 m in length and 4 mm in diameter were cut into 80 mm-long pins. These pins were mounted in a drill press and sanded to a smooth, tarnish-free finish using 400 and 2000 grit sandpaper. To minimize adhesion between the dip-coated polyurethanes and the brass pins, a thin coating of PTFE mold release spray was applied to each pin and sintered using a butane torch. Using a linear translating platform, a set of four pins was mounted on a custom fixture and dipped into the polymer solution over a 51 mm range at a rate of 0.67 mm/s. The pins were held at the bottom of the dip for 20 s and removed from the solution at 0.67 mm/s. Before

another dip-coating layer was applied, the pin fixtures were placed in an oven at 45 °C

for 20 min to facilitate solvent evaporation. The dipping process was repeated 6 to 10

times to vary the wall thickness of the polymer tubes that formed on the outside surface

of the brass pins. In order to remove residual THF without causing bubbling to occur in

the dip-coated tubular samples, the pins were left at ambient temperature for 24 h, heated

to 45°C in an oven at ambient pressure for 72 h, and then heated to 50°C for 48 h at 1

torr. The dried tubes, which varied in wall thickness from 140-220 μm, were transferred

from the brass pins to 4 mm OD high density polyethylene tubing and irradiated at 150

kGy. The tubes were transferred back to the brass pins and post-cured at 80°C for 24 h at

1 torr.

3.2 CO_2 Laser Machining

Complex stent patterns were designed using SolidWorks 2011 software and were

converted to the .eps file format before stent machining. The stent patterns were

machined on the e-beam crosslinked tubes using a Gravograph LS100 CO_2 laser

machining assembly in its cylindrical engraving mode. After laser machining, the stents

were carefully removed by hand from the brass pins and stored under desiccation.

C. Results and Discussion

Results for experimental techniques utilized to demonstrate the successful

achievement of control of crosslink density this e-beam crosslinkable SMP are included

in this section. Additional shape memory characterization experiments were run to

demonstrate the effects of covalent crosslinking on recoverable strain and recovery stress (i.e., to demonstrate runnable mechanical properties), and two medical device prototypes were also fabricated to demonstrate the advanced processing capabilities of this new SMP system.

1. Molecular Weight Characterization Results

The GPC results for all thermoplastic polyurethanes synthesized are provided in Table 3. Without the addition of methanol (MeOH), all thermoplastic polyurethanes exhibited molecular weights (M_w) in the range of 60-160 kDa. As MeOH content was increased from 0 to 10 mole % for 2-but-co-TMHDI SMPs, molecular weight decreased from 85 kDa to 3.6 kDa. Polydispersity index (PDI) values were in the range of 2.0-3.0 and generally decreased as molecular weight decreased, although the variation in PDI was large. The monofunctional methanol molecules limited the polyurethane step growth polymerization by introducing chain ends at sites that would otherwise have been available for step growth.

Table 3- GPC quantifies thermoplastic polyurethane behavior of synthesized samples.

Sample	Equiv. TMHDI	Equiv. 2-but	Eq. 2x MeOH	Eq. DEG/ 1,4-but	M_n (kDa)	M_w (kDa)	PDI
2-but-160*	1.000	1.000	-	-	46	160	3.5
2-but-85	1.000	1.000	-	-	33	85	2.5
2-but-40	1.000	0.990	0.010	-	18	40	2.5
2-but-20	1.000	0.975	0.025	-	5.2	20	3.2
2-but-7	1.000	0.950	0.500	-	2.8	7.0	2.4
2-but-3.6	1.000	0.900	0.100	-	1.7	3.6	2.0
DEG-60	1.000	0.500	-	0.500	27	60	2.2
DEG-78	1.000	0.800	-	0.200	29	78	2.7
1,4-but-98	1.000	-	-	1.000	42	98	2.3
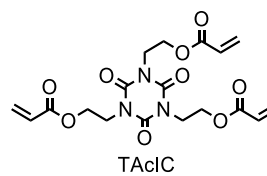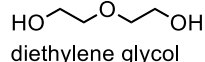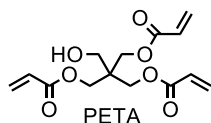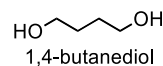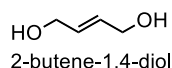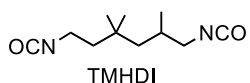
Note: 0.1 wt % Zr catalyst was used in the synthesis of the 2-but-160 polymer sample, while 0.01 wt % Zr catalyst was used in the synthesis of all other samples. Increasing the catalyst resulted in increased molecular weight and increased polydispersity index.

As methanol content increases, the average functionality, f_{av}, for the polymerization decreased, and polymer dispersity also decreases. This relationship between molecular weight and polymer dispersity was expected and follows reported trends.[61] It is noteworthy that the sample 2-but-160, which had an M_w of 160 kDa, was prepared using 0.1 wt % Zr Cat (all other samples were prepared using 0.01 wt% Zr Cat). This increased amount of catalyst resulted in an increased reaction rate. Since urethane polymerization reactions are exothermic, an increased reaction rate enabled an increased amount of heat to be generated simultaneously during polymerization, and the

increased kinetic energy in the system drove the polymerization reactions to greater completion.

2. Sol/Gel Analysis Results and Discussion

Gel fraction was most strongly dependent on the ratio of sensitizer to polymer, but it also increased with increasing dose, increasing C=C double bond composition, and increasing molecular weight. Plots of gel fraction (GF) versus dose for 2-but-co-TMHDI samples with varying molecular weights are provided in Figure 8(a), 8(b), and 8(c) for 0%, 10%, and 20% PETA samples, respectively. Figure 8(d) shows plots of GF versus dose for 2-but-40 samples containing varying amounts of PETA sensitizer. Figure 8 indicates that increasing the amount of sensitizer has the most drastic influence on increasing GF, although GF also increases with increasing dose and molecular weight. Figure 9(a)-9(d) show Charlesby-Pinner analysis plots of $s + s^{1/2}$ versus $1/d$ for the gel fraction data provided in Figure 8. A linear fit of each data series in Figure 9 was used to calculate d_0 and p_0/q_0 values for each sample, and these calculated Charlesby-Pinner parameters are provided in Table 4.

Table 4- Values for p_0/q_0 and d_0 for samples with varying sensitizer composition and varying molecular weight. These parameters were calculated from Charlesby-Pinner plots of $s + s^{1/2}$ versus 1/dose, such as the ones shown in Figure 2.

Sample Information		p_0/q_0	d_0 (kGy)
0% PETA	2-but-85	0.539	10.95
	2-but-40	0.583	35.04
	2-but-20	1.005	106.84
10% PETA	2-but-40	0.098	4.82
	2-but-20	0.293	9.98
	2-but-7.0	0.897	22.51
20% PETA	2-but-3.7	1.246	53.66
	2-but-20	0.311	8.44
	2-but-7.0	0.654	12.74
	2-but-3.6	1.049	17.85

The trends in Figure 9(b-d) are consistent with reported results from other radiation crosslinking studies in which molecular weight was varied in the presence of sensitizer.[55] Increasing molecular weight in the presence of sensitizer in Figure 9(b) and 9(c) result in a downward vertical shifting of the Charlesby-Pinner trend lines without causing a significant change in trend line slope. In Figure 9(c), the 2-but-40 sample had gel fractions approaching 1.0 for all doses tested, so plotting $s + s^{1/2}$ versus $dose^{-1}$ resulted in a straight line with a slope and y-intercept of zero. In 9(d), the slope of the trend lines approaches zero with increasing sensitizer composition, and this trend is also consistent with data reported in other studies.[62] In Figure 9(a), which contains Charlesby-Pinner data for sensitizer-free 0% PETA samples, a more pronounced change in the slope of the trend lines was observable as M_w increased from 20 to 40 to 85 kDa. This trend line behavior resembles that of the increasing sensitizer series, shown in

Figure 9(d), which contains samples with varying sensitizer and a constant M_w of 40

kDa. Figure 9(a) contains data only for the 2-but-20, 2-but-40, and 2-but-85 samples

because no gel fractions occurred for the lower molecular weight samples at any dose

tested.
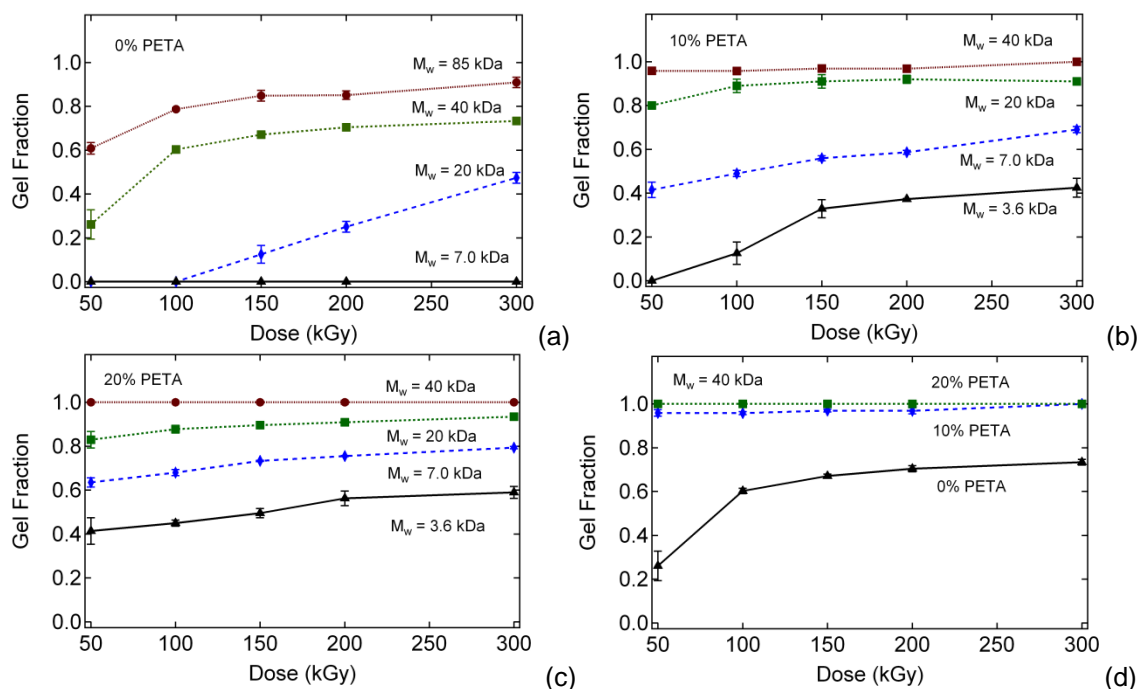
Figure 8- The effect of increasing radiation dose on gel fraction for samples with Mw varying from 3.6 kDa to 40 kDa. Plots for samples containing 0% (a), 10% (b) and 20% (c) PETA are shown. 1(d) shows gel fraction data for samples 2-but-40 samples with varying PETA.
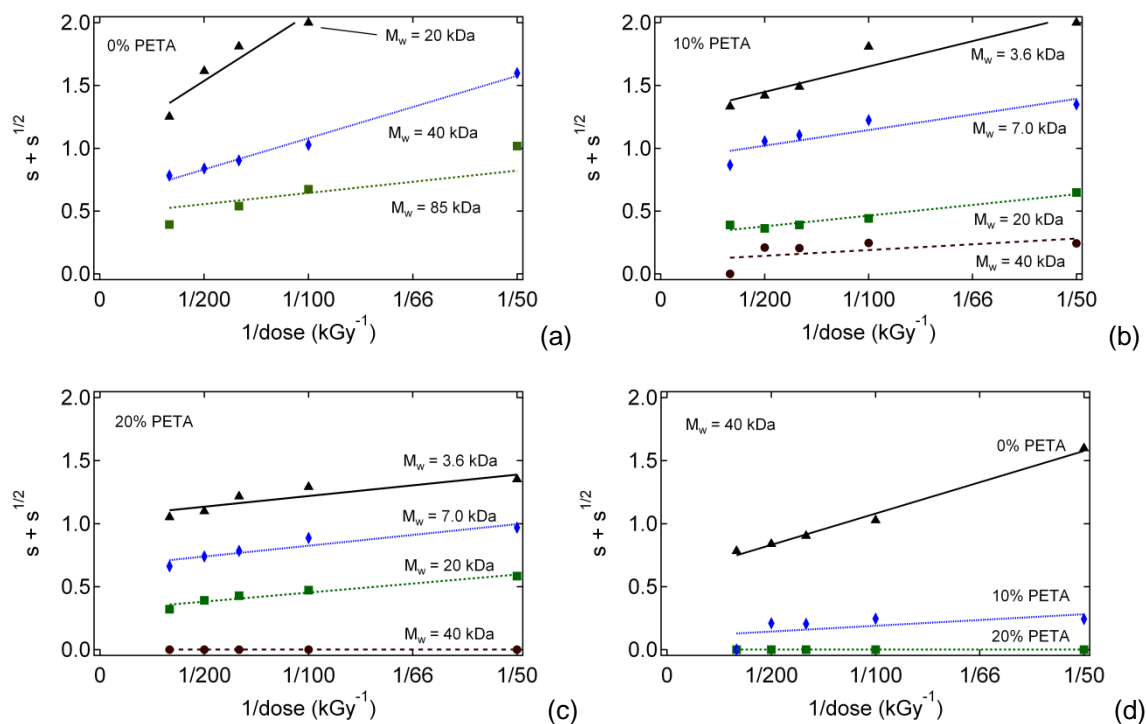
Figure 9- Charlesby-Pinner analysis plots of s + s1/2 versus 1/dose for irradiated samples with varying molecular weights and (a) 0% PETA, (b) 10% PETA, and (c) 20% PETA; in (d), Mw = 40 kDa, and PETA is varied.

As indicated in Table 4, minimum dose to gelation (d_0) decreased with increasing sensitizer composition and increasing molecular weight, in accordance with trends reported in previous works.[49, 54] Since the molecular weights in this study are much lower than those reported in many other studies,[41, 42] the d_0 values in this study are generally higher than those in other studies that used higher-molecular weight polymers (this study's lowest d_0 value was 4.82 kGy for the 10% PETA, 2-but-40 sample, although a d_0 value for the 2-but-40, 20% PETA could not be calculated because all gel fraction values were 1.0). The scission-to-crosslinking ratio, p_0/q_0, appeared to be highly dependent on molecular weight, especially for low-molecular weight samples. Since the

lowest molecular weight samples had no gel fractions for 0% PETA, and the highest

molecular weight samples had only gel fractions of 1.0 for 20% PETA, a four data-point

trend was only complete for 10% PETA. However, for the other PETA compositions,

this same trend was still evident. P_0/q_0 did appear to decrease slightly with increasing

PETA, especially in the case of 0% versus 10% PETA. Also, p_0/q_0 appeared to remain

relatively constant as PETA composition was increased from 10% to 20%, and this trend

is consistent with data reported in previous studies.[56]

3. DSC Results and Discussion

DSC results for 2-but-160 samples containing varying PETA and TAcIC

sensitizer and irradiated at 50 kGy are provided in Figure 10 and are indicative of the

DSC results of all samples. All samples appeared to be amorphous with glass transitions

in the range of 37 to 80°C. Samples containing TAcIC generally appeared to have glass

transitions approximately 10 to 15°C higher than those containing PETA, although the

trend was less pronounced for samples containing low sensitizer compositions.
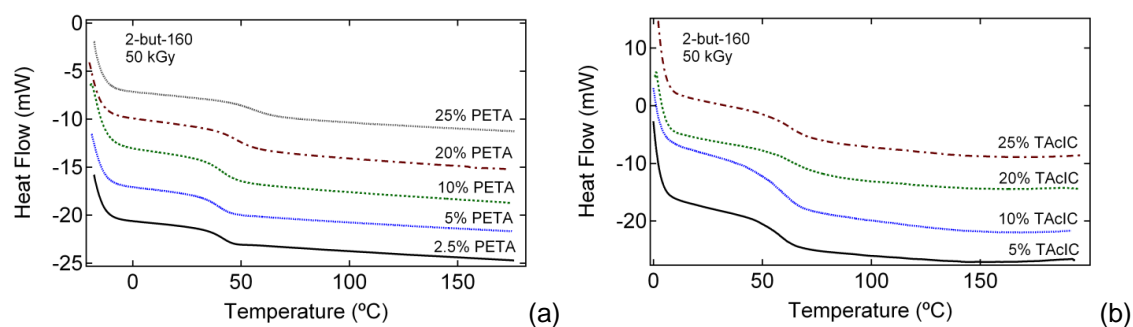
Figure 10- DSC results for samples with increasing (a) PETA and (b) TAcIC composition irradiated at 50 kGy.

4. DMA Results and Discussion

Rubbery modulus increased significantly with increasing sensitizer composition and also increased with increasing dose, increasing C=C double bond composition, and increasing molecular weight. DMA storage modulus plots for 50 kGy, 2-but-160 samples containing varying PETA and TAcIC sensitizer are provided in Figure 11(a) and 11(b), respectively, and Figure 11(c) and 11(d) contain the corresponding tan delta plots. Figure 11(a) shows that for 2-but-160 samples irradiated at 50 kGy, as PETA sensitizer increased from 2.5 to 25 mole %, rubbery modulus (E_r) increased from 0.5 MPa to 30 MPa. Figure 11(b) shows a very similar trend for otherwise identical samples containing TAcIC sensitizer. As TAcIC composition increased from 5 to 25 mole %, rubbery modulus increased from ~5.0 to ~39 MPa. In contrast to the irradiated samples, the thermoplastic sample in Figure 11(b) did not exhibit a significant rubbery plateau after its glass transition. Above T_g, its storage modulus tailed off and approached zero as the polymer began to flow, as is characteristic of amorphous thermoplastic polymers. The rubbery moduli of samples containing TAcIC were approximately 15 to 25% higher than the moduli of samples containing PETA. One explanation for this trend could be that the TAcIC sensitizer contained approximately 100 ppm monomethyl ether hydroquinone inhibitor, while the PETA sensitizer contained approximately 400 ppm 4-methoxyphenol inhibitor. Since our working hypothesis, which is discussed in later in this section, states that electron beam crosslinking proceeds by a free radical mechanism, the presence of free radical inhibitor could potentially have an inverse influence on radiation crosslinking.[63] For practical systems, increasing inhibitor helps the balance of

67

enhanced resin shelf life (to avoid premature polymerization and crosslinking) at the expense of ease of crosslinking under a given dose. Thus, a non-linear optimization among radiation dose, inhibitor content, sensitizer content, and polymer molecular weight can be used in real systems to pinpoint desired thermo-mechanical properties and resin shelf life.
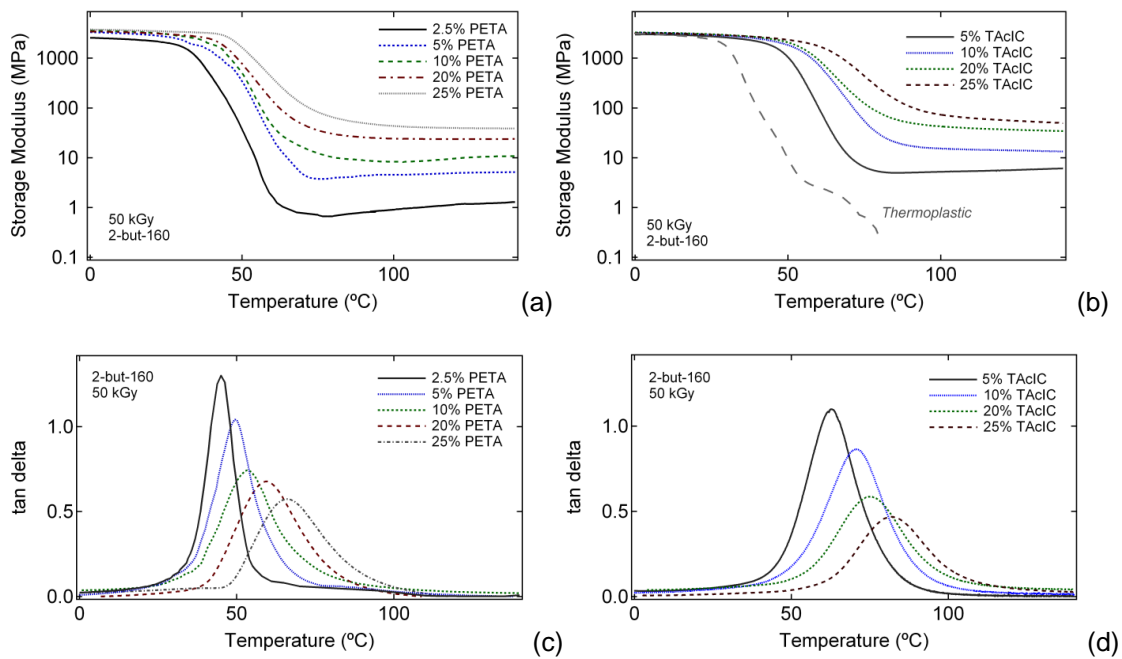
Figure 11- Storage modulus, 4(a) and 4(b), and tangent δ, 4(c) and 4(d), as a function of temperature from DMA for samples containing varying amounts of PETA and TAcIC. The thermoplastic sample is included in 4(b) for comparison. Maximum rubbery moduli of 30 MPa (PETA) and 45 MPa (TAcIC) were achieved.

Peaks of tangent δ, seen in Figure 11(c) and 11(d), correspond to the viscoelastic changes around T_g seen in Figure 11(a) and 11(b) and indicate that T_g increased with increasing sensitizer composition. Glass transition has often been shown to increase

with increasing crosslink density because crosslinking can reduce chain mobility,[22] so the general T_g trends in Figure 11(c) and 11(d) are in accordance with previously published trends. As shown in 11(c), T_g increases from approximately 52°C to 65°C as PETA is increased from 5% to 25%. The TAcIC samples shown in 11(d) generally had higher T_g than the PETA analogs: T_g increased from approximately 62 to 78°C as TAcIC increased from 5% to 25%.   The central isocyanurate ring structure of TAcIC is expected to be more rigid than the more flexible PETA structure, so a higher T_g for TAcIC samples was expected.[64]

Figure 12, which contains a large series of DMA storage modulus plots, illustrates that rubbery modulus was also dependent on dose, repeat unit C=C composition, and thermoplastic molecular weight. This figure represents the breadth of control that can be exerted on thermo-mechanical properties by altering both the underlying chemistry and the processing parameters. As Figure 12(a) shows, as dose was increased from 25 to 100 kGy, E_r increased from 2.5 to 14.0 MPa for 2-but-160, 5% TAcIC samples. As Figure 12(b) shows, as C=C double bond composition per repeat unit was increased from 50% (DEG-60) to 80% (DEG-78) to 100% (2-but-40), E_r increased from 1.5 to 3.0 to 7.0 MPa, respectively for 100 kGy, 10% PETA samples. As Figure 12(c) shows, as M_w increased from 7.0 to 160 kDa, E_r increased from 10.8 to to 23.5 MPa for 50 kGy, 20% PETA samples. The positive correlations observed in this study between gel fraction and sensitizer, dose, and molecular weight are in accordance with observed trends reported in previous electron beam crosslinking studies.[55] It is

noteworthy, however, that a comparatively significant positive correlation between these same three variables and rubbery modulus was also observed in this study.

We have hypothesized previously that it may be possible to increase the electron beam crosslinking susceptibility of a polymer by tailoring its chemistry to favor such crosslinking reactions.[65] As illustrated in Scheme 2, the alpha hydrogen theory of electron beam crosslinking, which has been supported in the literature since the 1950's, states that one of the dominant mechanisms of e-beam crosslinking may be the hydrogen extraction and ensuing radical formation at carbons in positions *alpha* to electron withdrawing groups (EWGs) during irradiation. Crosslinking is then proposed to occur via radical graft polymerization by radical-radical coupling.[50, 51] Illustrated in Scheme 3 is our working hypothesis, which states that, assuming that the processes described in alpha hydrogen theory do play some role in e-beam crosslinking, then the incorporation of a C=C double bond in the *beta* position to an EWG in a polymer may enhance a polymer's susceptibility to radiation crosslinking by providing resonance stabilization of e-beam-induced α-carbamate radicals. This delocalization could increase radical life, and longer radical life could increase the probability of crosslinking events' occurring, therein enhancing a polymer's susceptibility to radiation crosslinking.

The powerful effect of C=C double bond presence on radiation crosslinking is illustrated in Figure 12(d), which shows DMA storage modulus plots of two polymers with identical dose (100kGy) and sensitizer (20% PETA) conditions.   One sample is comprised of 2-butene-1,4-diol (2-but-40), and the other of 1,4-butanediol (1,4-but-98). The 2-butene-1,4-diol sample, which contains C=C double bonds in the *beta* positions to

electron withdrawing carbamate groups in addition to alpha hydrogens, appears

significantly crosslinked. This sample has a minimum rubbery modulus of 25.8 MPa

and exhibits a slight increase in E_r with increasing temperature, which is characteristic of

ideal elastomeric behavior. In contrast, 1,4-butanediol sample, which does contain α-

carbamate hydrogens, but lacks β-carbamate C=C motifs, appears only lightly

crosslinked. This sample maintains a temporary rubbery plateau modulus of

approximately 3.0 MPa, and its modulus begins to slope downward above 150°C.

Although the results provided in Figure 12(b) and 12(d) clearly indicate that a

correlation exists between thermoplastic carbon-carbon double bond composition and

electron beam crosslinking, alternative crosslinking processes other than the

hypothesized radical graft polymerization mechanism should also be considered. For

example, radiation crosslinking could instead proceed by free radical chain growth

polymerization, or it could involve a combination of multiple chemical processes. As

Dannoux and others have reported, numerous chemical reactions occur during the high-

energy irradiation of polymers, and the most dominate of these processes dictate whether

scission and/or crosslinking events occur.[66] The hypothesis presented in this study

appears sound, but it should be regarded only as a working scientific theory.

One major implication resulting from the data in Figure 12(d) is that this SMP

system is very well-suited for processing by thermoplastic melt processing techniques

such as injection molding because high crosslink densities are achievable upon

irradiation of even low molecular weight thermoplastics. High molecular weight

thermoplastics can be difficult to process, and molecular weights often must be lowered

71

before thermoplastics can be injection molded or extruded on a mass scale.[28] Figure 12(e) shows storage modulus plots for a very low molecular weight sample ($M_w = 7.0$ kDa) containing varying PETA and irradiated at 50 kGy. While the 0% PETA sample exhibits no rubbery plateau, the 10% PETA sample appears to have undergone some degree of molecular weight increase during irradiation and exhibits a small rubbery plateau region. The 20% PETA sample appears to have undergone a network formation during irradiation and has a rubbery modulus of roughly 11.0 MPa. Considering that the starting M_w of this polymer was only 7.0 kDa, this rubbery modulus value is considerably high. In Figure 12(d), even with 20 mole % triacrylate sensitizer, high crosslink densities were not achievable in the 1,4-butanediol sample, even though its molecular weight (98 kDa) was more than twice that of the 2-butene-1,4-diol sample (40 kDa).

The crosslink density of this polyurethane SMP system can thus be controlled by varying four factors: sensitizer, dose, carbon-carbon double bond composition, and molecular weight. There are inherent advantages to having multiple methods of achieving a particular material design criterion. For example, if a particular application were to require that a specialty monomer replace some of the 2-butene-1,4-diol monomer content, a target crosslink density could still be achievable by compensatively increasing sensitizer, dose, molecular weight, or any combination of the three. If an application should instead require an SMP with a low crosslink density, but should also require a high electron beam dose (e.g., for sterilization purposes), C=C composition, sensitizer composition, or molecular weight could be lowered to compensate for the

72

increased dose. In this study, these four parameters were varied in order to create materials that met two design criteria: (1) the ability for glass transition to be controlled independently of rubbery modulus, and (2) the ability for rubbery modulus to be controlled independently of glass transition. As Yakacki and others have reported, since actuation temperature and recovery stress are two of the most important properties in an SMP system, the ability to control each of these properties independently of the other could be extremely important from an application-based standpoint, and demonstrating control over these parameters can broaden the material application range.[67, 68]

In Figure 12(f), DMA for samples with glass transitions of 45 °C and 62 °C and a constant rubbery modulus of 5.0 MPa are shown. In Figure 12(g), DMA for samples with rubbery moduli of 3.0, 7.0, and 26.0 MPa and a glass transition of approximately 60 °C are shown. The various plots in Figure 12 highlight different approaches to manipulate the thermo-mechanical properties of radiation crosslinked SMPs.
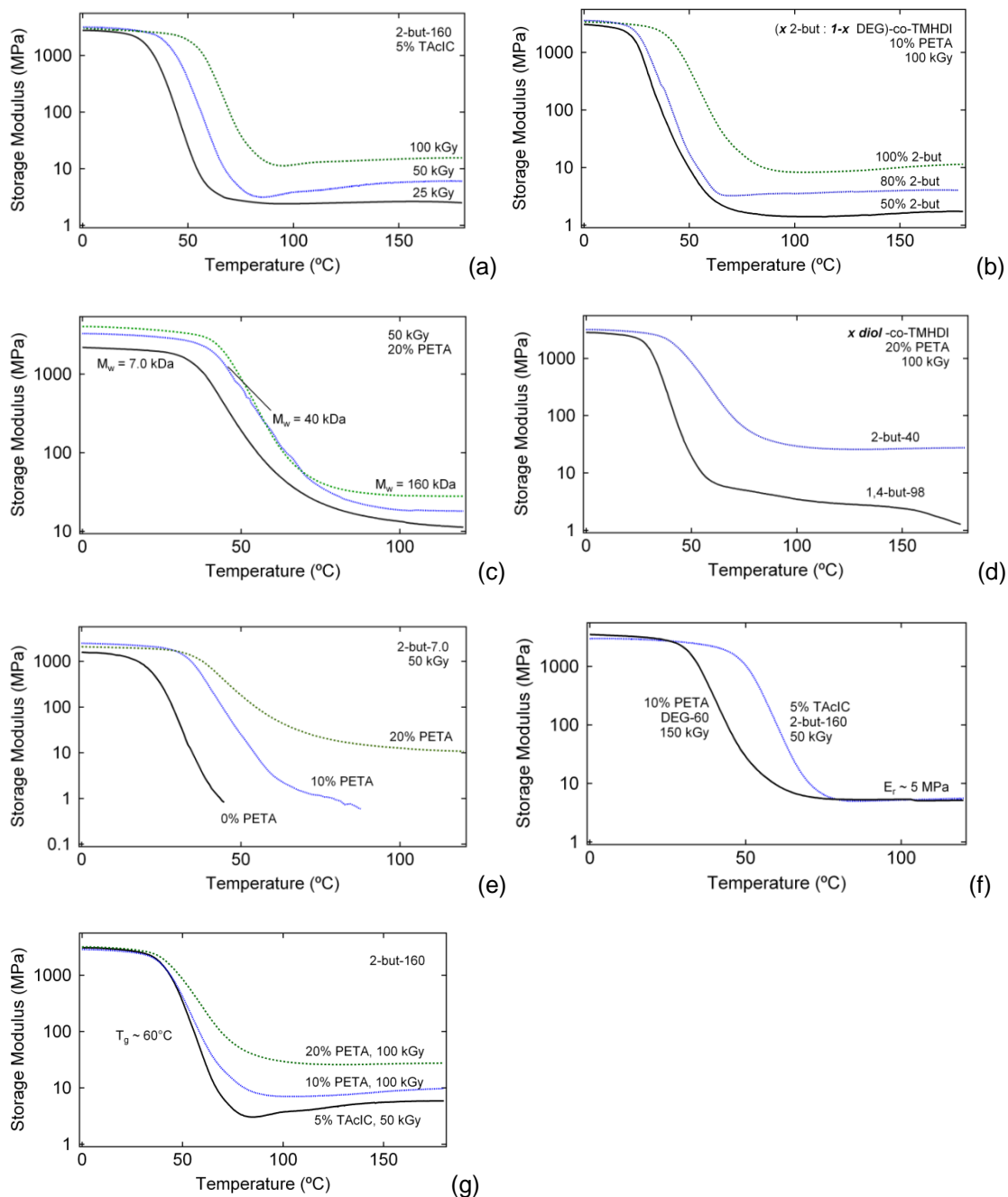
Figure 12- The thermomechanical effects of (a) dose, (b) the presence of double bonds in the polyurethane backbone, and (c) molecular weight on electron beam crosslinking. The effects of repeat unit C=C composition of radiation crosslinking for samples made from 2-butene-1,4-diol and 1,4-butanediol (d). A rubbery modulus of approximately 10 MPa was achievable upon irradiation of a sample with an Mw of 7.0 kDa (e). Independent control of Tg with respect to crosslink density (f) and independent control of crosslink density with respect to Tg (g)

74

5. Tensile Testing Results and Discussion

The tensile testing results followed anticipated trends: stress-at-failure increased with increasing crosslink density, and strain-to-failure decreased with increasing crosslink density. The experiments were performed at T_g (as measured from DMA tangent δ peaks) on the 2-but-160, 50 kGy, varying PETA series, for which DMA data is provided in Figure 11. Stress/strain plots for strain-to-failure experiments are provided in Figure 13(a), and a summary plot of ultimate tensile stress and strain versus PETA composition is provided in Figure 13(b). As PETA composition was increased from 2.5% to 25%, average strain-to-failure decreased from 2.1 mm/mm to 0.4 mm/mm, and average stress-at-failure increased from 8.1 to 29.3 MPa. The tensile tests indicate sample strengths and toughness that could make these systems appealing candidates for engineering applications traditionally selecting from moldable thermoplastics.

6. Shape Memory Characterization Results and Discussion

Free strain recovery results, which are provided in Figure 14(a), demonstrated 100% recoverable strains for the 2-but-160, 50 kGy, 10% PETA sample selected for the test (0.30 mm/mm applied strain). Since high percent recoverable strains are generally thought to be an advantage of covalent crosslinking, this sample's ability to fully recover its strain was anticipated. The constrained recovery results in Figure 14(b) indicate that the recovery stresses of samples strained to 0.25 mm/mm increased with increasing sensitizer composition (i.e., increasing crosslink density). For PETA compositions of 0% (thermoplastic), 2.5%, 5.0%, and 10%, peak recovery stress values were measured to

be 0.0 MPa, 0.9 MPa, 1.3 MPa, and 2.3 MPa, respectively. This observed positive

correlation between crosslink density/rubbery modulus and recovery stress of SMPs

confirms trends noted in previous investigations by Yakacki and others[36]
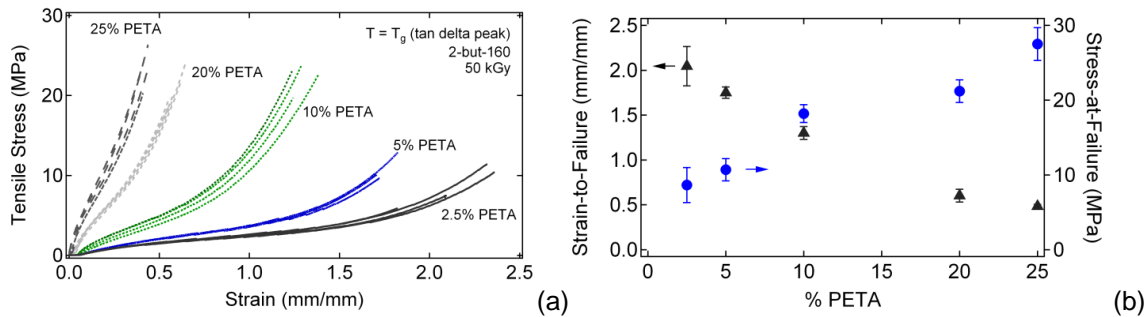
Figure 13- (a) Stress-strain data for strain-to-failure tests run on samples with varying PETA irradiated at 50 kGy. Testing was performed at tan delta peak. (b) The effect of PETA composition strain-to-failure and stress-at-failure
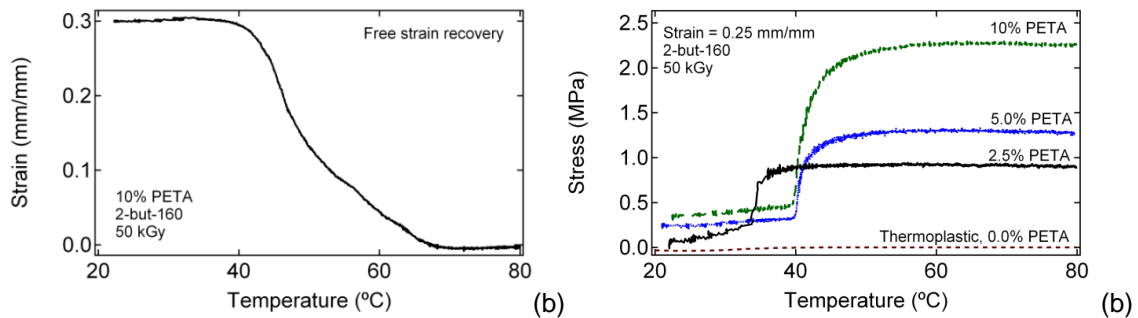
Figure 14- Shape memory characterization: (a) Free strain recovery demonstrated fully recoverable strains of 0.30 mm/mm for 2-but-160, 50 kGy, 10% PETA samples; (b) Constrained recovery tests at 0.25 mm/mm demonstrated that recovery stress increased with increasing PETA composition (i.e., crosslink density, rubbery modulus) for 2-but-160, 50 kGy samples with varying PETA

The primary objective of this study was to demonstrate control of the crosslink

density of electron beam crosslinked SMPs using low molecular weight thermoplastics.

Although the DMA results in Figure 11 and Figure 12 are the best experimental evidence that this specific objective was met, the stress-strain data in Figure 13 and shape memory characterization data in Figure 14 provide compelling validation that the strategy of controlling crosslink density is an effective method of tuning thermo-mechanical properties. By controlling crosslink density, control over stiffness, ultimate strain capacity, and ultimate tensile strength was also achieved, and the stress-strain data in Figure 13 illustrates this point. The constrained recovery data in Figure 14(b) then serve as a fitting parallel conclusion to the DMA data in Figure 11(a), as this figure brands the tangible concept of physical force onto an otherwise intangible concept of crosslink density.

7. Stent Fabrication Results and Discussion

The purpose of fabricating a medical device from the polyurethane SMPs in this study was to demonstrate their novel capability to be processed into desired geometries by dip-coating and subsequently crosslinked after processing using electron beam irradiation to tune thermo-mechanical properties. From a medical device standpoint, an SMP neurovascular stent was selected as the target medical device prototype because we have investigated similar polyurethane neurovascular SMP stents in previous studies.[59] The stents in these studies were determined to have collapse pressures above (tubular) or very near (laser etched) the maximum expected pressures to be exerted by an artery, and the expansion ratios of the tubular and etched stents were approximately 2.1 and 2.7, respectively. In this study, our objective was to introduce a new SMP system that could

77

potentially offer improved processing capability and better tunability of thermo-mechanical properties for numerous medical device applications, including neurovascular stents.

The automated assembly used to dip-coat sets of four 80 mm-long, 4 mm-diameter brass pins is pictured in Figure 15(a). Figure 15(b) shows a brass pin that was dip-coated in 2-but-160 polyurethane SMP, irradiated at 150 kGy, and engraved using CO_2 laser machining. The SEM images in Figure 15(c), taken after the stent's removal from the brass pin, provide a close-up view of the complex, laser-engraved stent geometry.

The final stent prototypes were approximately 25 mm in length, with wall thicknesses ranging from 150 to 220 μm and outer diameters (ODs) of approximately 4.30 mm. To qualitatively demonstrate the ability of these SMP stent devices to store temporary, compressed geometries, the stents were crimped from their original 4.30 mm ODs to final diameters of 1.40 mm using a Machine Solutions, Inc. SC150-42 Stent Crimper, which is pictured in Figure 15(d). Each stent was heated to 55 ˚C (T_g + 15 ˚C) and given one hour to equilibrate. The stents were then crimped to final diameters of 1.4 mm using a constant applied pressure of 45 psi. Figure 15(e) shows a crimped stent and a stent in its primary geometry. Ongoing and future work involves stent-specific thermo-mechanical characterization and testing on the bench top and *in vivo*. The engineering of this polyurethane SMP system will also continue, with device-specific material demands largely driving this engineering process.
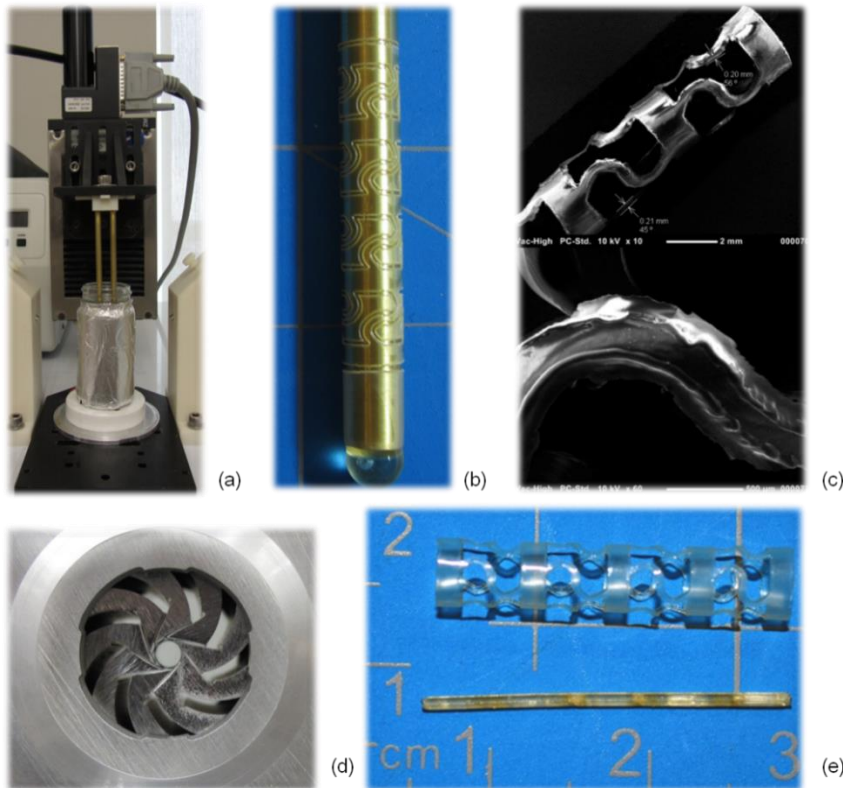
Figure 15- (a) Dip-coating assembly use to fabricate stents; (b) Brass pin surrounded by thin SMP tube, after dip-coating, drying, electron beam crosslinking, and CO2 laser machining; (c) SEM image of the stent after removal from brass pin. (d) Machine Solutions, Inc. SC150-42 Stent Crimper; (e) SMP neurovascular stent in primary geometry and crimped geometry.

D. Summary and Conclusions

As the shape memory polymer community continues to diversify, a broadening application range demands that SMPs have more versatile material capabilities. Covalent crosslinking can improve certain thermo-mechanical properties and act as an avenue to finely tune these properties, but it also creates major processing difficulties for complex thermoset SMP prototypes. This work introduces novel polyurethane SMPs with highly tunable mechanical properties that can be processed into desired geometries

as thermoplastics and then crosslinked using electron beam irradiation at significantly lower molecular weights than previously described in the literature. The potential impacts of this study span the confines of multiple disciplines. From a radiation physics standpoint, the observed dependence of e-beam crosslinking on carbon-carbon double bond composition suggests that a "polymer chemistry" factor could be missing from the classical radiation crosslinking model. Furthermore, while classical theory has sought to quantify radiation crosslinking in terms of gel fraction trends, this study suggests that exploring an alternative model that uses both rubbery modulus and gel fraction to define crosslinking may be an interesting future course of study. From a materials engineering standpoint, the demonstrated ability to control crosslink density and the material properties that depend on it by varying dose, sensitizer composition, C=C composition, or molecular weight may be very useful when application-specific requirements limit what factors can be varied to control crosslink density. For example, for a hypothetical medical device that requires processing by injection molding but also requires high crosslink density, molecular weight could be kept low to facilitate injection molding, and high crosslink density could still be achieved by varying other factors. Finally, from a biomedical engineering standpoint, new SMP medical devices with highly tunable mechanical properties may now be able to fabricated and characterized, and current devices already being investigated may now be fabricated in a more efficient manner. The demonstrated use of dip-coating and laser machining to fabricate an SMP neurovascular stent is promising evidence that other devices can also be made using this novel SMP system. As intelligent polymer systems continue to gain attention in the

80

scientific community, materials engineers bear the responsibility of ensuring that these materials remain relevant for increasingly complex applications.

E. Acknowledgements

CHAPTER V

THERMAL STABILIZATION OF A SENSITIZED E-BEAM CROSSLINKABLE

POLYURETHANE SMP SYSTEM USING FREE RADICAL INHIBITOR*

The development of a series of new SMP systems that are capable of being processed into desired geometries as thermoplastics and subsequently crosslinked using post-polymerization crosslinking techniques is the focus of this work. In Chapter III, a polyurethane SMP system than can undergo post-polymerization thermally induced crosslinking is reported. To overcome two limitations of this thermally crosslinkable SMP system, an electron beam crosslinkable PU SMP system was developed and is reported in Chapter IV, in which control of crosslink density is demonstrated using acrylic radiation sensitizer additives. One drawback of using radiation sensitizer additives such as polyacrylate sensitizers is sensitizer thermal instability during elevated temperature processing, which can lead to undesired premature sensitizer auto-polymerization. Chapter V reports a study in which free radical inhibitor is added to sensitizer containing thermoplastics comprised of similar formulations to those reported in Chapter IV, and the effects inhibitor on both e-beam crosslinking susceptibility and on thermal stabilization of sensitizer are investigated.

A. Introduction and Literature Review

One drawback of the sensitized electron beam crosslinkable PU SMP system reported in Chapter IV is sensitizer thermal instability during elevated temperature processing, which can lead to undesired premature sensitizer auto-polymerization. Chapter V reports a study in which free radical inhibitor is added to sensitizer-containing thermoplastics comprised of similar formulations to those reported in Chapter IV, and the effects inhibitor on both e-beam crosslinking susceptibility and on thermal stabilization of sensitizer are investigated in order to quantify the improvements in elevated temperature working times that result from varying quantities of free radical inhibitor addition.

As discussed in Chapter IV, many studies have reported the use of radiation sensitizer additives to increase the electron beam crosslinking susceptibility of thermoplastic polymers. First reported by Pinner and others in the 1950's, sensitizers have high mobility in comparison with that of bulky polymer chains and are highly reactive with polymer radicals induced during irradiation [41, 43, 69]. Unfortunately, while the high reactivity of radiation sensitizers can be extremely useful in facilitating radiation crosslinking, sensitizers are often so reactive that they can potentially undergo premature thermally-induced auto-polymerization reactions during high-temperature processing [31]. Many thermoplastic processing techniques such as blow molding, extrusion, and injection molding are performed at elevated temperatures, and the machinery used for such techniques could be ruined if premature sensitizer crosslinking were to occur during processing. Furthermore, the reaction of sensitizers before

irradiation could prevent radiation crosslinking from occurring and consequently prevent target mechanical properties from being achieved. To address this problem, free radical inhibitors such as benzoquinone or hydroquinone can be added to thermoplastic/ sensitizer blends to stabilize the sensitizer [70]. For decades it has been an industry standard for chemical distributors to add free radical inhibitors to reactive monomers capable of undergoing runaway uncontrolled radical polymerizations [48], and several patents have reported that adding free radical inhibitor to thermoplastic polymer/sensitizer blends before processing successfully prevents premature sensitizer crosslinking.[71] In addition to providing thermal stabilization, free radical inhibitor may also inhibit electron beam crosslinking by reacting with e-beam induced radicals generated during irradiation. As illustrated in Scheme 4, which expounds on the resonance stabilization hypothesis for enhanced e-beam crosslinking that is reported in Chapter IV, if inhibitor is present during irradiation, it can potentially react with e-beam-induced radicals and prevent radical graft polymerization from occurring. Consequently, competing effects can occur if both sensitizer and inhibitor are present [40]. Reported efforts to quantify these competing effects to determine optimal processing conditions for sensitizer-containing thermoplastic polymer blends are largely lacking in the literature, and such effects are investigated in this study.

Scheme 4- Flow chart illustrating potential problems that can arise during high-temperature processing and attempted e-beam crosslinking of polyurethane SMPs containing radiation sensitizer and inhibitor: (1) undesired premature sensitizer crosslinking during processing; (2) undesired inhibition of radiation crosslinking by inhibitor; (3) desired sensitizer stabilization without undesired radiation crosslinking inhibition
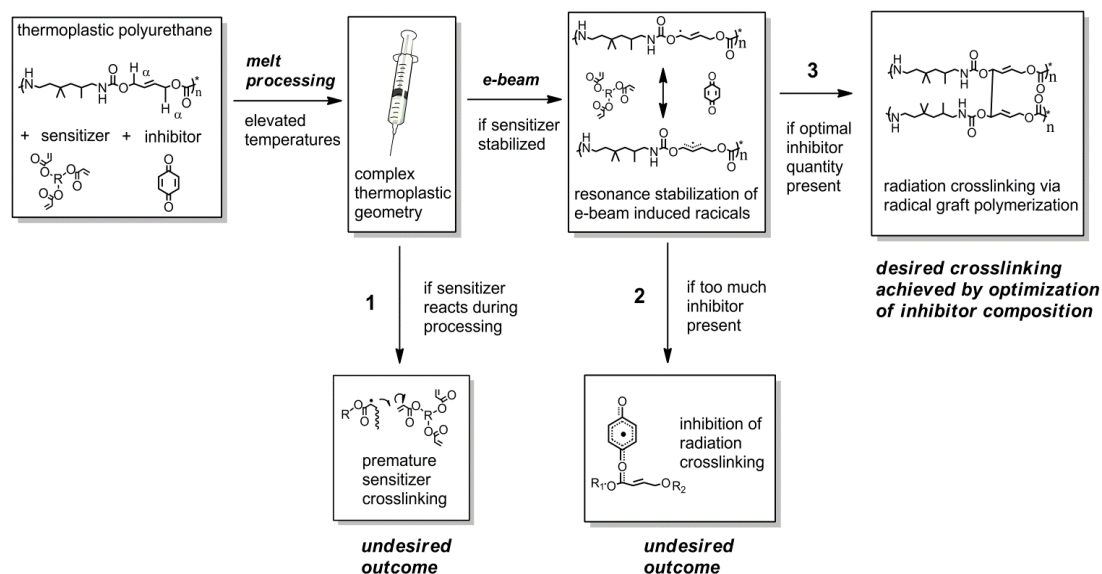
B. Materials and Methods

In Chapter IV, a polyurethane SMP system prepared from 2-butene-1,4-diol and trimethylhexamethylene diisocyanate (TMHDI) is reported that can be crosslinked to tunable crosslinking densities by blending thermoplastics with acrylic sensitizer additives and subjecting these blends to electron beam irradiation after thermoplastic processing. To improve the industrial relevance of this SMP system, it is desirable to improve these polymers' ability to be processed at elevated temperatures. In this study, we introduce free radical inhibitor to the sensitized polyurethane SMP system reported in Chapter IV to determine optimal sensitizer and inhibitor compositions that allow for

both sufficient e-beam crosslinking and sufficient sensitizer thermal stabilization. There are two main objectives in this study: (1) to determine effects of sensitizer, inhibitor, and radiation dose on e-beam crosslinking and (2) to quantify the thermal stabilization effects of the inhibitor for varying temperatures and varying heat exposure times.

1. Synthetic Strategy, Polyurethane Synthesis and Sample Preparation

Pentaerythritol triacrylate (PETA), which is utilized as a radiation sensitizer additive in Chapter IV [31], is also utilized as a sensitizing agent in this study. The free radical inhibitor 1,4-benzoquinone (BQ) is utilized in this study because of its chemical inertness in the presence of isocyanate monomers and because of its reported oxygen insensitivity. Other inhibitors such as hydroquinone or 4-methoxyphenol contain hydroxyl groups and are expected to react with isocyanates or other electrophilic monomers. Since the underlying motivation in this work is to improve the industrial relevance of shape memory materials, the BQ inhibitor was chosen because it can be used in the presence of isocyanates or other electrophilic monomers if necessary. Also, BQ has been shown to act as an oxygen-independent inhibitor, while other inhibitors such as hydroquinone may require oxygen to form peroxy radicals to be effective inhibitors [52]. Certain processing procedures such as injection molding may take place in oxygen-poor or oxygen-free environments, and consequently an oxygen-independent free radical inhibitor is desirable.

1.1. Polyurethane Synthesis

The polyurethane shape memory polymers characterized in this work were
prepared from trimethylhexamethylene diisocyanate (TMHDI) and 2-butene-1,4-diol.
All reagents and starting materials were used as received unless otherwise stated.
TMHDI (97%), 2-butene-1,4-diol (97%), and 1,4-benzoquinone (99%) were purchased
from TCI America. Anhydrous THF and 4-methoxyphenol inhibitor removal columns
for were purchased from Sigma Aldrich, and pentaerythritol triacrylate (97%) was
purchased from Alfa Aesar. Monomers and anhydrous THF were stored in a glove box
under dry air until use to prevent moisture absorption. The as-received PETA contained
300 ppm 4-methoxyphenol inhibitor, which was removed using the inhibitor removal
columns. Samples were solution cast in polypropylene containers. The chemical
structures of the monomers, inhibitor, and sensitizer used in this study are provided
along with the GPC data in Table 5.

Thermoplastic polyurethanes were synthesized from 2-butene-1,4-diol and
TMHDI. A 100g monomer batch was prepared in a glove box under dry air using a 1%
stoichiometric excess of NCO:OH. The polymerization reaction was catalyzed by 0.01
wt% zirconium(IV) 2,4-pentanedionate and carried out in a 33% anhydrous THF
solution at 80°C for 24h under mild vortexing conditions. A LabConco RapidVap
concentrator was used to heat and vortex the samples at its 150 rpm during
polymerization. After polymerization, the viscous polymer solution was diluted to 10%
by adding THF and was subsequently allowed to dry for 12 hours in a fume hood. The
samples were then heated to 80°C for 12 h, after which they were evacuated at 1 torr at

80°C for an additional 24 h. After solvent removal, five 20 g, 0.3 mm-thick, optically clear, bubble-free samples were removed from the polypropylene dishes and stored in a desiccation chamber.

1.2. Size Exclusion Chromatography

Size exclusion chromatography was used to measure M_n and M_w for the thermoplastic urethane synthesized in this study. Molecular weight was determined using a Waters Chromatography 1515 HPLC equipped with a Waters 2414 differential refractometer, a Precision Detectors PD2020 dual-angle (15° and 90°) light scattering detector, and Polymer Laboratories three-column series PL gel 5 μm Mixed C, 500 Å, and 104 Å 300 mm × 7.5 mm columns. The system was equilibrated at 35 °C in anhydrous THF, which was used as both the polymer solvent and eluent, with a flow rate of 1.0 mL/min. Polymer solutions of about 3 mg/mL were prepared, and an injection volume of 200 μL was used. Data collection was performed using Precision Acquire software, and data analysis was performed using Waters Empower 3 software. Using a nearly monodisperse polystyrene standard purchased from Pressure Chemical Co. for calibration (M_p = 90 kDa, M_w/M_n< 1.04), the interdetector delay volume and light scattering detector calibration constant were determined. Standard polystyrene reference material (SRM 706 NIST) of known S-2 specific refractive index increment (dn/dc = 0.184 mL/g) was used to calibrate the differential refractometer. The dn/dc values of the analyzed polymers were then determined from the differential refractometer response.

1.3. Solution Blending of Sensitizer and Inhibitor and Film Casting

5g polyurethane samples were massed and placed in 40 mL glass vials. 25 mL THF was added to each vial, and the polymers were re-dissolved in THF by vortexing in a LabConco RapidVap at 35 speed setting at 50°C for 5h. After allowing the samples to cool to ambient temperature, inhibitor-free PETA was added to four sets of vials in 0, 5, 10, and 20 mole % ratios, and 1,4-benzoquinone inhibitor was added to each four-vial series in 0, 100, 1000, and 10,000 ppm ratios. The ratio of sensitizer to polymer was selected because it contained min and max limits in accordance with previous studies [56]. The inhibitor range of 0-10,000 ppm was selected because many commercially available acrylic monomers (and other monomers requiring stabilization) generally contain inhibitor additives in the range of 10-500, ppm, with some highly unstable monomers containing inhibitor in the 500-1000 ppm or higher range. The 10,000 ppm upper inhibitor composition limit was chosen so that the BQ composition could be varied over a four-order-of-magnitude range, with the upper limit's being roughly 1-2 orders of magnitude greater than inhibitor compositions generally contained in commercial products. 0.3-mm-thick films were solution cast by pouring the solutions into 2" x 2" polypropylene compartmentalized boxes and placing the boxes in a fume hood for 24 h. All samples were then evacuated at 1 torr at 25°C for 72 h to remove residual solvent. It is noteworthy that significant effort was made to prevent the PETA-containing samples from ever being subjected to elevated temperatures during the solution blending and film casting processes.

1.4. Sample Irradiation

The thermoplastic films were placed in 2" x 3" polyethylene sample bags. They were then irradiated at 25, 50, 100, 150 and 200 kGy using a 10 MeV electron accelerator located at the Texas A&M University National Center for Electron Beam Research (NCEBR). The dose range of 25-200 kGy was selected because numerous previous studies have demonstrated successful electron beam crosslinking of various polymer systems over this dose range [39, 54, 72]. The irradiations were carried out at 40°C (reported by NCEBR staff) on a conveyor belt, and doses were delivered in 25 kGy/pass increments. Doses were measured using alanine strips, and the uncertainty of dose to product was reported by the NCEBR operators to be 5%.

2. Radiation Crosslinking Studies: Varying Inhibitor, Sensitizer

To evaluate the effects of inhibitor and sensitizer on electron beam crosslinking, sol/gel analysis and DMA experiments were performed on irradiated samples containing varying BQ and PETA compositions. These studies were employed to determine optimal amounts of inhibitor additives that provide sufficient sensitizer thermal processing stabilization while also allowing for desirable e-beam crosslinking to occur.

2.1. Sol/Gel Analysis

Before being subjected to sol/gel analysis experiments, irradiated samples were dried at 80°C for 24 h at 1 torr and stored in a desiccated environment until use. Triplicate samples with masses of about approximately 0.050 g were cut from the dried,

irradiated films, massed with a precision balance, and placed in 20 mL glass vials. 10

mL THF was added to each vial to give a 1:125 sample to solvent mass ratio. The

sample-solvent mixtures were heated to 50°C for 48 h and vortexed every 5 h to

facilitate dissolution of thermoplastic content. The THF-swollen gels were then

removed from the vials and dried at 80°C for 72 h at 1 torr to remove residual solvent.

Dried samples were re-massed, and gel fractions were calculated using Equations 6 and

7, which are provided in Chapter II.

2.2. Dynamic Mechanical Analysis

To evaluate the effect of inhibitor and sensitizer on rubbery modulus, irradiated

0.3 mm-thick rectangular samples were cut into 4.5 x 30 mm samples using a

Gravograph LS 100 40W laser cutting system. Samples were cut at 20% power and at

12% speed. DMA experiments were carried out in tension on each sample composition

in triplicate using a TA Instruments Q800 dynamic mechanical analyzer in the DMA

Multifrequency/Strain mode at 1 Hz frequency, 0.1% strain, 0.01 N preload force, and

150% Force Track settings. Experiments were run from 0 to 140°C at 2°C/min, and data

was recorded and analyzed using TA Instruments QSeries software. Rubbery modulus

values were determined by taking the storage modulus values at T= T_g + 35°C.

3. Thermal Stabilization Studies

To determine the stabilization effects of the free radical inhibitor on sensitizer-

blended PU thermoplastics during subjection varying temperatures and for varying time

periods, thermal stabilization studies were designed using DSC and sol/gel analysis

experiments. In this particular set of sol/gel analysis experiments, gel fractions for

thermoplastic/sensitizer blends subjected to varying heating conditions were measured

after heating as means of determining if undesired sensitizer crosslinking occurred

during heating. Zero gel fractions were interpreted as indications that the sensitizer

additives remained stable.

3.1 Differential Scanning Calorimetry Thermal Stabilization Studies

To determine the onset of the thermally-induced PETA polymerization reaction,

thermoplastic samples containing varying amounts of sensitizer and inhibitor were

subjected to DSC studies using a TA Instruments Q200 differential scanning

calorimeter. 5-10mg samples were massed and placed in TA Instruments aluminum

DSC pans. DSC experiments were run from 25-200°C at 20°C/min under dry air. Data

were recorded using TA Instruments QSeries software.

3.2 Thermal Conditioning and Sol/Gel Analysis to Determine Thermal Stabilization

Thermoplastic polyurethane samples that had been blended with varying

inhibitor and sensitizer were cut to 0.050 g specimens and were then subjected to 100,

125, and 150°C temperatures under air for time increments of 5 min, 30 min, 1 h, 5 h,

and 24 h at atmospheric pressure. These temperatures were selected because they were

below, between, and above the DSC exotherm peaks shown in Figure 19. After thermal

conditioning, the samples were left at ambient temperature under dry air for 24 h to

allow for the delayed reaction of radicals generated during heating to occur. After 24 h,

a sol/gel analysis was performed on all samples according to the procedures described in

2.1 It is important to note that the samples were not dried at 90°C to remove moisture

before massing because of potential thermal effects that could occur during the drying

process. All thermoplastic samples were, however, stored in a desiccated environment

after solution blending with inhibitor and sensitizer. In these sol/gel analysis studies,

zero gel fractions were interpreted as being indicative that crosslinking did not occur

during heating. Any other gel fraction values indicated that an undesired sensitizer

crosslinking reaction had taken place.

C. Results

Both sol/gel analysis and DMA results demonstrated that inhibitor and sensitizer

exhibit competing effects on electron beam crosslinking, with the PETA sensitizer

appearing to have a more dominant enhancement effect on crosslinking than BQ's

inhibitory effect on it. However, the thermal stabilization studies showed that the

addition of inhibitor significantly improved the thermal stability of sensitizer-containing

thermoplastics.

1. Molecular Weight Characterization Results

The molecular weight data for the thermoplastic polyurethane characterized in

this work are provided in Table 5 along with chemical structures. M_n and M_w were

measured to be 26,500 and 47,000 Da, respectively, and PDI was 1.76.

Table 5- GPC results and chemical structures of monomers, sensitizer, and inhibitor

2-butene-1,4-diol-	M_n (Da)	M_w (Da)	PDI
co-TMHDI	26,500	47,000	1.76

2-butene-1,4-diol	HO⌒⌒OH
TMHDI	OCN⌒⌒⌒NCO
1,4-benzoquinone	O=⬡=O
PETA	(structure)

2. Radiation Crosslinking Study Results

        Both sol/gel analysis and DMA results demonstrated that desirable crosslink densities were still achievable even in the cases of the highest inhibitor compositions, although BQ addition was shown to exhibit a more pronounced inhibitory effect on rubbery modulus than on gel fraction.

2.1. Sol/Gel Analysis Results for Radiation Crosslinking Study

        Irradiated samples containing varying amounts of sensitizer and inhibitor were characterized using sol/gel analysis and dynamic mechanical analysis. In Figure 16, plots of gel fraction versus (a) benzoquinone composition, (b) dose, and (c) PETA composition are shown. Gel fraction increased significantly with increasing PETA and

also increased with increasing dose. However, gel fraction only decreased slightly with increasing inhibitor composition. In Figure 17, Charlesby-Pinner plots of $s + s^{1/2}$ versus $1/d$ are shown. The classical Charlesby-Pinner equation describes the random radiation crosslinking of thermoplastic polymers and is provided and defined in Chapter IV.

A linear fit of each data series was used to calculate p_0/q_0 and d_0 values, which are shown in Table 6 along with the R^2 values for each linear regression equation. Minimum dose to gelation, d_0, decreased significantly with increasing sensitizer composition and increased slightly with increasing inhibitor composition. The scission-to-crosslinking ratio, p_0/q_0, decreased slightly with increasing sensitizer composition and showed almost no dependence on inhibitor composition for PETA-containing samples. However, in the absence of sensitizer, the effect of inhibitor composition on p_0/q_0 was more pronounced: it increased from 0.496 to 0.731 as benzoquinone was increased from 0 ppm to 10,000 ppm. Also, it is notable that the R^2 values for the linear regression equations were very close to 1.0 in the absence of sensitizer, but R^2 values generally decreased with increasing sensitizer.
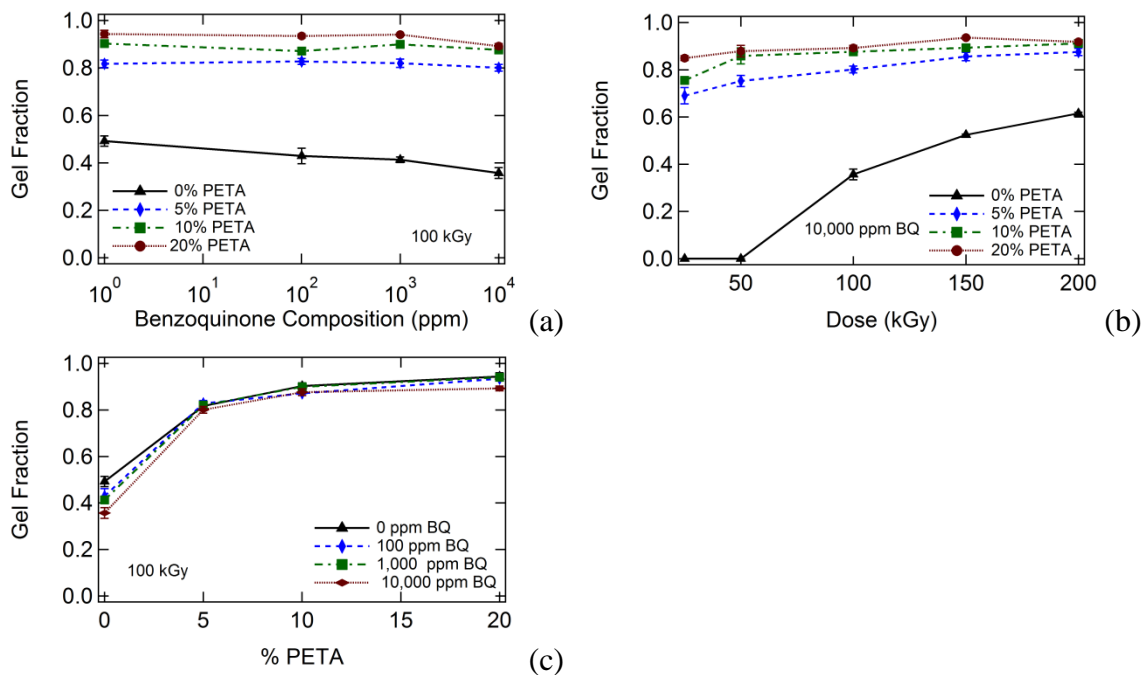
Figure 16- A comparison of the effects of benzoquinone composition, radiation dose, and sensitizer composition on gel fraction. Gel fraction is plotted against (a) inhibitor composition, (b) dose, and (c) sensitizer composition. In general, gel fraction increased significantly with increasing dose and increasing sensitizer composition. Gel fraction also decreased slightly with increasing benzoquinone composition; however, this effect was minimal.
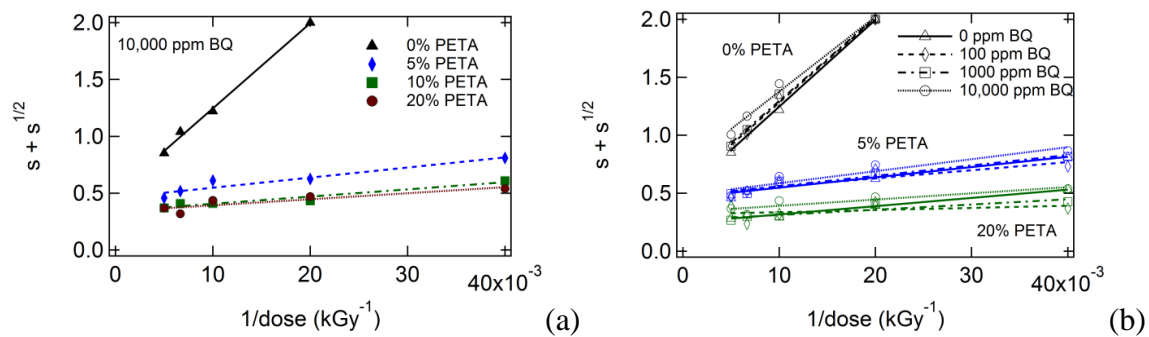
Figure 17- Charlesby-Pinner analysis plots for (a) samples with varying PETA composition and 10,000 ppm BQ and (b) samples with varying BQ composition and 0%, 5%, and 20% PETA.

Table 6- Charlesby-Pinner analysis calculations of p0/q0 and d0 for samples with varying inhibitor and sensitizer compositions.R2 values for each linear regression equation are also plotted.

% PETA	ppm	p_0/q_0	d_0	R^2
0	0	0.496	49.9	0.996
0	100	0.551	50.4	0.996
0	1,000	0.575	50.6	0.994
0	10,000	0.731	50.9	0.987
5	0	0.459	5.8	0.914
5	100	0.462	5.6	0.898
5	1,000	0.470	5.9	0.943
5	10,000	0.482	6.8	0.888
10	0	0.343	3.8	0.942
10	100	0.343	3.8	0.942
10	1,000	0.342	3.9	0.907
10	10,000	0.357	5.7	0.975
20	0	0.295	1.8	0.708
20	100	0.273	2.2	0.821
20	1,000	0.268	2.6	0.816
20	10,000	0.338	3.2	0.805

2.2. DMA Results for Radiation Crosslinking Study

DMA plots of storage modulus versus temperature for samples with (a) varying inhibitor, (b) varying irradiation dose, and (c) varying sensitizer are shown in Figure 18. The storage modulus data for each sample is characteristic of an amorphous thermoset; that is, each DMA plot shows a glassy regime, a glass transition (T_g) region characterized by a several orders-of-magnitude drop in storage modulus, and a rubbery regime at $T > T_g$, in which storage modulus reaches a rubbery plateau value and does not tail off and approach zero with increasing temperature [25]. Rubbery modulus increased

significantly with increasing sensitizer composition and increasing dose and decreased to

a lesser extent with increasing inhibitor.
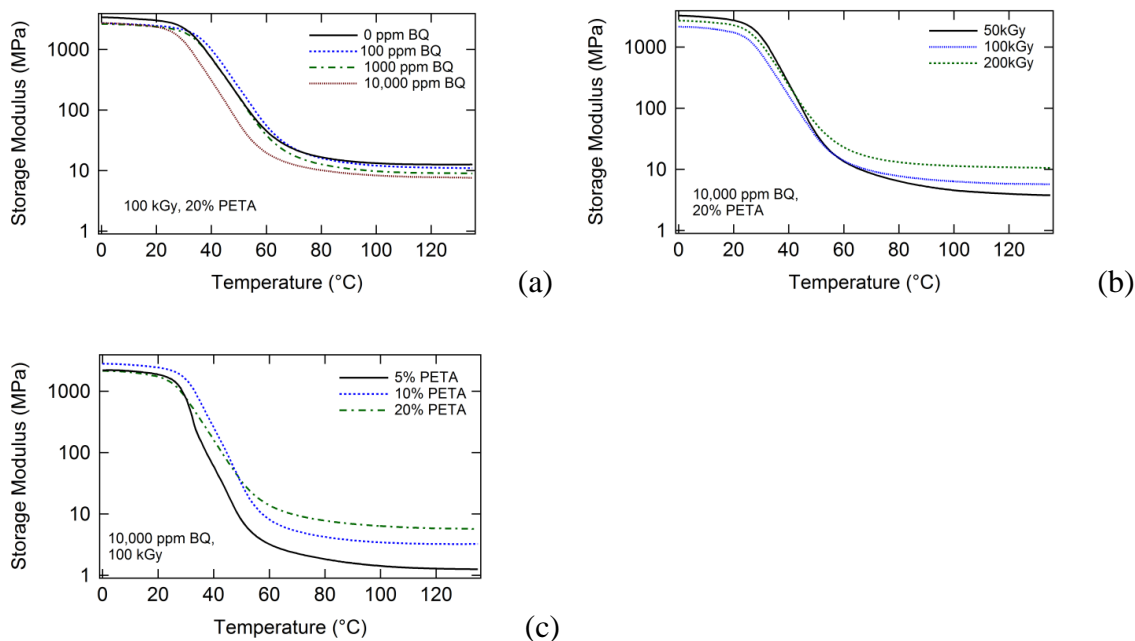
Figure 18- DMA plots of storage modulus versus temperature for (a) samples irradiated at 100 kGy containing varying BQ composition and 20% PETA, (b) samples irradiated at varying doses containing 10,000 ppm BQ and 20% PETA, and (c) samples irradiated at 100 kGy containing varying % PETA and 10,000 ppm BQ. Rubbery modulus increased most significantly with increasing PETA. Rubbery modulus also increased with increasing dose, and decreased slightly with increasing BQ composition.

3. Thermal Stabilization Study Results

The addition of the free radical inhibitor 1,4-benzoquinone was shown to

increase the elevated temperature working times for sensitizer-containing thermoplastics

for up for 24 h, and maximum acceptable working times decreased with increasing heat

exposure temperature.

3.1 Differential Scanning Calorimetry Results

In Figure 19, DSC thermograms for thermoplastic 10% PETA samples

containing 0, 1000, and 10,000 ppm benzoquinone are shown. As inhibitor composition

increased, the exotherm onsets, which were attributed to the thermally-induced onset of

the auto-polymerization reaction of the acrylic double bonds in the PETA molecules,

increased from 120°C to 131°C to 142°C. Based on these DSC results, test temperatures

of 100°C (below all exotherm onsets), 125°C (above 0 ppm BQ onset and below others),

and 150°C (above all exotherm onsets) were selected for comprehensive sol/gel analysis

studies of thermoplastics containing 10% PETA and varying BQ subjected to the

selected test temperatures for varying time increments. There was little difference

between the DSC data of 0 ppm and 100 ppm BQ samples, and the 100 ppm BQ DSC

data is consequently omitted for clarity. The temperatures and heat exposure times in

this study were of comparable magnitudes to those used to determine benzoquinone

induction period measurements (BQ's ability to delay thermal polymerization) in the

literature [52].
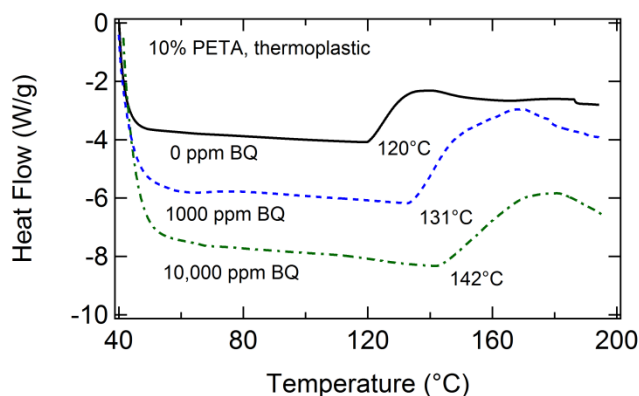
Figure 19- DSC data for thermoplastic 10% PETA samples containing 0, 1000, and 10,000 ppm benzoquinone. As inhibitor composition increased, the exotherm onset, which corresponds to the thermally-induced onset of the auto-polymerization reaction of the acrylic double bonds in the PETA molecules, increased from 120°C to 131°C to 142°C.

3.2 Thermal Conditioning Study Results

Figure 20 shows the effect of increasing inhibitor composition on gel fraction for thermoplastic 10% PETA samples subjected to (a) 100°C, (b) 125°C, and (c) 150°C temperatures for varying amounts of time. Gel fraction increased with both increased temperature and increased heat exposure time. Gel fraction decreased with increased benzoquinone composition. Figure 21, which is an alternate way of looking at the data in Figure 20, shows the effect of increased temperature on gel fraction for thermoplastic 10% PETA samples containing (a) 0 ppm BQ, (b) 100 ppm BQ, (c) 1000 ppm BQ, and (d) 10,000 ppm BQ subjected to 100°C, 125°C, and 150°C temperatures for varying time increments. Gel fraction increased with both increased temperature and increased heat exposure time. Gel fraction decreased with increased benzoquinone composition. The decrease in gel fraction for the 24 hour, 150°C samples in 21(a) and 21(b) in comparison

100

to the respective 125°C samples can be attributed to thermal degradation in the samples

after prolonged exposure to 150°C temperatures in the presence of oxygen.
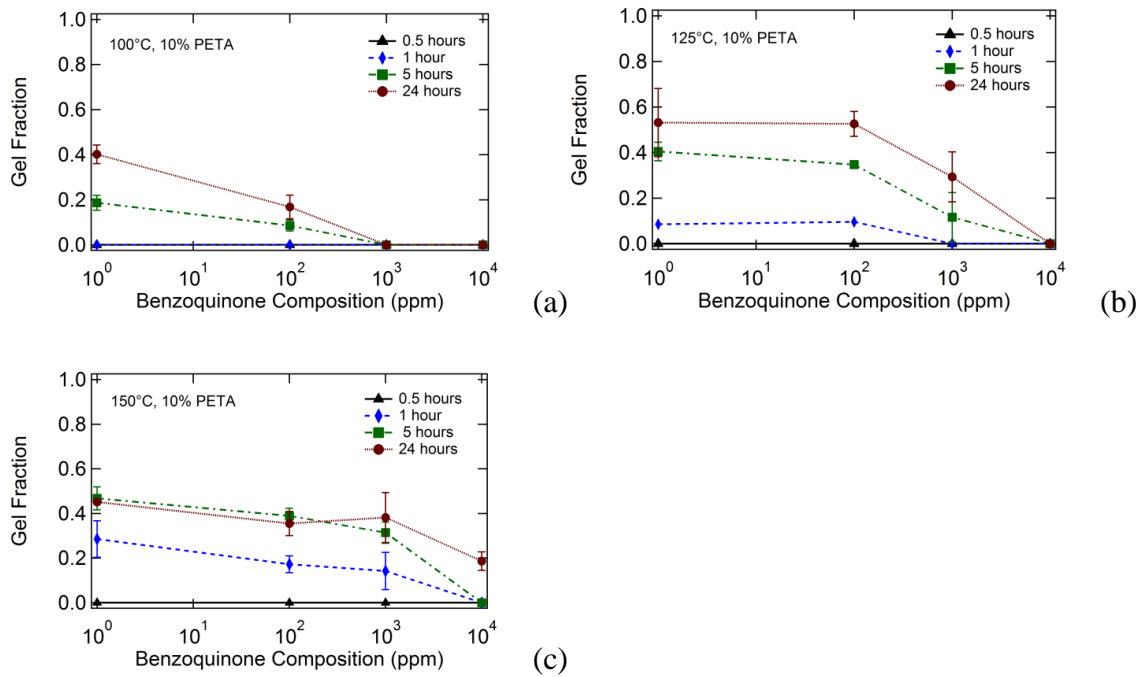
Figure 20- Effect of increasing inhibitor composition on gel fraction for thermoplastic 10% PETA samples exposed to (a) 100°C, (b) 125°C, and (c) 150°C temperatures for varying amounts of time. Gel fraction increased with both increased temperature and increased heat exposure time. Gel fraction decreased with increased benzoquinone composition.
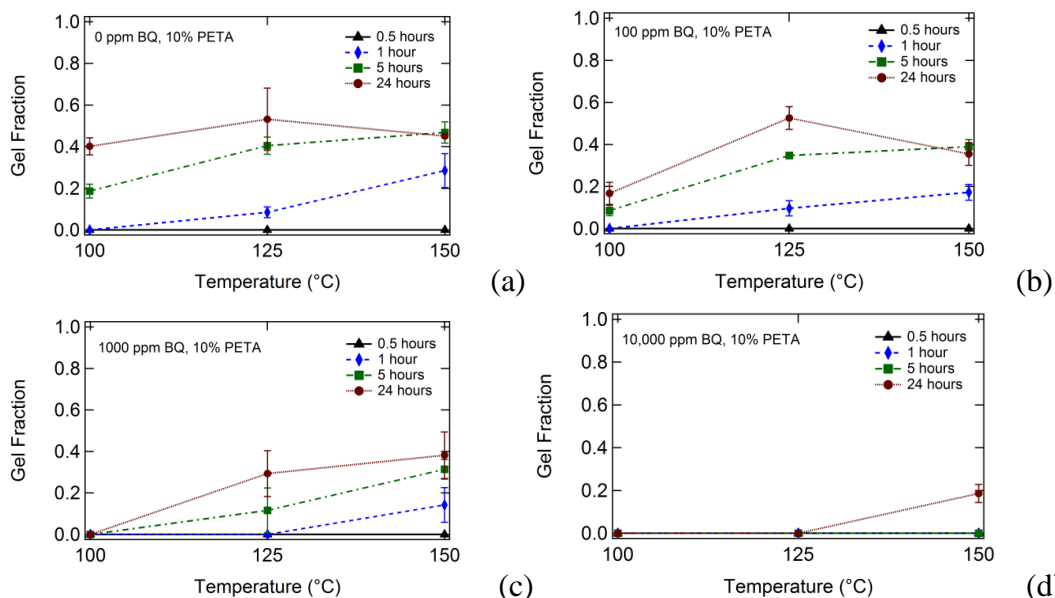
Figure 21- Effect of heating on gel fraction for thermoplastic 10% PETA samples containing (a) 0 ppm BQ, (b) 100 ppm BQ, (c) 1000 ppm BQ, and (d) 10,000 ppm BQ exposed to 100°C, 125°C, and 150°C temperatures for varying amounts of time.

D. Discussion

The ability to process thermoset shape memory polymers into complex geometries using thermoplastic processing methods and a subsequent crosslinking step may help enable the mass-manufacturing of complex thermoset SMP-based devices. Radiation crosslinking is an effective means of crosslinking various thermoplastic polymer systems, and the use of radiation sensitizers can significantly enhance a polymer system's susceptibility to radiation crosslinking. Unfortunately, the high reactivity of radiation sensitizer monomers could potentially cause premature sensitizer crosslinking to occur during high-temperature processing of thermoplastic-sensitizer blends. Free radical inhibitors can be used to stabilize the sensitizer monomers; however, inhibitors can also inhibit radiation crosslinking, which we have hypothesized

102

occurs by radical graft polymerization in our polyurethane SMP system. The objectives of this study were twofold: (1) to determine the effect of free radical inhibitor on radiation crosslinking of sensitizer-containing PU SMPs and (2) to quantify the stabilization effect of free radical inhibitor on thermoplastic-sensitizer blended samples subjected to varying temperatures for varying time increments.

4.1 Molecular Weight

It is notable that high crosslink densities were achievable in this study for samples with an initial M_w of only 47,000 Da. Many other polymers subjected to radiation crosslinking studies in the literature have had higher molecular weights, such as acrylics made by uncontrolled radical polymerization [33] or UHMWPE [41]. The Charlesby-Pinner equation, shown in Equation 3, indicates an inverse relationship between sol fraction and initial molecular weight, μ_1. Consequently, gel fraction and radiation crosslinking are expected to increase with increasing initial molecular weight. In comparison with other radiation crosslinked polymers of similar molecular weights reported in the literature, the polyurethane in this study generally exhibited a higher susceptibility to radiation crosslinking. For example, d_0 and p_0/q_0 values of 182 kGy and 1.65 were reported for a PCL-based SMP with an M_w of 40,000 Da irradiated in the absence of sensitizer [55]. In comparison, the 0% PETA, 0% BQ sample in this study had d_0 and p_0/q_0 values of 49.9 and 0.496, respectively. Thus, almost four times less energy was needed for the polyurethane in this study to reach its minimum dose for gelation, and its crosslinking efficiency was nearly four times greater than that of the PCL sample

with a similar M_w. As illustrated in Scheme 4 , our working theory for the radiation crosslinking mechanism of this SMP system states that radicals generated at α-carbamate sites during irradiation undergo resonance stabilization because of their adjacency to the double bond in the 2-butene-1,4-diol segments. We have hypothesized that this resonance stabilization could enhance radiation crosslinking by extending radical life and increasing the odds that a crosslinking event will occur via radical graft polymerization. Although radiation crosslinking mechanisms are very difficult to prove quantitatively, this SMP system does appear to have a greater susceptibility to radiation crosslinking than other SMPs, and our proposed radiation crosslinking mechanism still appears to be viable.

One potential benefit of enhanced susceptibility to radiation crosslinking is the facilitation of melt-based processing. If desired crosslink densities are achievable in this SMP system at low molecular weights, then these low molecular weight thermoplastics should exhibit low melt viscosities, which should enable easier melt-based processing. Furthermore, since lower molecular weight polymers generally flow at lower temperatures than higher molecular weight samples, heating to lower temperatures would be required for the melt processing of the lower molecular weight samples. As the thermal crosslinking study data in Figures 19, 20 and 21 show, the lower the processing temperature and the shorter the processing time, the lower the likelihood is that premature sensitizer crosslinking will occur.

4.2 Radiation Crosslinking Study

The presence of 0-10,000 ppm 1,4-benzoquinone inhibitor had little effect on gel fraction for the irradiated polyurethane samples in this study, although gel fraction generally decreased slightly with increasing inhibitor. Benzoquinone had the greatest inhibitory effect on gel fraction for the 0% PETA samples irradiated at 100 kGy, where average gel fraction decreased from 0.49 to 0.35 as BQ concentration was increased from 0 ppm to 10,000 ppm, respectively. Both sensitizer and dose had much more significant impacts on gel fraction, as shown in Figure 16. Figure 24(a) shows gel fraction versus dose data for all irradiated samples except 10% PETA samples (these data were omitted for clarity because the 10% PETA gel fraction data essentially overlapped the 20% PETA gel fraction data). As Figure 24(a) shows, the gel fraction trends for the irradiated samples were highly dependent on PETA composition, and varying inhibitor composition caused this data to deviate little from these trends. It is not surprising, then, that inhibitor composition also had little effect on the behavior of the Charlesby-Pinner regression lines shown in Figure 17(b) for 0%, 5%, and 20% PETA samples containing all BQ compositions. Calculated d_0 values for all samples, listed in Table 6, follow this same trend: minimum dose to gelation decreased significantly with increasing PETA and only increased slightly with increasing BQ. In other words, the presence of sensitizer greatly reduced the amount of energy necessary for crosslinking, and the presence of inhibitor only slightly increased the amount of energy necessary for crosslinking for the inhibitor compositions in this study. Benzoquinone had the greatest effect on d_0 for the 10% PETA samples, where d_0

increased from 3.8 to 5.7 kGy as BQ concentration was increased from 0 ppm to 10,000 ppm, respectively.

Concerning p_0/q_0 values, the presence of inhibitor had virtually no effect on the scission-to-crosslinking ratios for the sensitizer-containing samples. For the 0% PETA samples, however, p_0/q_0 increased from 0.496 to 0.731 as BQ concentration was increased from 0 ppm to 10,000 ppm, respectively. Since the effects of sensitizer composition on crosslinking have repeatedly been shown in this study to be much greater than those of inhibitor composition, it is not surprising that sensitizer composition is the dominant factor in determining p_0/q_0. However, when no sensitizer was present, the scission-to-crosslinking ratio increased by roughly 60% as BQ composition was increased from 0 ppm to 10,000 ppm. This trend is very interesting because it sheds light onto the radiation crosslinking mechanism of this polymer system. Given that crosslinking and chain scission events are predicted to occur randomly during irradiation for the sensitizer-free samples (the randomness of the crosslinking events is evidenced by the data's high correlation to the linear fits in the Charlesby-Pinner plots, for which the R^2 values all approach 1.0), the reaction of benzoquinone with any reactive species generated during irradiation should occur in a random statistical distribution, with the highest number of reactions occurring for the most chemically favorable processes. Since benzoquinone is known to react preferentially with free radicals, if both the dominant scission and crosslinking events were to occur via free radical mechanisms, then p_0/q_0 should not be effected by inhibitor composition for a given polymer system because the inhibitor would react randomly with all radical species

106

generated, and the overall scission-to-crosslinking ratio would remain unchanged. The increase in p_0/q_0 with increased inhibitor is evidence that the benzoquinone is either acting as a chain scission agonist or a crosslinking antagonist in the sensitizer-free samples. The most likely explanation for this observed phenomenon is that the BQ is reacting with radicals randomly generated during irradiation that would otherwise contribute to crosslinking events. This explanation is consistent with our previously reported radiation crosslinking mechanism proposed in Scheme 4, and it is also consistent with other proposed free radical based radiation crosslinking mechanisms in the literature [50]. Of course, this postulation is based on the assumption that all free radical species have equal reactivities with benzoquinone, which is undoubtedly not the case. Furthermore, it is also possible that, instead of the dominant crosslinking events' occurring via a free radical mechanism, the chain scission events could result in the formation of free radicals at scission sites, and the inhibitor could be effectively preventing the chains from re-forming by inhibiting free radical recombination. Thus, although absolute conclusions about the radiation crosslinking mechanisms of this polymer system cannot be made based on this p_0/q_0 data alone, the data serves as further evidence of the validity of our working theory for the radiation crosslinking mechanism of this polymer system.

The DMA results in Figure 18 show the effects of (a) inhibitor composition, (b) radiation dose, and (c) sensitizer composition on rubbery modulus for various irradiated samples. In general, the relationships between rubbery modulus and inhibitor, dose, and sensitizer followed similar trends to those of the gel fraction data; however, increased

inhibitor composition did have more of a pronounced inhibitory effect on rubbery modulus. Figure 22(b) shows plots of average rubbery modulus versus inhibitor composition for 20% PETA samples irradiated at 50, 100, 150, and 200 kGy. From this figure, it is clear that dose had a more significant effect on rubbery modulus than did inhibitor composition; however, the effects of inhibitor on rubbery modulus are by no means negligible. In the case of the 100 kGy series in Figure 22(b), average rubbery modulus decreased from 12.1 to 6.7 MPa as inhibitor composition was increased from 0 ppm to 10,000 ppm BQ. It is not surprising that the presence of free radical inhibitor had a more pronounced effect on rubbery modulus than on gel fraction. Gel fraction is only a measure of the percentage of a polymer's chains that are incorporated into a crosslinked network, and samples with drastically different crosslink densities could both have identical gel fractions. Rubbery modulus, which is inversely proportional to the average molecular weight between crosslinks, is dependent on *how crosslinked* a polymer network is [39]. Thus, although the amounts of free radical inhibitor in this study may have not been significant enough to prevent networks from forming during irradiation, they were significant enough to lower the amount of radiation crosslinking that occurred in these networks. As Figure 22(b), indicates, however, the inhibitory effect of BQ on rubbery modulus could be circumvented by irradiating at higher doses. For example, a rubbery modulus of ~12.2 MPa could be achieved by irradiating the 0 ppm BQ sample at 150 kGy or by irradiating the 10,000 ppm BQ sample at 200 kGy. Thus, the data indicates that significant inhibitor can still be added to this SMP for

thermal stabilization without a significant inhibition of radiation crosslinking's

occurring.
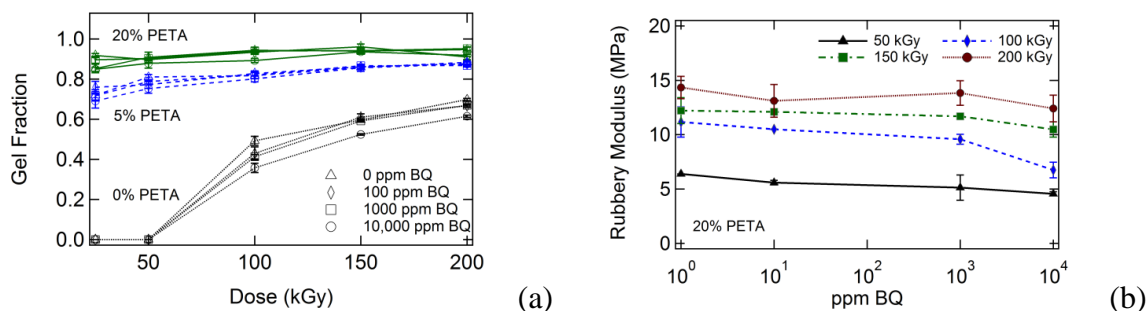
Figure 22- Comparative figures summarizing the effects of benzoquinone composition, dose, and PETA composition on (a) gel fraction and (b) rubbery modulus. Figure 22(a) shows that PETA composition and dose have much more significant impacts on gel fraction than benzoquinone composition. Figure 22(b) illustrates that PETA composition and dose have much more significant impacts on rubbery modulus than benzoquinone composition.

4.3 Thermal Stabilization Study

The DSC thermograms in Figure 19 show exotherm onset temperatures of

120°C, 131°C, and 142°C for 10% PETA thermoplastic samples containing 0, 1000, and

10,000 ppm BQ compositions, respectively. Although differential scanning calorimetry

in itself does not provide concrete evidence that these exotherms are attributed to

polymerization reactions in the sensitizer, DSC is commonly used in the literature for

cure studies of various polymer systems, including acrylic, vinyl, and epoxy systems [73].

In fact, because of its ease of use, DSC is often the preferred method for conducting cure

studies [45]. A heating rate of 20°C/min was used because faster heating rates better

mimic the heating conditions that a sample would experience during heating in an industrial processing machine such as an injection molder or extruder. The purpose of the DSC experiments was not to provide conclusive data about the stability of a given sample at a specific temperature, but to provide a general scientific backing for the results in the thermal conditioning studies.

In Figure 23, the results from the thermal conditioning studies are plotted in the form of zero gel fraction threshold plots. These plots show the conditions for which a sample of a given BQ composition can be subjected to elevated temperatures and still maintain a zero gel fraction (i.e., not undergo thermally-induced sensitizer crosslinking). In 23(a), the maximum times for each test temperature that still yielded zero gel fractions are plotted against inhibitor concentration, and in 8(b), maximum temperatures for each test time are plotted. For all data points in Figure 23, gel fraction equals 0, and non-zero gel fractions thus occurred for higher temperatures or longer heat exposure times for each BQ composition. Figure 23(a) indicates that gel fractions never occurred for any 5 min or 30 min samples exposed to any of the test temperatures. Figure 23(b) shows that zero gel fractions never occurred at any of the tested temperatures for the for the 5 h and 24 h samples containing less than 1000 ppm benzoquinone.

The summary data in Figure 23 quantifies the thermal stabilization effects of the benzoquinone inhibitor on the PETA sensitizer. In general, the presence of inhibitor increased both maximum allowable heat exposure times and maximum exposure temperatures. Consequently, it appears that benzoquinone may be useful in increasing

the maximum working times and working temperatures during thermal processing of this

sensitizer-containing SMP system.
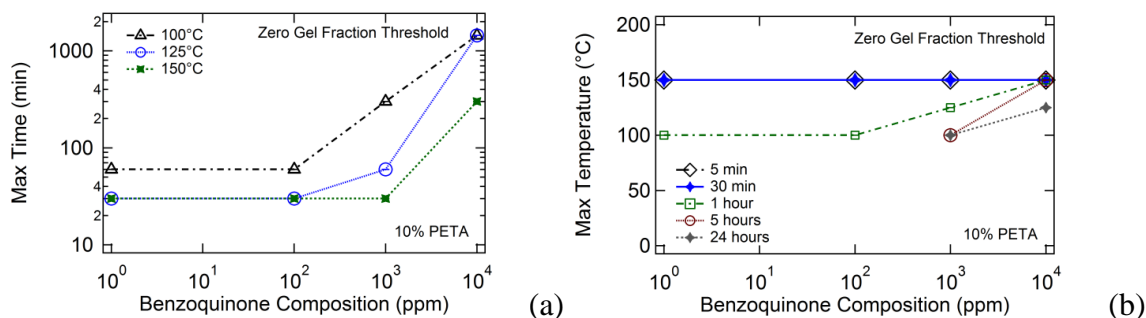
Figure 23- Summary figures showing zero gel fraction thresholds for 10% PETA samples containing varying benzoquinone compositions exposed to 100°C, 125°C, and 150°C temperatures for varying amounts of time. For all data points in Figure 23, gel fraction = 0, and the maximum temperatures or heat exposure times for each benzoquinone composition are reported (non-zero gel fractions thus occurred for higher temperatures or heat exposure times for each BQ composition).

E. Summary and Conclusions

As a result of this study, a potentially viable solution to the processing issue of

radiation sensitizer thermal instability for a potentially industrially relevant shape

memory polymer system has been reported. The effects of the free radical inhibitor 1,4-

benzoquinone on the radiation crosslinking and thermal stabilization of sensitizer-

containing polyurethane SMPs were quantified. PETA effectively sensitized the

radiation crosslinking of the 2-butene-1,4-diol-co-TMHDI polyurethane, and rubbery

moduli greater than 20 MPa, more than four times greater than our previously reported

E_r values, were achievable. DMA results showed that high rubbery modulus values (>

15 MPa) were achievable for samples containing as much as 10,000 ppm benzoquinone

111

inhibitor; consequently, BQ can be used without a significant tradeoff in maximum achievable mechanical properties occurring. Also, a Charlesby-Pinner analysis for irradiated samples containing varying inhibitor provided further evidence for the validity of our proposed radical graft polymerization-based crosslinking mechanism for this SMP system. Thermal stabilization studies showed that 1,4-benzoquinone was effective in stabilizing the PETA sensitizer at temperatures up to 150°C for up to 5 hours. Consequently, the addition of BQ to thermoplastic-sensitizer blends appears to be an effective means of increasing the maximum working time and maximum working temperature during processing at elevated temperatures.

Nonetheless, completely sensitizer-free electron beam crosslinkable PU SMP system is still desirable because such an SMP system is predicted to exhibit significantly better thermal processing stability than that of even the highest inhibitor-containing formulations reported in this study. In Chapter VI, the development of a sensitizer-free e-beam crosslinkable PU SMP system is reported.

F. Acknowledgements

provided by the National Science Foundation (NSF) Graduate Research Fellowship

Program (GRFP) fellowship.

CHAPTER VI

A SENSITIZER-FREE ELECTRON BEAM CROSSLINKABLE POLYURETHANE

SMP SYSTEM*

In Chapter III, a thermally crosslinkable PU SMP system is reported. While glass transitions in this SMP system are tunable in the range of 35 to 80°C, its industrial relevance may be limited because of the high temperatures required to achieve crosslinking and because of the limited control of crosslink density that is demonstrated. To enable crosslinking at ambient temperature of bulk thermoplastics after processing and to provide a wider range of control of crosslink density, an electron beam crosslinkable PU system was developed and is reported in Chapter IV. Although crosslink density is shown to be tunable from 1 to 40 MPa, this SMP system relies heavily on the addition of thermally unstable radiation sensitizer additives as a means of tuning crosslink density. To counteract the thermal instability of this sensitizer-based SMP system, the effects of free radical inhibitor addition on e-beam crosslinking and thermal stability are reported in Chapter V. In Chapter VI, the development of a sensitizer-free PU SMP system is reported in order to further improve industrial relevance.

A. Introduction and Literature Review

As discussed in Chapter III, the crosslinking of bulk thermoplastic polymers has been achieved in multiple polymeric systems using electron beam irradiation.[37] Two drawbacks often associated with e-beam crosslinkable thermoplastics are rheologically unfavorable high molecular weight requirements and the required addition of thermally unstable sensitizer additives to achieve desired crosslink densities. To improve the overall functional utility of e-beam crosslinkable polymers, it is desirable that crosslinking be achievable in lower molecular weight thermoplastics, that it be attainable without the use of sensitizer additives, and that it be a favorable enough process to afford highly crosslinked networks when desired. As discussed in Chapters IV and V, we have hypothesized that the e-beam crosslinking susceptibility of a thermoplastic polymer can be enhanced by the incorporation of specific structural motifs into the polymer repeat units, as shown in Scheme 5.[65] Although the PU SMPs in Chapter IV and V exhibit high e-beam crosslinking susceptibility in comparison with that of other thermoplastic polymers reported in the literature, acrylic sensitizer additives are still required to achieve desired tunability of crosslink density in these SMPs, with as much as 25 mole percent radiation sensitizer being required.[74] In this study, a structural approach to achieving tailorability of crosslink density in a new class of aliphatic, amorphous polyurethane SMPs that undergo e-beam crosslinking as low molecular weight thermoplastics without the use of radiation sensitizers is presented. As shown in Scheme 5, we hypothesize that e-beam crosslinking can be further enhanced by shifting the EWG-$CH_{2\alpha}$-C=C structural motifs from the polyurethane backbones to the polymer side

chains because of increased mobility of side chain e-beam induced α-carbamate radicals.

Since no alkene diol monomer capable of enabling an EWG-CH$_{2\alpha}$-C=C side chain motif

was found to be commercially available, a custom monomer, referred to as "DEA-diol"

in this study, is prepared from diethanolamine and allyl chloroformate using a one-pot

synthesis and subsequent purification. To compare the effects of side chain electron

withdrawing groups on e-beam crosslinking with those of side chain electron donating

groups on e-beam crosslinking, an analog is prepared from the commercially available

trimethylolpropane allyl ether (TMPAE) monomer. The radiation crosslinking

susceptibility of equivalent molecular weight DEA-diol, TMPAE, and 2-butene-1,4-diol

polymers are quantified using sol/gel analysis and dynamic mechanical analysis

experiments. The general structures of polymers based on these monomers are provided

in Table 7.   Other DEA-diol and TMPAE-based polymers with varying C=C content

and molecular weights are also synthesized, and the effects of radiation dose, molecular

weight, and side chain C=C composition on e-beam crosslinking are quantified using

subsequent sol/gel analysis and DMA experiments. The new SMPs were then subjected

to multi-temperature strain-to-failure experiments and shape memory characterization

experiments to determine tensile and shape memory properties.

Scheme 5- In this study, the approach is the synthesis of polyurethane shape memory polymers with EWG-CH2α-C=C structural motifs in the polymer side chains to enhance susceptibility to electron beam crosslinking and eliminate the need for sensitizer additives.

Previous Approach

E-beam induced alpha hydrogen abstraction and radical formation

Sensitizer additives required to achieve desired crosslink densities and resulting desired thermomechanical properties

Backbone Alpha Hydrogens with Adjacent Double Bond
(EWG-CH$_{2\alpha}$-C=C motifs)

Resonance stabilization of α-carbamate e-beam induced radicals enhances radiation crosslinking susceptibility.

New Approach (Custom Diol Monomer Synthesis Required)

+ regioisomers

Side Chain Allylic Group
(EWG-CH$_{2\alpha}$-C=C motifs)

Sensitizer-free tailorable e-beam crosslinking achieved by increasing mobility of EWG-CH$_{2\alpha}$-C=C motifs

B. Materials and Methods

In the study, the approach is the synthesis of polyurethane shape memory polymers with EWG-CH2α-C=C structural motifs in the polymer side chains to enhance susceptibility to electron beam crosslinking and eliminate the need for sensitizer additives.

1. Materials, Monomer and Polymer Synthesis and Sample Preparation

1.1 Materials

Hexamethylene diisocyanate (HDI), trimethylhexamethylene diisocyanate (TMHDI), 2-butene-1,4-diol (2-but), diethylene glycol (DEG), diethanolamine (DEA), 4-dimethylaminopyridine (DMAP), triethylamine (TEA) and zirconium (IV) acetylacetonate (Zr catalyst) were purchased from TCI America and used as received. Allyl chloroformate (ACF), allyl alcohol (AA), trimethylolpropane allyl ether (TMPAE), and 3-methyl-1,5-pentanediol (3-MPD), and 4 Å molecular sieve beads were purchased from Sigma Aldrich and used as received. Anhydrous dichloromethane (DCM) and tetrahydrofuran (THF) were purchased from BDH Chemicals and used as received.

1.2. One-Pot Synthesis of DEA-Diol Monomer from Diethanolamine and Allyl Chloroformate

Synthesis of the DEA-diol monomer from diethanolamine and allyl chloroformate is depicted in Scheme 6. Diethanolamine (0.476 mol), triethylamine (0.952 mol) , and dimethylaminopyridine (4.76 mmol) were dissolved in 1760 mL of anhydrous DCM at 25°C. The solution was then cooled to -20°C using a saturated NaCl water bath and stirred vigorously under a dry nitrogen atmosphere. Allyl chloroformate (0.571 mol) was then added dropwise over the course of 2 h. The final reaction mixture had a concentration of 0.11 g/mL in DCM. After 2 h, the solution temperature was allowed to equilibrate at 25°C and was allowed to stir under dry nitrogen for an

additional 6 h. Upon consumption of the starting material, the reaction was quenched by

adding the reaction mixture to 1000 mL of ice water. The aqueous layer was extracted

with 500 mL (2x) of DCM. The organic layers were combined and washed with aq. sat.

NaHCO$_3$, 0.5 M HCl and brine. The organic layer was then dried with MgSO$_4$, filtered,

and concentrated under reduced pressure. The resulting crude oil was purified by column

chromatography with 50% ethyl acetate/50% acetone as an eluent to afford the product

as a clear oil (84.4 g, 71% yield). ^{1}H NMR (CDCl$_3$, 500 MHz): δ 5.91-5.78 (dddd, 1H,

J = 16.9, 15.5, 5.4, 5.1), 5.25-5.18 (ddd, 1H, J = 17.2 Hz, 3.5, 1.5), 5.16-5.11 (ddd, 1H, J

= 10.5, 2.9, 1.5), 4.64 (s, br, 2H, OH) 4.52-4.49 (td, 2H, J = 5.5, 1.5), 3.69 (d, 4H, J =

4.3), 3.39 (t, 4H, J = 4.8) ppm. ^{13}C NMR (CDCl$_3$, 125 MHz): δ 156.6 (C=O), 132.6

(C=C), 117.54 (C=C), 66.2, 61.4, 61.1, 52.4, 51.9 ppm.

Scheme 6- One-step synthesis of DEA-diol monomer from diethanolamine (DEA) and allyl chloroformate (ACF).
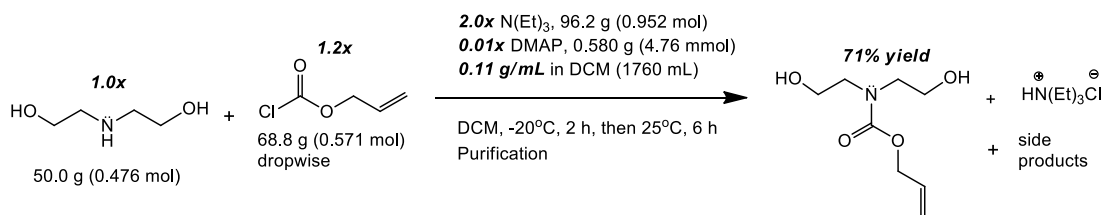
1.3. Thermoplastic Polyurethane Synthesis

All thermoplastic polyurethanes were synthesized in 33.0 vol % solutions in

anhydrous THF. All monomers, solvents, and catalysts were mixed to 100 g scale

reaction mixtures under dry air in a LabConco glove box. Using a 1.01:1.00 NCO:OH

ratio, all polymerization reaction products were mixed in the glove box in 225 mL glass

jars that were previously flame dried, after which the THF and Zr catalyst solution

(0.010 wt % catalyst) were added. After adding approximately 80 mL of 4 Å molecular

sieves to each polymerization mixture, the polymerizations were carried out in sealed

jars using a LabConco RapidVap instrument at 80 °C for 24 h at a vortex setting of 150

RPM. The RapidVap was used to heat and mix the monomer solutions. After 24h, the

viscous polymer solutions were filtered to remove molecular sieve dust using flash

chromatography and then decanted into 12" × 9" rectangular polypropylene (PP) dishes,

which were placed under vacuum at 80°C for 72 h to remove solvent.

1.4. Polymer Film Preparation and Irradiation

To prepare films suitable for DMA and tensile testing experiments, 2" × 5" × 0.4

mm thick films were prepared by dissolving approximately 5 grams of each

thermoplastic polymer into 40 mL of THF. The polymer solutions were then re-

decanted into polypropylene 2" × 5" × 2" polypropylene dishes purchased from

McMaster Carr. The THF was allowed to evaporate at ambient pressure at 50°C for 24 h

and then at 80°C for an additional 24 h using a vacuum oven. The samples were then

evacuated at 80°C at 1 torr for an additional 24 h and then stored under desiccation until

irradiation. The thermoplastic films were irradiated doses varying between 1 and 500

kGy using a 10 MeV electron accelerator located at the Texas A&M University National

Center for Electron Beam Research (NCEBR). The dose range of 1-500 kGy was

selected because numerous previous studies have demonstrated successful electron beam

crosslinking of various polymer systems over this dose range, including our own

previous studies. The irradiations were carried out at 40°C (reported by NCEBR staff)

on a conveyor belt, and doses were delivered in 50 kGy/pass increments. Doses were

measured using alanine strips, and the uncertainty of dose to product was reported by the

NCEBR operators to be 5%. After irradiation, all samples were post-cured at 80°C at 1

torr for 24 h.

1.5. Nuclear Magnetic Resonance Spectroscopy

^{1}H NMR and ^{13}C NMR spectra were recorded on a Varian Inova 500

spectrometer. Chemical shifts were referenced to the solvent resonance signals.

1.6. Molecular Weight Characterization

Gel permeation chromatography (GPC) was performed on a Waters

Chromatography, Inc., 1515 isocratic HPLC pump equipped with an inline degasser, a

model PD2020 dual angle (15° and 90°), a model 2414 differential refractometer

(Waters, Inc.), and four PLgel polystyrene-co-divinylbenzene gel columns (Polymer

Laboratories, Inc.) connected in series: 5 μm Guard (50×7.5 mm), 5 μm MixedC

(300×7.5mm), 5 μm 104 (300×7.5mm), and 5 μm 500Å (300×7.5mm) using the Breeze

(version 3.30, Waters, Inc.) software. The instrument was operated at 35 °C with THF as

eluent (flow rate set to 1.0 mL/min). Data collection was performed with Precision

Acquire 32 Acquisition program (Precision Detectors, Inc.) and analyses were carried

out using Discovery32 software (Precision Detectors, Inc.). A system calibration curve

generated from plotting molecular weight as a function of retention time for a series of

broad polydispersity poly(styrene) standards was used to determine the molecular weight values of polycarbonates, and the value was determined using dn/dc values that were calculated for each sample.

2. Materials Characterization

2.1. Sol/Gel Analyis

After irradiation and post-curing, dry 50 mg samples irradiated at varying doses and comprised of varying monomer combinations were massed in triplicate and placed in 20 mL glass vials, after which THF was added in approximately a 150:1 solvent:polymer mass ratios. The vials were capped and vortexed at 50 RPM at 50°C for 48 h using a LabConco RapidVap instrument. After 48 h, the solvent swollen polymer samples were removed from the THF/sol fraction solutions and placed in new 20 mL glass vials, dried at 80 C for an additional 48 h at 1 torr, and then re-massed to provide sufficient mass data to determine the gel fractions of each irradiated sample.

2.2. Dynamic Mechanical Analysis

4 mm x 30 mm x 0.4 mm rectangular DMA samples were machined using a Gravograph LS100 40 W CO_2 laser machining device. All laser machined samples were sanded around the edges using 400, then 800, then 1200 grit sandpaper. DMA was performed using a TA Instruments Q800 Dynamic Mechanical Analyzer in the DMA Multifrequency/Strain mode in tension using a deformation of 0.1% strain, a frequency

of 1 Hz, a force track of 150%, and a preload force of 0.01 N. Each experiment was run

from -20 to 140°C using a heating rate of 2°C/min.

2.3. Differential Scanning Calorimetry

Differential scanning calorimetry (DSC) experiments were run using a TA

Instruments Q200 differential scanning calorimeter on 5-10 mg samples. Two-cycle

heat-cool-heat experiments were run from 0 to 150°C using a heating and cooling rate of

20°C/min. In between heating and cooling cycles, the samples were held isothermally at

0 or 150°C for 2 min. Only the second-cycle heating data is shown in this publication.

2.4. Uniaxial Tensile Testing

ASTM Type V dog bone samples were machined using a Gravograph LS100 40

W CO_2 laser machining device. All laser machined samples were sanded around the

edges using 400, then 800, then 1200 grit sandpaper. Strain-to-failure experiments were

conducted on select samples (n $\geq$ 5) using an Instron Model 5965 electromechanical,

screw driven test frame, which was equipped with a 500 N load cell, 1 kN high

temperature pneumatic grips, and a temperature chamber that utilizes forced convection

heating. An Instron Advanced Video Extensometer with a 60 mm field-of-view lens

was used to optically measure the deformation of the samples by tracking parallel lines

applied at the ends of the gauge length. The samples were heated to varying desired

temperatures under zero load (unclamped bottom grip). The temperature was held at the

desired temperature for 30 minutes to allow for thermal equilibrium to be reached, after

which the bottom grip was clamped, and then experiments were started thereafter using a deformation rate of 10 mm/min. Data were recorded using Instron Bluehill 3 software.

2.5. Shape Memory Characterization

Shape memory characterization experiments were performed using a TA Instruments 800 Dynamic Mechanical Analyzer on the same size 4 mm × 30 mm × 0.4 mm rectangular specimens used for the DMA experiments for select samples. In the DMA Strain Rate Mode in tension, the rectangular specimens were heated to $T_g + 25°C$ (glass transitions were determined by the peak of the tangent deltas from the previous DMA results), allowed to equilibrate for 30 min, and then strained to deformations of 25% or 50%. The strained samples were then cooled to 0°C and allowed to equilibrate for an additional 30 min. For constrained recovery experiments, which were used to measure the recovery stress of the materials, the drive force of the DMA instrument was maintained to fix 25% strain, and the samples were heated to 120°C at 2°C/min. For free strain recovery experiments, which were used to measure percent recoverable strain, the drive force was set to zero after equilibration at 0°C, after which 50% prestrained samples were re-heated to 80°C at 2°C/min as recoverable strain was measured, and upon reaching 80°C, the samples were cooled back to $T = T_g + 25°C$, and four more free strain recovery cycles were subsequently carried out to afford a five-cycle experiment. Percent recoverable deformation was recorded using TA Instruments QSeries software.

C. Results and Discussion

The objective of this study is the development of a low-molecular weight thermoplastic polyurethane shape memory polymer system that can be crosslinked to tailorable crosslink densities while in the bulk state using electron beam irradiation without the use of radiation sensitizer additives. Such an SMP system is desirable because the combined processability of a thermoplastic SMP and thermomechanical tailorability of a thermoset SMP results in a highly versatile SMP system with a potentially broad application range.   To accomplish this objective, a new custom diol monomer predicted to be highly favorable for electron beam crosslinking was synthesized, and the radiation crosslinking susceptibility of polyurethanes prepared from this monomer was quantified and compared to that of polyurethanes made from two other commercially available diol monomers.

1. Molecular Weight Characterization Results and Discussion

The GPC results for all samples synthesized in this study are provided in Table 7. The objective in synthesizing these samples was to quantify the effects of varying chemistry adjacent to C=C motifs, as well as varying dose, molecular weight, and C=C composition on electron beam crosslinking of sensitizer-free polyurethane shape memory polymer samples in order to work towards establishing a platform chemistry to enable facile, tunable, bulk crosslinking of polyurethane shape memory polymers. Since molecular weight has been shown to significantly influence the susceptibility of a polymer to electron beam crosslinking,[55] it was important that equivalent molecular

125

weight samples for DEA-diol, TMPAE, and 2-butene-1,4-diol containing samples be synthesized so that the effects of the adjacent C=C chemistry on e-beam crosslinking could be accurately evaluated. After the series of polymers containing varying DEA-diol composition was synthesized and the M_w of the DEA-1.0 sample was determined to be ~21.5 kDa, the syntheses of TMPAE and 2-butene-1,4-diol based polymers of similar molecular weights were attempted. To accomplish this objective, varying amounts of the capping agent allyl alcohol (AA) were added to the polymerization mixtures of TMPAE and 2-but based polymers to control molecular weight. Allyl alcohol was selected for the purpose of creating polymer chain ends with the potential for incorporation into the crosslinked networks after irradiation to minimize the number of dangling chain ends and maximize toughness.[75] For TMPAE-based polymers, molecular weight decreased from ~215 to ~24 kDa as AA composition increased from 1 to 10 mole %. For 2-butene-1,4-diol based polymers, which have been the focus of multiple previous studies, the 5% AA formulation has been previously shown to give an M_w in the range of 20-25 kDa, and the 2-butene-1,4-diol based polymer synthesized in this study was determined to have an M_w of roughly 25.7 kDa.

Table 7- Compositions and GPC data for all samples synthesized.

(a) Formulations prepared for achieving tailorable crosslink densities

Varying DEA-diol	Eq. TMHDI	Eq. DEA-Diol	Eq. DEG	Eq. AA	M_n	M_w	PDI
DEA-0	1.01	0.00	1.00	0.00	2.7	5	1.57
DEA-0.1	1.01	0.10	0.90	0.00	2.5	5.2	2.06
DEA-0.5	1.01	0.50	0.50	0.00	3.6	13.5	3.73
DEA-1.0	1.01	1.00	0.00	0.00	3.9	21.5	5.48
Varying TMPAE	Eq. TMHDI	Eq. TMPAE	Eq. 3-MPD	Eq. AA	M_n	M_w	PDI
TMPAE-0.1	1.01	0.10	0.89	0.01	15	26.9	1.79
TMPAE-0.2	1.01	0.20	0.79	0.01	17.2	30.7	1.79
TMPAE-0.3	1.01	0.30	0.69	0.01	1.9	5.2	2.78
TMPAE-0.5	1.01	0.50	0.49	0.01	1.3	3.7	2.81
TMPAE-0.7	1.01	0.70	0.29	0.01	1.1	3.5	3.01
TMPAE-0.9	1.01	0.90	0.09	0.01	2.8	9.5	2.69
Varying AA	Eq. HDI	Eq. TMPAE	Eq. Diol	Eq. AA	M_n	M_w	PDI
AA-0.01	1.01	0.99	0.00	0.01	73.3	215	3.07
AA-0.03	1.01	0.97	0.00	0.03	38.2	76	1.99
AA-0.05	1.01	0.95	0.00	0.05	26.7	45.9	1.719
AA-0.10	1.01	0.90	0.00	0.10	15.3	24.2	1.587
2-but-co-TMHDI	Eq. TMHDI	Eq. 2-but	Eq. Diol	Eq. AA	M_n	M_w	PDI
2-but-0.95	1.01	0.95	0.00	0.05	9.1	25.7	2.82
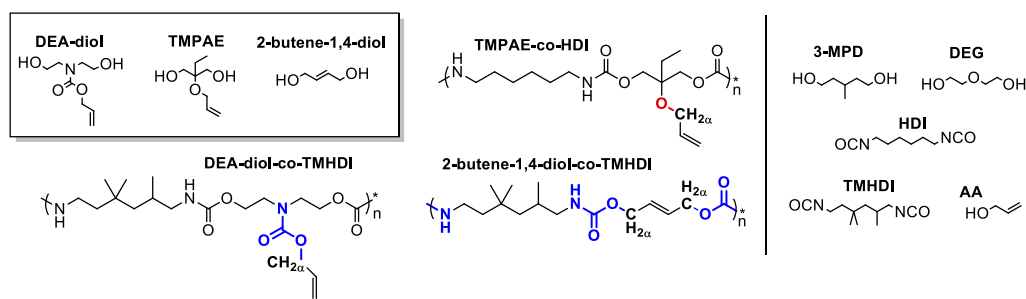
Table 7 Continued

(b) Formulations prepared for manipulating glass transitions

Diol Structure	Identity	Eq. TMHDI	Eq. TMPAE	Eq. Diol	Eq. 2x AA	M_n (kDa)	M_w (kDa)	PDI
HO~O~OH	DEG-0.9	1.020	0.100	0.900	0.010	16.3	38.7	2.37
HO~~OH	1,4-BD-0.9	1.020	0.100	0.900	0.010	11.5	28.6	2.49
HO~OH	2-MPD-0.9	1.020	0.100	0.900	0.010	18.7	57.3	3.06
HO~OH	2,2-DMPD-0.9	1.020	0.100	0.900	0.010			
HO~OH	1,3-PrD-0.9	1.020	0.100	0.900	0.010			
HO~OH	2,5-HD-0.9	1.020	0.100	0.900	0.010	16.4	38.6	2.35
HO~OH	1,3-BD-0.9	1.020	0.100	0.900	0.010	17.0	41.4	2.44
HO~~OH	3-MPD-0.9	1.020	0.100	0.900	0.010			
HO~OH	2,2-DEPD-0.9	1.020	0.100	0.900	0.010			
HO~OH	2B,2E-PD-0.9	1.020	0.100	0.900	0.010			
OH~OH	2,3-BD-0.9	1.020	0.100	0.900	0.010			
HO~OH	TCD-0.9	1.020	0.100	0.900	0.010	11.8	31.2	2.64
HO~OH	CHDM-0.9	1.020	0.100	0.900	0.010	18.7	57.3	3.06
HO~~~~OH	1,8-oct-0.5	1.020	0.500	0.500	0.010			
HO~~~~~OH	1,10-dec-0.3	1.020	0.700	0.300	0.100			

Diisocyanate Structure	Identity	Eq. DCHMDI	Eq. HDI	Eq. TMPAE	Eq. 2x AA	Mn (kDa)	Mw (kDa)	PDI
OCN—cyclohexyl-CH2-cyclohexyl—NCO	DCHMDI-0.0	0.00	1.02	1.00	0.01	21.2	65.4	3.08
	DCHMDI-0.1	0.10	0.92	1.00	0.01	10.0	20.6	2.06
OCN~~~NCO	DCHMDI-0.5	0.50	0.52	1.00	0.01	5.5	11.0	2.00
	DCHMDI-1.0	1.00	0.02	1.00	0.01	5.4	9.7	1.80

2. Results and Discussion for Synthetic Objective of Achieving Control of Crosslink

Density

2.1. Sol/Gel Analysis Results and Discussion

The susceptibility of the polymers in Table 7 to electron beam crosslinking was

quantified using sol/gel analysis and dynamic mechanical analysis. The random

radiation crosslinking of thermoplastic polymers is described by the classical Charlesby-

Pinner equation, as discussed in Chapter III. E-beam irradiation causes both random

chain scission and random inter-chain bond formation (*i.e.*, crosslinking), and the

calculated parameter d_0, the minimum dose to gelation, represents the theoretical dose

required to achieve crosslinking in 1% of a polymer's chains.[48] A polymer that is

highly susceptible to electron beam crosslinking has a low d_0, while a polymer that is not

favorable for electron beam crosslinking has a high d_0. D_0 has been shown in previous

studies to decrease with increasing molecular weight,[55, 74] and one of the objectives in

this study is to determine the extent to which d_0 is dependent on adjacent C=C chemistry

(*i.e.*, backbone *vs*. side chain C=C position and adjacent C=C EWG's *vs*. adjacent C=C

EDG's).

Sol/gel analysis plots of gel fraction *versus* dose for the irradiated polymer

samples in Table 7 are provided in Figure 24(a), (c), and (e), Charlesby-Pinner analysis

plots of $s + s^{1/2}$ *versus* $1/d$ for each respective gel fraction plot are provided in Figure

24(b), (d), and (f), and calculated Charleby-Pinner parameters are provided in Table 8.

Figure 24(a) and 24(b) demonstrate that, for polymer samples with M_w's in the range of

20-25 kDa, DEA-diol-based polymers are the most susceptible to e-beam crosslinking, TMPAE-based polymers are the second-most susceptible, and 2-butene-1,4-diol polymers are the least susceptible. The calculated d_0 values provided in Table 8 profoundly demonstrate the differences in e-beam crosslinking susceptibility for these polymers. D_0 increases roughly an order of magnitude, from 0.88 to 10.91 to 106.73 kGy, as the polymer repeat unit chemistry changes from side chain EWG-$CH_{2\alpha}$-C=C (DEA-diol) to side chain EDG-$CH_{2\alpha}$-C=C (TMPAE) to backbone EWG-$CH_{2\alpha}$-C=C (2-butene-1,4-diol) chemistry. The linearity of the Charlesby-Pinner plots in Figure 24(b) is greatest for 2-butene-1,4-diol, second greatest for TMPAE, and lowest for DEA-diol polymers, as indicated by the R^2 values in Table 8, which decrease from 0.896 to 0.639 to 0.490, respectively. Deviation from linearity in a Charlesby-Pinner plot indicates that crosslinking events are occurring in a less random and more directed manner, and previous studies have shown that adding sensitizer to thermoplastic polymer blends results in deviations from linearity that are similar to those observed in Table 8.[56, 74] In this study, the DEA-diol chemistry (and to a lesser degree the TMPAE and 2-butene-1,4-diol chemistries) effectively act as in-chain sensitizers. The gel fraction *versus* dose trends in Figure 24(c) and (d) show that radiation crosslinking susceptibility increases with increasing C=C composition for DEA-diol co-polymers, and the gel fraction versus dose trends in Figure 24(e) and (f) show that radiation crosslinking susceptibility increases with increasing M_w for TMPAE copolymers. Both these results are consistent with those for 2-butene-1,4-diol based copolymers reported in previous studies.
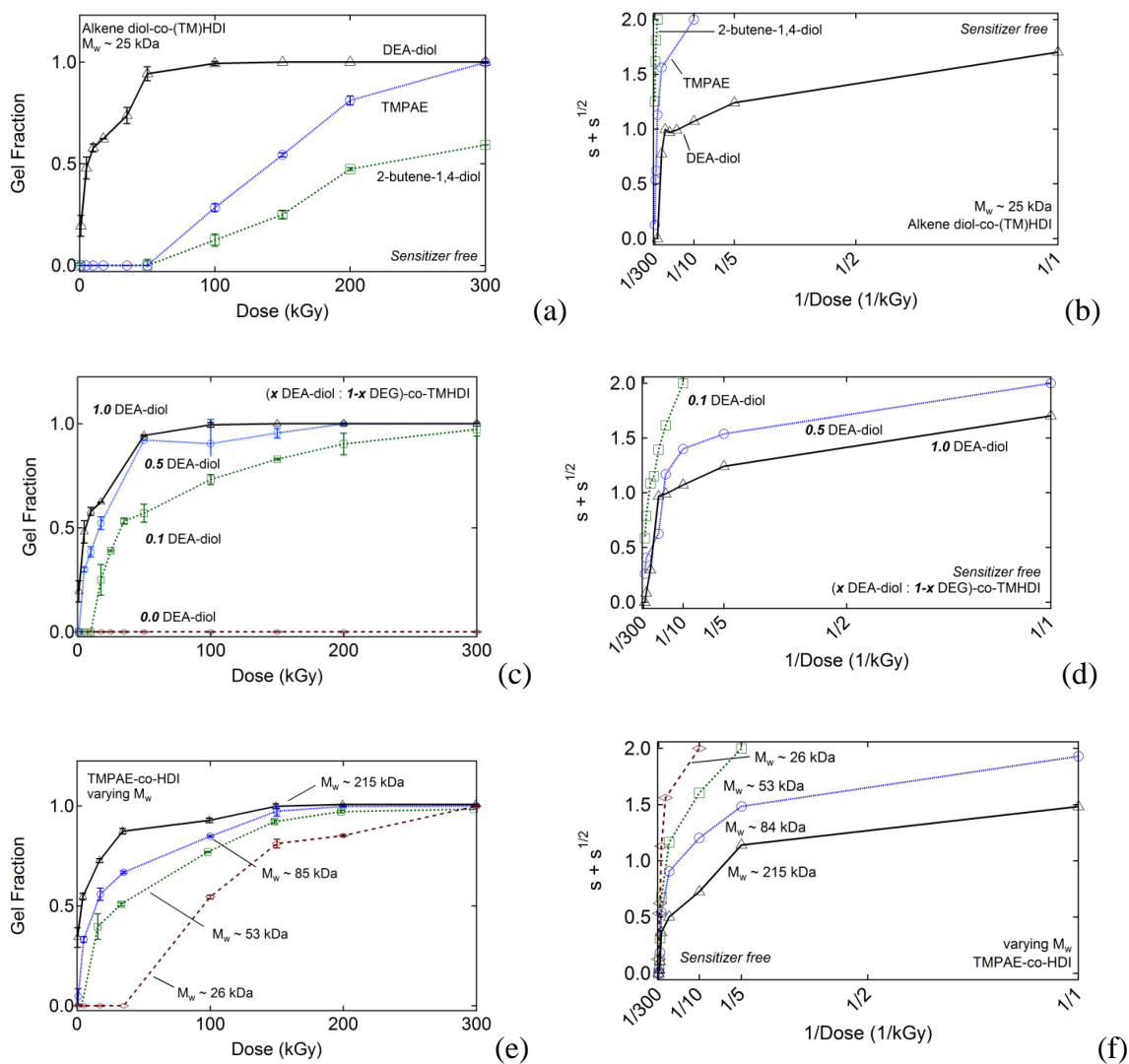
Figure 24- **(a) plots of gel fraction versus dose as determined by sol/gel analysis for polyurethane samples with M_w's of approximately 25 kDa: DEA-diol-co-TMHDI (-EWG-CH$_{2\alpha}$-C=C motif in polymer side chain), TMPAE-co-HDI (-EDG-CH$_{2\alpha}$ -C=C motif in polymer side chain), and 2-but-co-TMHDI (-EWG-CH$_{2\alpha}$ -C=C motif in polymer backbone). Structures of each polymer repeat unit are provided. (b) Charlesby-Pinner analysis plots of s + s$^{1/2}$ versus 1/dose for the gel fraction data in (a), where *s* is sol fraction; (c) plots of gel fraction versus dose for samples containing varying DEA-diol composition; (d) Charlesby-Pinner analysis plots of s + s$^{1/2}$ versus 1/dose for the gel fraction data in (c); (e) plots of gel fraction versus dose for TMPAE-co-HDI samples with varying molecular weight; (f) Charlesby-Pinner analysis plots of s + s$^{1/2}$ versus 1/dose for the gel fraction data in (e).**

131

Table 8- Charlesby-Pinner parameters calculated for irradiated PU's made from varying alkene diols, varying alkene diol composition, and vaying molecular weight

Description	Identity	d_0	p_0/q_0	R^2
Varying C=C Composition	DEA-0.10	10.96	0.695	0.929
	DEA-0.50	1.13	0.709	0.709
	DEA-1.00	0.88	0.620	0.466
Varying M_w	AA-0.10	10.92	0.635	0.639
	AA-0.05	5.68	0.373	0.373
	AA-0.03	1.08	0.516	0.588
	AA-0.01	0.77	0.324	0.324
Varying C=C Adjacent Chemistry	2-but-0.95 (2-but)	106.73	1.000	0.896
	AA-0.10 (TMPAE)	10.91	0.630	0.639
	DEA-1.00 (DEA-diol)	0.88	0.640	0.490

2.2. Dynamic Mechanical Analysis Results and Discussion

Figure 25(a) and (b) show plots of storage modulus and tangent delta, respectively, versus temperature for the $M_w \sim$ 20-25 kDa DEA-diol, TMPAE, and 2-but samples irradiated at 100 kGy. Rubbery modulus, E_r, defined by the equation of an ideal rubber to be inversely proportional to the average molecular weight between crosslink sites, is greatest for DEA-diol polymer (~15 MPa) and significantly lower for TMPAE polymer (~0.5 MPa).[18, 76] The 2-butene-1,4-diol polymer does not have a rubbery plateau regime after irradiation at 100 kGy and, therefore, does not exhibit thermomechanical behavior characteristic of that of a covalently crosslinked polymer (*i.e.*, a glassy modulus plateau at temperatures below its glass transition, a transition region in which modulus decreases with increasing temperature, and a rubbery plateau

132

region in which modulus increases linearly with increasing temperature).[77] When the d_0

values in Table 8 are combined with the storage modulus data in Figure 25(a), the

calculated order-of-magnitude variations appear consistent with the observed DMA data.

The 2-butene-1,4-diol sample was determined to have a d_0 of 106.73 kGy, which

indicates that, upon irradiation at 106.73 kGy, roughly 1% of this polymer's chains

should be incorporated into a network. The lack of a rubbery plateau modulus altogether

for this sample in Figure 25(a), which shows plots of storage modulus versus

temperature for samples irradiated at 100 kGy, is consistent with a d_0 of 106.73 kGy.

The significant increases in rubbery modulus for TMPAE and then for DEA-diol

samples, respectively also support the calculated d_0 values for these samples in Table 8.

DSC results for these three polymers are also provided in Figure 25(**c**) and indicate that

all three samples are amorphous.
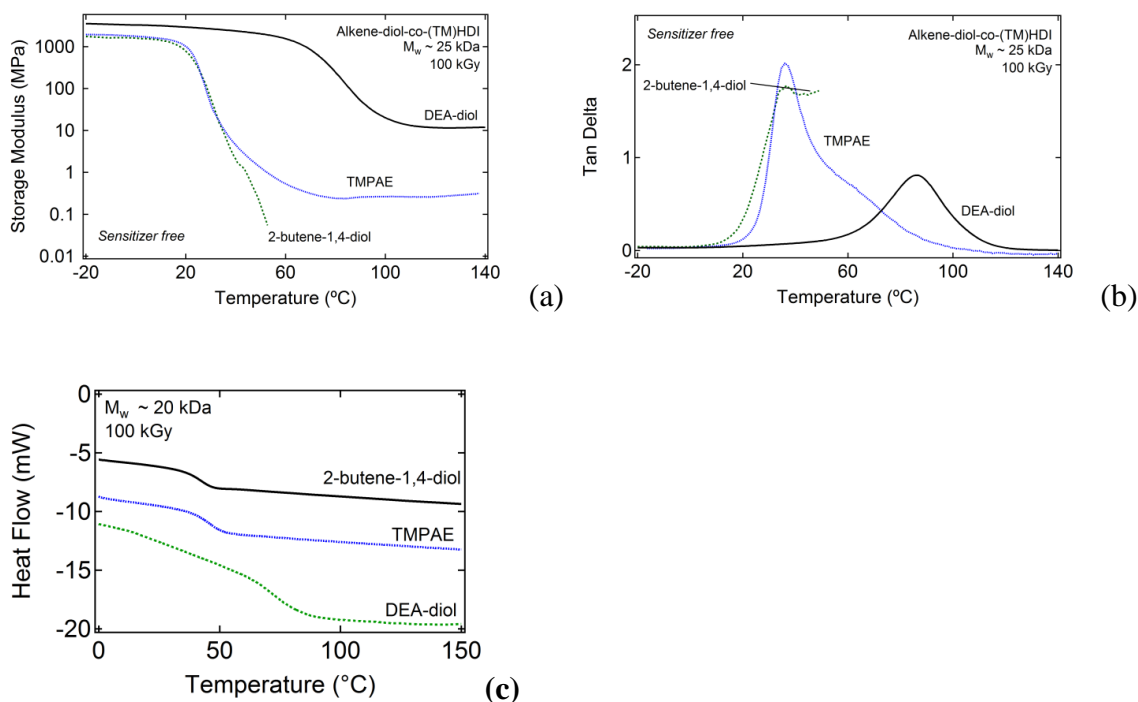
Figure 25- Plots of (a) storage modulus and (b) tangent delta versus temperature as determined by DMA for polyurethane samples with Mw's of approximately 25 kDa irradiated at 100 kGy: DEA-diol-co-TMHDI,TMPAE-co-HDI and 2-but-co-TMHDI (c) DSC thermograms for the same 2-but, TMPAE, and DEA-diol samples

Figure 26(a) and (b) demonstrate that crosslink density increases with increasing dose and increasing C=C composition, respectively, for DEA-diol based polymers. Figure 26(a) shows that increasing the dose for the DEA-0.5 sample from 25 to 100 kGy results in an increase in rubbery modulus from ~0.9 to ~10.1 MPa. Figure 26(b) shows that increasing DEA-diol composition from 0.1 diol mole fraction to 1.0 diol mole fraction results in an increase in rubbery modulus from ~0.4 to 15 MPa for samples irradiated at 100 kGy. Similar trends are shown for TMPAE-based polymers in Figure 27.

134
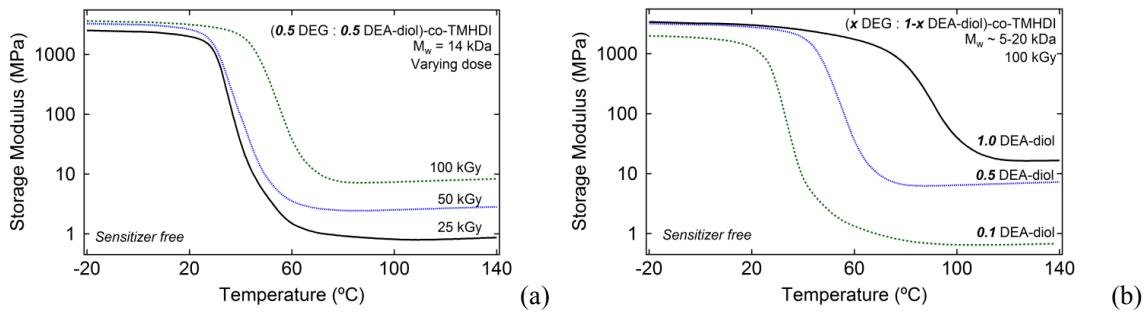
Figure 26- DMA results tailoring rubbery modulus, DEA-diol: (a) varying dose; (b) varying DEA-diol composition
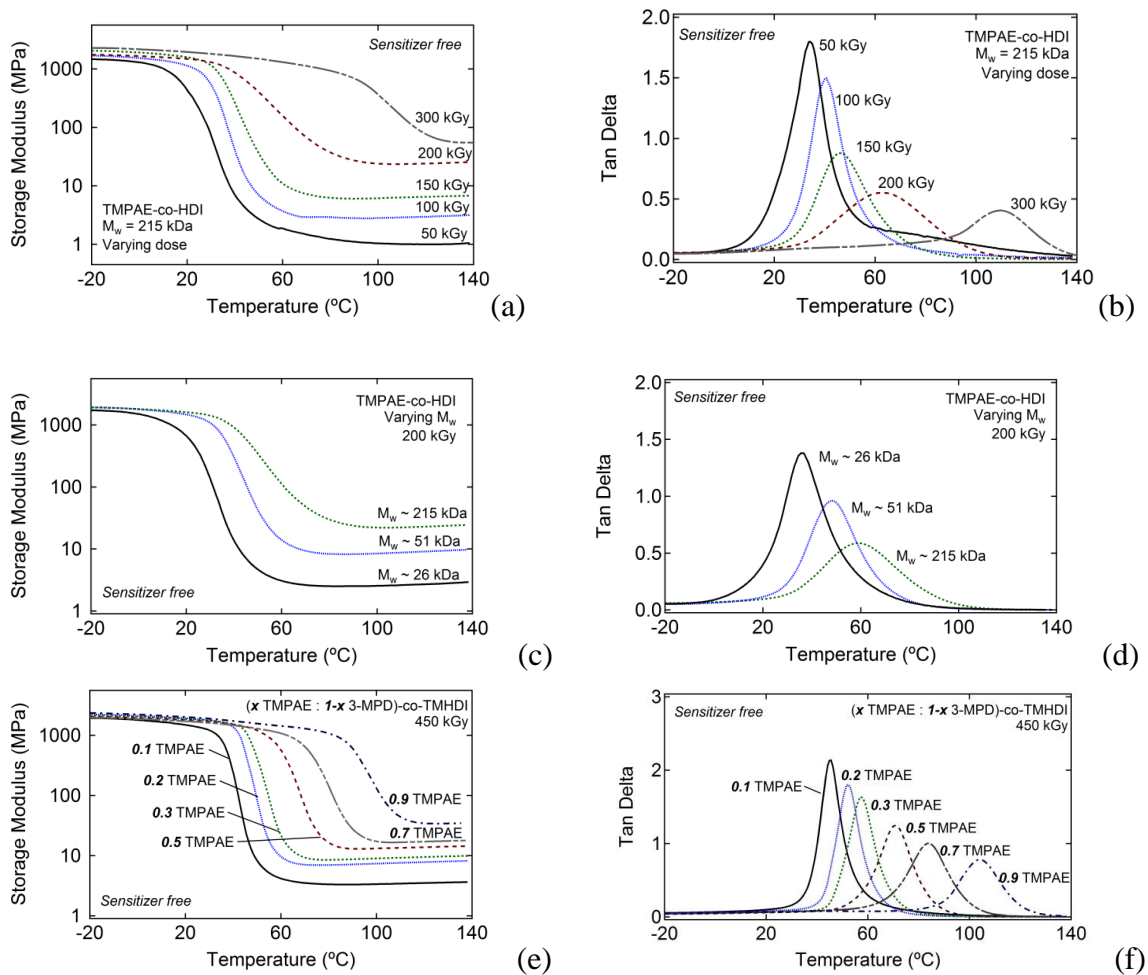
Figure 27- Storage modulus and corresponding tan delta plots for TMPAE-containing samples that demonstrate that crosslink density can be moved over a significant range by varying dose (a-b), molecular weight (c-d), side chain C=C composition (e-f)

For all three series, T_g breadth generally increases with increasing rubbery modulus, although several points should be noted. First, for the varying TMPAE series, T_g breadth only varies over a FWHM range of 10 to 19°C, while that of the varying dose and varying M_w series varies over larger ranges of 16 to 43°C and 21 to 39°C, respectively. One possible explanation for this behavior is that, since both the varying dose and varying molecular weight series are comprised of 1.0 TMPAE diol fractions and possess a maximum number of crosslinking sites for this SMP system, the materials in these series may be able to undergo crosslinking at lower irradiation doses given their high TMPAE composition, while the materials in the varying TMPAE series, which possess fewer crosslinking sites and have lower molecular weights in most cases, must be subjected to higher doses to enable crosslinking. It is possible that irradiation at high doses (450 kGy) in the varying TMPAE series results in a high percentage of the TMPAE crosslinking sites' undergoing crosslinking and affords networks with high degrees of homogeneity. If this same reasoning is applied to the varying dose and varying M_w series, the argument could be made that the materials in this series are susceptible enough to e-beam crosslinking such that some, but not all, of their crosslinking sites undergo e-beam crosslinking, and this "partial" crosslinking could increase network heterogeneity and broaden glass transitions. This argument is supported by the fact that the T_g breadth of the varying dose series decreases from 43 to 30°C as dose increases from 200 to 300 kGy, even though rubbery modulus also increases from 23.4 to 54.5 MPa. A key concept to take away from the glass transition breadth trends shown in Figure 28 is that, if a specific rubbery modulus value is

136

desirable for an SMP from this series, although multiple methods of achieving this rubbery modulus value may be viable, it appears that keeping TMPAE (or an alternative C=C containing monomer) functionality to a minimum value and irradiating at sufficient dose to cause the majority of the crosslinkable sites to become incorporated in the polymer network may be the best synthetic approach to achieving narrow glass transitions. Figure 28(b), which shows plots of storage modulus and tan delta versus temperature for a 1.0 TMPAE sample irradiated at 150 kGy (Point 1 in 28(a)) and a 0.2 TMPAE sample irradiated at 450 kGy (Point 2 in 28(a)), illustrates this concept. While both samples exhibit rubbery moduli of approximately 6.5 MPa, the T_g FWHM value for the 1.0 TMPAE, 150 kGy sample is 25°C, while that of the 0.2 TMPAE, 50 kGy sample is 10°C.
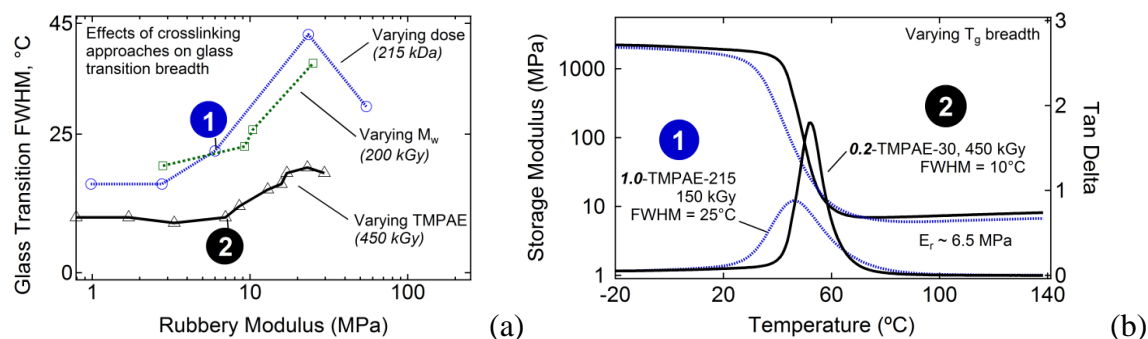
Figure 28- (a) Plots of glass transition breadth as determined by tangent delta full width half maximum values (FWHM) versus rubbery modulus for the three series of samples shown in Figure 27, in which crosslink density is controlled by varying dose, varying molecular weight and varying TMPAE composition; (b) plots of storage modulus and tan delta versus temperature corresponding to points 1 and 2 in Figure 28(a), which show near equivalent rubbery modulus values of ~6.5 MPa but glass transition FWHM breadths of approximately 25°C for composition 1 and 10°C for composition 2.

137

3. Results and Discussion for Synthetic Objective of Achieving Tailorable Glass Transitions

Control of glass transition was attempted using two synthetic approaches: (1) varying diol co-monomer chemistry in thermoplastics comprised of *0.1* : *0.9* TMPAE : diol ratio and equivalent diisocyanates composition and (2) varying DCHMDI : HDI diisocyanate co-monomer ratio in thermoplastics with equivalent diol composition. While both approaches resulted in tunable glass transitions in the range of approximately 40 to 80°C, the varying diol approach resulted in significantly sharper glass transitions and consequently appears to be the preferred method of tuning glass transition.

3.1 Moving T_g by Varying Aliphatic Diol Co-Monomer Chemistry

The first approach to controlling glass transition constituted varying diol co-monomer composition for thermoplastics comprised of low C=C diol monomer composition (0.10 TMPAE, 0.90 diol), as shown in Table 7. Instead of selecting a "high-T_g and "Low-T_g" diol and moving glass transition by blending such diols in varying ratios, the 0.10 TMPAE : 0.90 diol varying T_g series was formulated to provide increased network homogeneity and more narrow glass transition breadths. Figure 29(a) and 29(b) contain storage modulus and tangent delta versus temperature plots, respectively, and show a T_g range of approximately 39 to 79°C and a roughly constant rubbery modulus of approximately 3.0 MPa for all samples. The 39°C T_g was observed for the 3-methyl pentanediol (3-MPD) co-monomer, and the 79°C T_g was observed for the tricyclo[5.2.1.0^{2,6}]decane-4,8-dimethanol (TCD) co-monomer. T_g breadths were

138

very narrow in this series and ranged from 9°C to 12°C (tangent delta full width half maximum, FWHM). This observed sharpness in glass transition breadth indicates that the synthetic strategy of varying T_g by changing the entire diol co-monomer compositions was effective and resulted in high network homogeneity.

3.2 Moving T_g By Varying Diisocyanate Co-Monomer Chemistry

To provide a second manner of tailoring glass transition, a series of thermoplastics was prepared from 0.9 TMPAE and varying ratios of HDI and DCHMDI diisocyanate co-monomers. As the DMA data in Figure 29(c) and 29(d) show, as DCHMDI composition is increased from 0.0 to 1.0, T_g increases from 46 to 75°C, and rubbery modulus for this SMP series remains roughly constant, in the range of 3.5 MPa. T_g breadth ranges from 19 to 32°C and is greatest for the 0.5 HDI : 0.5 DCHMDI composition, which is comprised of the most heterogeneous formulation.

3.3 Achieving Independent Control of Rubbery Modulus with Respect to T_g

After extensive DMA characterization, select formulations were shown to exhibit thermomechanical behavior representative of independent control of crosslink density with respect to T_g. Plots of storage modulus and tangent delta versus temperature are provided in Figure 29(e) and 29(f) for one such series of formulations, which exhibit rubbery moduli ranging from 1.2 to 15.8 MPa and equivalent glass transitions of approximately 70°C. The SMPs whose DMA data are shown in Figure 29(e) and 29(f) are predicted based on this observed thermomechanical behavior to exhibit equivalent

actuation temperature and varying recovery stresses when subject to equivalent prestrains. When combined with the independent control of T_g with respect to crosslink density that is shown for the SMPs in Figure 29(a)-29(d), this overall independent control of actuation temperature and recovery stress constitutes the thermomechanical behavior of a true SMP system.
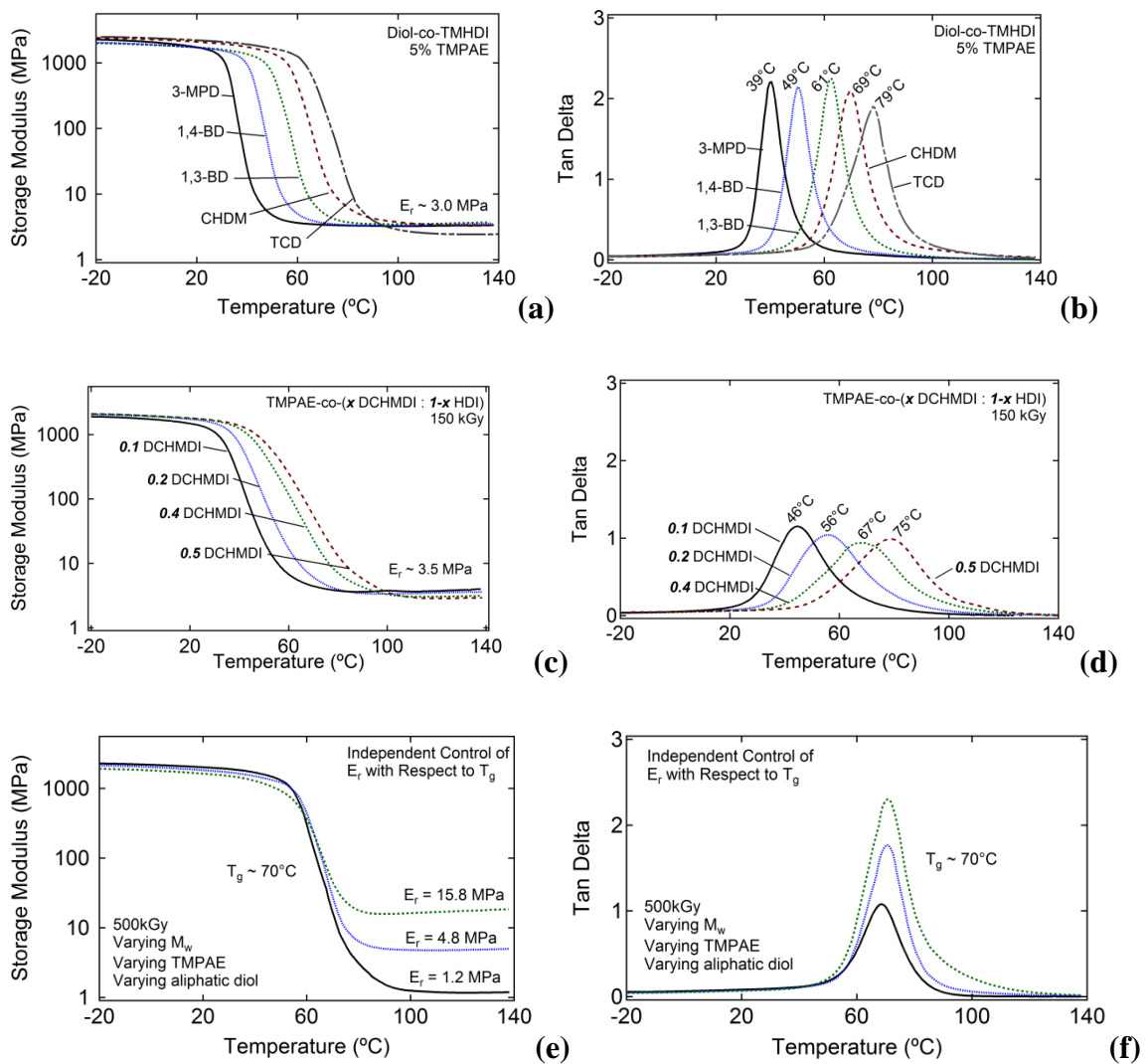
Figure 29- Moving Tg, independent control of glass transition and crosslink density

4. Shape Memory Characterization Results and Discussion

The shape memory characterization data provided in Figure 30 demonstrate that the polymers synthesized in this study exhibit good shape memory behavior. The free strain recovery data in Figure 30(a) and 30(b) show five-cycle thermomechanical cycling for 0.50 mm/mm prestrain for a 0.1 TMPAE, 450 kGy SMP in (a) strain-temperature and (b) strain-time and stress-time planes. As noted in Figure 30(a), the recoverable strain, σ_{rec}, was 90% for Cycle 1 and was greater than 99% for Cycles 2 to 5. Covalent crosslinking is expected to result in good cyclic shape recovery for SMPs, and Figure 30(a) and 30(b) demonstrate such behavior.[25] The constrained recovery data in Figure 30(c) shows increasing recovery stress for TMPAE samples with increasing crosslink density under 25% constrained deformation conditions. Recovery stress increases from 0.5 to 3.0 MPa at tangent delta peak temperature + 25°C as rubbery modulus increases from 3.1 to 15.2 MPa (TMPAE-0.1 to TMPAE-0.7, 450 kGy). Achieving tailorable recovery stress through the control of crosslink density using e-beam irradiation in low molecular weight thermoplastics without the use of sensitizer was one of the underlying motivations in designing the SMP system in this study, and Figure 30(c) demonstrates the successful achievement of this objective in for thermoplastics with initial molecular weights of 26.9, 5.2, 3.7, and 3.5 kDa.
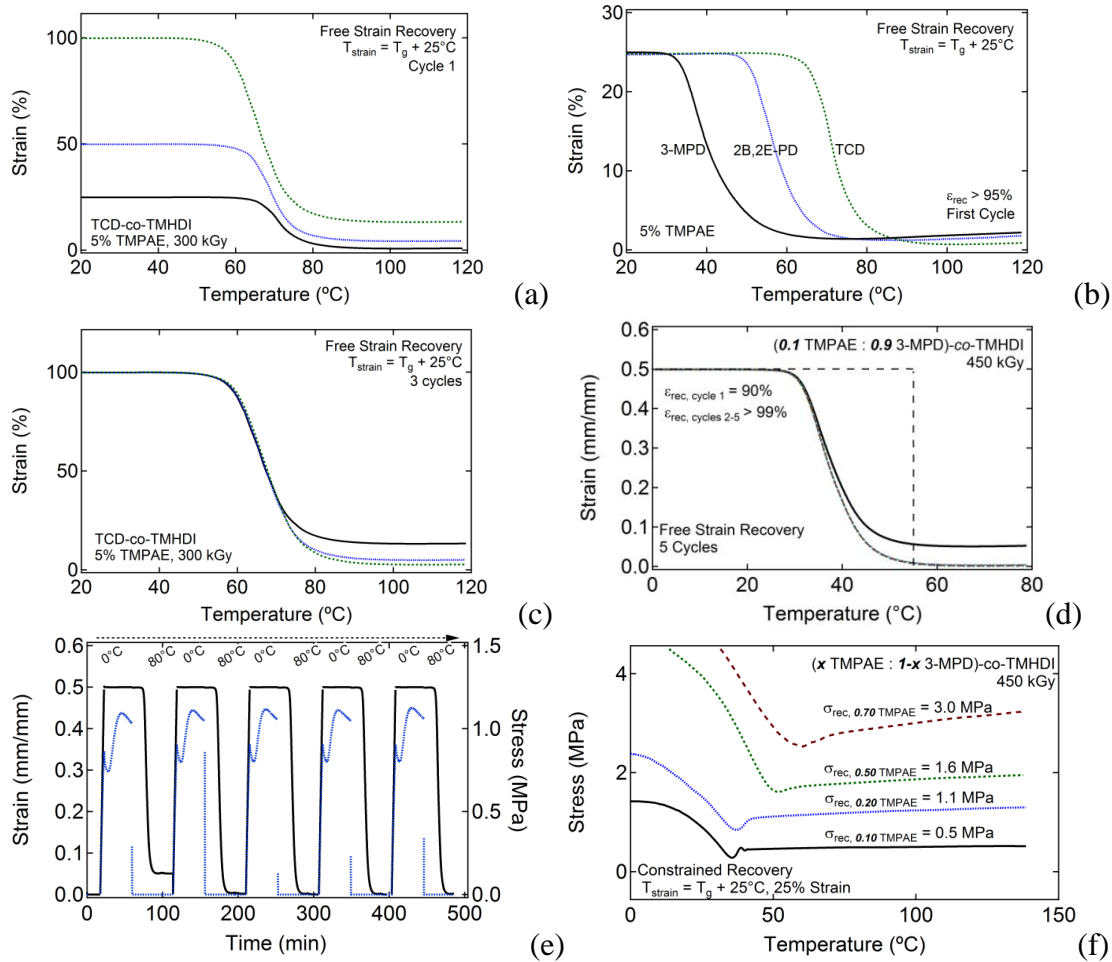
Figure 30- **Five-cycle free strain recovery data for a 0.1 TMPAE, 450 kGy SMP
subjected to 0.50 mm/mm prestrain shown in (a) strain-temperature and (b) strain-
time and stress-time planes. For Cycle 1, 90% recoverable strain was observed,
and for Cycles 2 to 5, greater than 99% recoverable strain was observed; (c)
contrained recovery analysis showing increased recovery stress with increasing
rubbery modulus for electron beam crosslinked SMPs comprised of varying
TMPAE composition irradiated at 450 kGy.**

5. *Strain-to-Failure Results and Discussion*

To provide a general indication of the performance that can be expected from this

new SMP system over a temperature range representative of that which an SMP used in

medical device applications could be subjected and to demonstrate that high radiation

dose does not result in decreased mechanical integrity as shown in some polymer

systems,[78] strain-to-failure experiments for TMPAE-0.1 samples irradiated at 450 kGy

were conducted at temperatures ranging from 0 to 65°C and are provided in Figure 31

along with calculated average toughness values for each straining temperature. The

temperatures selected for the strain-to-failure experiments were 65 °C (T_g + 20 °C), 45

°C (T_g), 35 °C (T_g – 10 °C), 20 °C (T_g – 25 °C), and 0 °C (T_g – 45 °C), where T_g was

defined by the tangent delta peak temperature as determined by DMA. The stress-strain

behavior at each temperature is consistent with that of typical temperature-dependent

polymeric behavior.[79]   While good mechanical integrity is generally predicted for

lightly crosslinked polyurethanes, it is important to demonstrate that good mechanical

integrity is still exhibited by materials in this SMP system after subjection to high doses.

Average toughness values of 59.3 MJ/m^3 ± 2.8 and 45.6 MJ/m^3 ± 3.2 were observed at

20 and 35°C, respectively, and consequently the strain-to-failure results demonstrate that

good mechanical integrity can be maintained upon high dose irradiation over a

temperature range that is relevant for medical device applications.
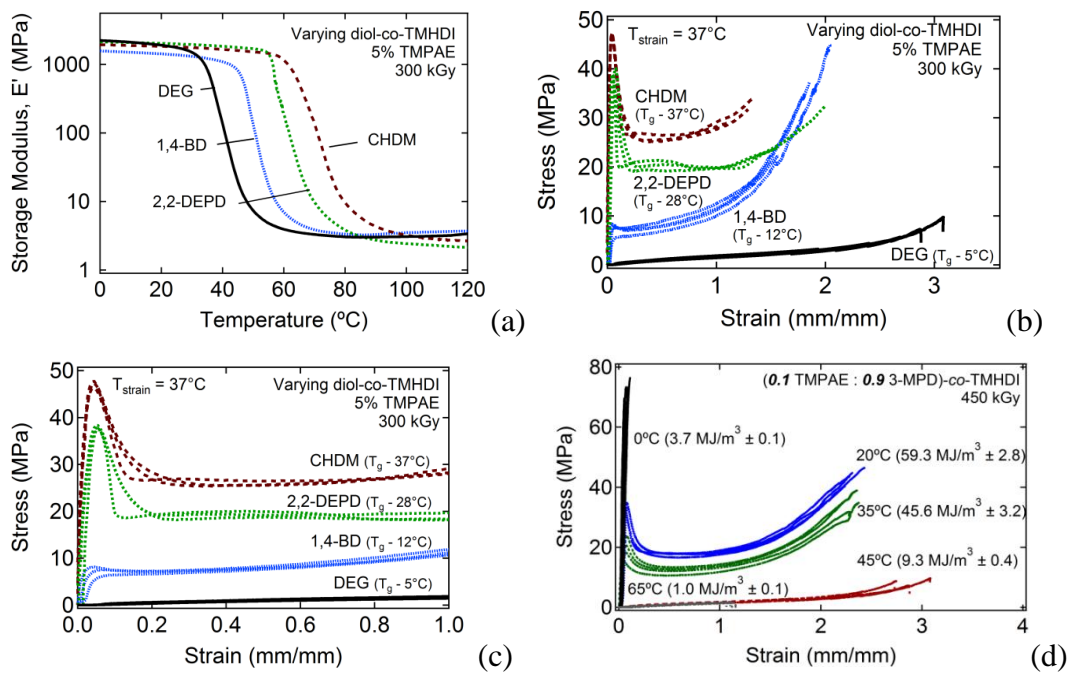
Figure 31- Strain-to-failure at various temperatures for 0.1 TMPAE SMP irradiated at 450 kGy. Average toughness values are provided in parentheses next to each straining temperature and ranged from 1.0 ± 0.1 MJ/m3 at 65°C to 59.3 MJ/m3 ± 2.8 at 20°C.

6. Demonstration of Thermoplastic Processing Capabilities

To demonstrate the thermoplastic processing capabilities of this e-beam crosslinkable polyurethane shape memory polymer system, the CHDM-0.90 formulation was subjected to extrusion and 3D printing. Extrusion was carried out using a Malvern RH7 Advanced Capillary Rheometer, and 3D printing of an ASTM Type V dog bone was carried out using a Cubify 3D Touch printer. Images of the extrusion process, extruded material, and 3D printed material are provided in Figure 32.
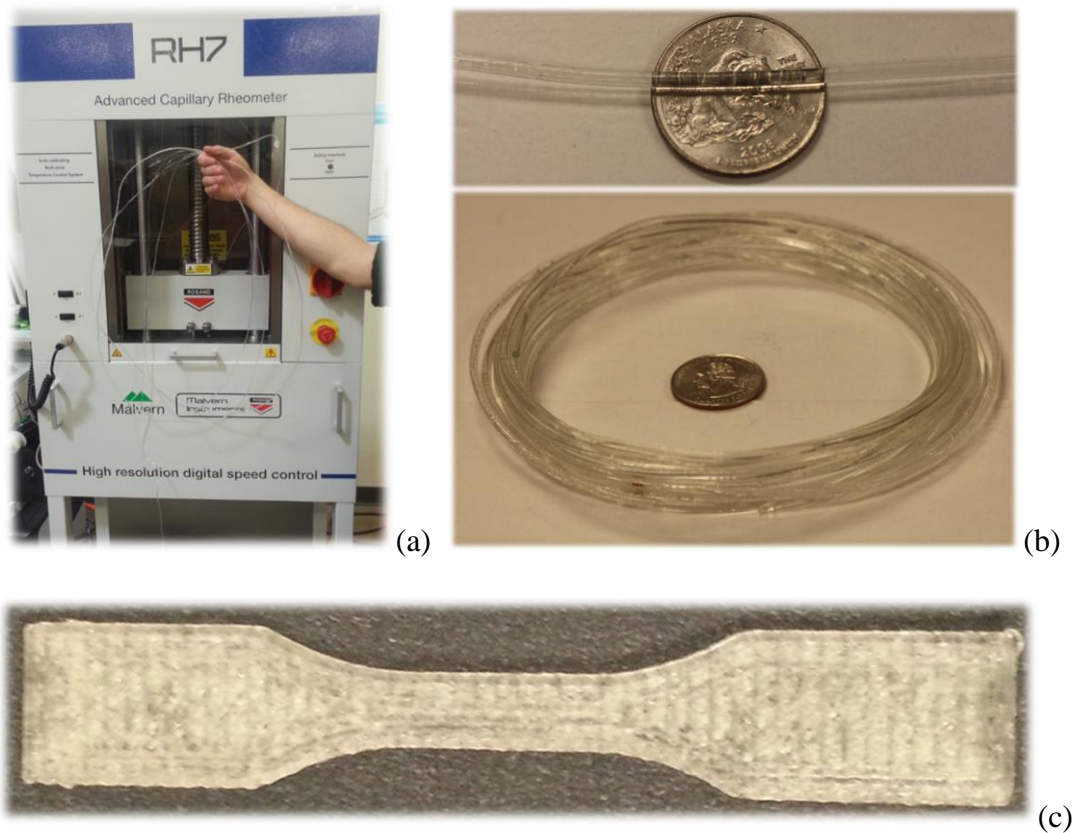
Figure 32- Demonstration of extrusion and 3D printing capability of sensitizer-free electron beam crosslinkable polyurethane SMP system. The formulation pictured is CHDM-0.90.

D. Summary and Conclusions

A structural approach to achieving both facile processability and significant tunability of thermomechanical properties in a versatile aliphatic polyurethane shape memory polymer system is reported in this study. The effects of varying chemistry adjacent to C=C motifs, as well as varying dose, molecular weight, and C=C composition on electron beam crosslinking of sensitizer-free polyurethane shape memory polymers are determined in order to work towards establishing a platform

145

chemistry to enable facile, tunable, bulk crosslinking of polyurethane shape memory polymers. As hypothesized, incorporation of EWG-$CH_{2\alpha}$-C=C motifs into the side chains of thermoplastic polyurethane SMPs, which was achieved by synthesizing the custom monomer DEA-diol, results in higher susceptibility to electron beam crosslinking than that which results from incorporating the TMPAE monomer's EDG-$CH_{2\alpha}$-C=C side chain motifs or the 2-butene-1,4-diol monomer's EWG-$CH_{2\alpha}$-C=C backbone motifs. However, SMPs containing the commercially available TMPAE monomer's EDG-$CH_{2\alpha}$-C=C side chain motifs were also shown to provide sufficient e-beam crosslinking susceptibility to enable control of shape memory properties over a notable range, with rubbery modulus being tailorable between 1 and 55 MPa. The crosslink density of the TMPAE-based SMPs was demonstrated to be tunable by varying dose, molecular weight, and/or C=C monomer composition. Consequently, the thermomechanical properties of this SMP system can be achieved by multiple routes, and the SMP system appears to be quite versatile. Based on the observed trends in glass transition breadth for the crosslinked SMPs in this study, the combination of minimizing C=C monomer functionality and irradiating at sufficient dose to drive crosslinking reactions to occur in a high percentage of whatever number of crosslinkable sites are necessary to achieve a desirable rubbery modulus appears to afford glass transition breadths that generally remain more narrow as crosslink density is increased than those that are afforded by higher C=C functionalized thermoplastics that are more susceptible to partial crosslinking at lower doses.

146

The ability to achieve tunable, bulk crosslinking in thermoplastics using the synthetic strategy hypothesized and supported herein may be of interest in a number of industrial applications outside the field of SMP research because the incorporation of even a small amount of the chemical functionalities in this study can be used to greatly influence and improve the resulting mechanical properties of a material system. Since tailorable crosslinking is achievable even for low molecular weight thermoplastics without sensitizer, these SMP materials may be very well-suited for high throughput thermoplastic melt processing techniques. The advanced processing capability and demonstrated tunability of material properties in this SMP system may enable a wide range of applications in biomedical engineering and other industries. Potential high-impact applications range in complexity from 3D printable tissue scaffolds with tailorable moduli possessing shape memory properties to shape memory catheters used in basic medical procedures that must be produced on a mass-scale to justify production costs. Future work will focus on the rheological characterization, complex fabrication and further thermomechanical optimization of this new polyurethane SMP system, including in-depth shape memory characterization and new synthetic strategies to achieving tunable glass transitions.

E. Acknowledgements

CHAPTER VII

A UV CATALYZED THIOL-ENE CROSSLINKABLE POLYURETHANE SHAPE MEMORY POLYMER SYSTEM

Although the e-beam crosslinkable SMP system reported in Chapter VI excels from numerous processing and mechanical characterization standpoints, the development of an additional alternative SMP system was desired that possesses advantages in the areas of practical utility and time required for fabrication. Instead of requiring researchers to wait for samples to be irradiated at what is most often and likely an external facility, the thiol-ene crosslinked system reported in Chapter VII allows for synthesis and curing of polymers and devices in a facility that is equipped with the resources generally characteristic of a polymer synthetic research laboratory.

A. Introduction

A high performance shape memory polymer (SMP) system with tunable thermomechanical properties, high toughness and good biocompatibility that can be readily synthesized and processed in atmospheric conditions into desired geometries for device fabrication is of importance for a variety of biomedical applications.[1, 5, 80] For SMP-based medical devices, the functional utility that arises from a clinician's ability to trigger geometric transformations after device implantation in the body is both multi-dimensional in nature and complex in conceptualization. The materials science of human physiology constitutes tremendous variations in tissue modulus and architecture, and consequently implantable devices may require SMPs that exhibit highly tunable material properties and advanced processing capabilities.[33] Various applications may demand SMPs with tailorable actuation temperature, recoverable strain, recovery stress, modulus at physiological conditions, and toughness, in addition to good biocompatibility.[81] Devices also often have complex geometric design requirements, and a material system's ability to be processed using techniques required to achieve such geometries is often a key determining factor in the materials selection process of device design.[82] The focus of this work is to introduce an amorphous, thermally actuated shape memory polymer system that exhibits highly tunable material properties and advanced processing capabilities and to demonstrate this SMP system's viability as a platform system for medical device design through the fabrication of a laser actuated SMP-based microgripper designed to facilitate microcatheter delivery of implantable endovascular devices.

The tunability of material properties, toughness and processability of many SMP systems has been shown to be highly dependent on the nature and extent of crosslinking in the SMPs.[75] The term "SMP system" is used in this study to refer to a series of formulations built around a core chemical foundation that have been reported together for the purpose of enabling tailorable material properties. Primarily, achieving independent control of T_{trans} (in thermally actuated SMPs) and rubbery modulus, E_r, is desirable.[67] E_r is proportional to recovery stress[83] and is predicted to increase with increasing crosslink density by the elastic theory of rubber.[76] For a thermally actuated, one-way SMP, the polymer constituents that undergo thermal transitions upon heating or cooling across the SMP switching temperature T_{trans} are referred to as "switching segments," and crosslinks, whether covalent, physical, or other, are referred to as "netpoints." Netpoints prevent switching segment chains from permanently sliding past one another during straining to a secondary geometry by effectively acting as anchors that enable shape recovery to occur.[3] Covalently crosslinked SMP systems often exhibit advantages in mechanical behavior over those of physically crosslinked SMP systems, including better cyclic shape memory and greater percent recoverable strains. In contrast, thermoplastic SMPs often possess significant processing advantages over thermosets, which do not flow at elevated temperatures and pressures and do not dissolve in solvents.[4] Thermoplastic processing techniques such as extrusion, injection molding and solution casting are especially useful when high-throughput processing and/or complex prototype fabrication are desired.[84] For medical device applications in particular, a thermoplastic SMP that is capable of being processed into a desired

151

geometry in atmospheric conditions and subsequently crosslinked in a secondary step may offer significant advantages over current SMP materials by exploiting the processing capabilities of a thermoplastic and the mechanical robustness of a thermoset.[65]

Reported herein is an amorphous, aliphatic polyurethane (PU) SMP system designed to exhibit tunable crosslink density and glass transition (T_g), high toughness, and good biocompatibility, as well as advanced processing capabilities in atmospheric conditions. One advantage of PUs is the high toughness that results from inter-chain hydrogen bonding between carbamate linkages,[85] and many aliphatic PUs have also been shown to exhibit good biocompatibility.[86] One major disadvantage of PUs is the fact that PU synthesis must be carried out in moisture-free environments such as glove boxes to prevent isocyanate side reactions, and consequently many commercially available PUs are thermoplastics that have been pre-synthesized by manufacturers to allow for processing into desired geometries in atmospheric conditions. If applications should require the high toughness provided by urethane chemistry and the mechanical robustness provided by covalent crosslinking while also demanding processability in atmospheric conditions, one strategy that allows for the incorporation of urethane linkages into covalently crosslinked networks in atmospheric synthetic environments is the synthesis of monomers, oligomers, or thermoplastic precursors containing internal carbamate linkages that are functionalized with groups that can be subsequently cured using alternative polymerization methods.[87] Thiol-ene "click" chemistry is a powerful synthetic tool that can proceed to high conversion in atmospheric conditions,[88] and Nair

and co-workers have reported an SMP system that is prepared by functionalizing isophorone diisocyanate (IPDI) to afford polyalkene and polythiol monomers with internal (thio)urethane linkages, which are curable using thiol-ene "click" reactions upon UV irradiation.[89] Beigi, et al. have recently investigated the use of alkene-functionalized IPDI as a co-monomer in thiol-ene-methacrylate systems as a resin matrix for dental applications,[90] and a number of studies have also reported the synthesis of thiol-ene crosslinked waterborne PU coatings from alkene end-capped urethane-ester-urethane trimers that possess internal side chain carboxylic acid functional groups that allow for water solubility.[91] Because of the high number of flexible thioether linkages that result from the bulk curing of thiol-ene monomers, even when such monomers contain internal carbamate linkages, the resulting hybrid networks often exhibit glass transitions below 25°C. Although T_g can be increased by increasing crosslink density, this increase in crosslinking is often accompanied by a tradeoff in decreased toughness, and achieving independent control of crosslink density and T_g in such systems is often a synthetic challenge.[22]

To afford a polyurethane SMP system that is processable in atmospheric conditions in which crosslink density and T_g can be controlled independently of one another to enable higher toughness and greater control of shape memory properties, we report a synthetic strategy in which thermoplastic PUs are prepared from aliphatic diisocyanates and varying ratios of C=C and non-C=C functionalized diols, as shown in Scheme 7. After thermoplastic synthesis, crosslinking is achieved by solution blending of thermoplastics with polythiol crosslinking agents and photoinitiator and subsequent

153

UV irradiation. This post-polymerization crosslinking approach allows for polyurethane-based SMP devices to be fabricated in atmospheric conditions, and the toughness and thermomechanical properties of these SMPs are primarily influenced by the linkages in the thermoplastic PUs, which statistically significantly outnumber the thioether linkages in the crosslinked materials. Furthermore, the incorporation of C=C linkages into PU side chains by PU step growth polymerization should result in a fairly uniform distribution of C=C functionalities, which, upon crosslinking with polythiols, should afford poly(thioether-co-urethane) networks with high network homogeneity and narrow glass transition breadths.[25]

To demonstrate the processing capability of this new SMP system, a prototype microactuator device was also synthesized and characterized in this work. One advantage to the solution blending aspect of this synthetic process in this study is the solvent's ability to uniformly disperse non-reactive additives throughout the thermoplastic PU/polythiol solutions. The device fabricated in this study constitutes a new design for a light-actuated SMP microgripper, which is designed for the purpose of delivering endovascular devices via microcatheter. Utilizing the properties of this new SMP system, we seek to improve upon a microactuator device previously reported by our group in 2002.[92] Our new device design, illustrated in Figure 33, offers significantly improved ease of fabrication over our previously reported design. By fabricating this microactuator device, we seek to demonstrate (a) the ease with which non-reactive additives can be blended with this new SMP system; (b) the use of post-polymerization crosslinking to enable the fabrication of a micro-scale medical device;

(c) the ability of this new SMP system to be subjected to device fabrication in

atmospheric conditions.

Scheme 7- Synthetic strategy utilized in this study.

- Synthesis in atmospheric conditions possible
- Thermoplastic processing techniques possible
- Nonreactive additives can easily be added (e.g., light absorbing die to enable laser-induced actuation)
- Thiol-modified functional chemistries can be easily incorporated into final network (e.g., thiol-functionalized UPy to enable triple shape behavior)

Highly versatile thiol-ene crosslinked PU SMP series: A platform SMP system for medical device design

Figure 33- Schematic diagram for laser actuated SMP microgripper. Solutions of thermoplastic PU and polythiol doped with Epolin 4121 were first solution cast over a cleaved optical fiber to form the SMP gripper. Pellet tipped nitinol was then axially crimped into the gripper, as shown in

B. Experimental

1. Materials, Synthetic Strategy, and Sample Preparation

1.1 Materials

To provide a monomer-based synthetic approach to tailoring crosslink density in the thiol-ene crosslinked PU SMP system in this study, the alkene diol trimethylolpropane allyl ether (TMPAE, > 98%) and the end-capping agent allyl alcohol (AA, > 99%) were purchased from Sigma Aldrich. To tailor glass transition by varying
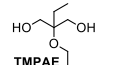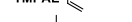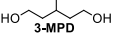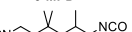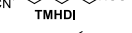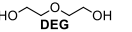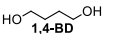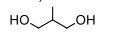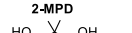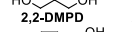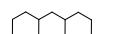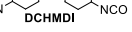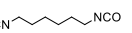
aliphatic diol co-monomer, diethylene glycol (DEG, > 99%), 3-methylpentanediol (3-MPD, > 99%), 1,4-butanediol (1,4-BD, > 99%), 2-methylpropanediol (2-MPD, > 99%), 2,2'-dimethylpropanediol (2,2-DMPD, > 99%), and 1,4-cyclohexanedimethanol, mixture of *cis* and *trans* (CHDM, > 99%) were purchased from Sigma Aldrich. To tailor glass transition by varying diisocyanate monomer composition, hexamethylene diisocyanate (HDI, > 98%), trimethylhexamethylene diisocyanate (TMHDI, > 97%), and dicyclohexylmethane 4,4'-diisocyanate (DCHMDI, > 90%) were purchased from TCI America. To absorb water during polyurethane polymerizations, 4 Å molecular sieves were purchased from Sigma Aldrich. The catalyst zirconium (IV) acetylacetonate (Zr Cat, > 99%), which has been shown to favor urethane formation over urea formation when water is present during urethane polymerizations, was purchased from Alfa Aesar and used in thermoplastic polyurethane synthesis. Anhydrous tetrahydrofuran (THF, > 99.98%) was purchased from EMD Chemicals and used as a polymerization and blending solvent. The polythiol crosslinking agents ethylene glycol bis(3-mercaptopropionate) (EGBMP, > 97%) and dipentaerythritol hexakis(3-mercaptopropionate) (DPHMP, > 97%) were purchased from Wako Chemicals, and trimethylolpropane tris(3-mercaptopropionate) (TMPTMP, > 95%), tris[2-(3-mercaptopropionyloxy)ethyl] isocyanurate (3TI, > 95%), and pentaerithritol tetrakis(3-mercaptopropionate) (PETMP, > 95%), as well as the photoinitiator 2,2'-dimethoxy-2-phenylacetophenone (DMPA) were purchased from Sigma Aldrich. All monomers, solvents, additives, catalysts, and crosslinking agents were purchased from the specified distributors and used as received without further purification.

157

For microgripper device fabrication, Epolight™ 4121 platinum dye was purchased from Epolin, Inc., and 200 μm optical fiber was purchased from Polymicro Technologies.

Formulations for all thermoplastic polyurethanes synthesized in this study are provided in Table 9. Each thermoplastic polyurethane formulation was synthesized in a 100 g scale polymerization batch in a 0.40 g/mL solution in anhydrous THF in a previously flame dried 240 mL glass jar in the presence of approximately 80 mL of 4 Å molecular sieves, which were also previously flame dried. All monomers, solvents, and catalysts were mixed under dry air in a LabConco glove box. Using a 1.02:1.01 NCO:OH ratio, all diisocyanate and hydroxyl starting materials were added to the molecular sieve-containing glass jars in the glove box, after which anhydrous THF and the Zr catalyst (0.010 overall wt % Zr Cat) were added. The polymerizations were carried out in sealed jars using a LabConco RapidVap instrument at 80 °C for 24 h at a vortex setting of 150 RPM. The RapidVap was used to heat and mix the monomer solutions. After 24 h, the viscous polymer solutions were diluted with additional THF to 0.10 g/mL concentrations and filtered to remove molecular sieve dust, residual starting materials and catalyst using flash chromatography through 15 cm tall, 10 cm diameter packed silica columns. After filtration, the purified, diluted polymer solutions were decanted into 30 cm × 22 cm rectangular polypropylene (PP) dishes for solvent removal. The solution-containing PP dishes were heated in a vacuum oven to 50°C at ambient pressure using a house air purge for 24 h, after which the oven temperature was increased to 80°C for an additional 24 h. The vacuum oven was then evacuated to a

158

pressure of 1 torr at 80°C for 72 h, after which neat, amorphous, thermoplastic

polyurethane films approximately 0.5 mm in thickness were removed from the PP dishes

and stored under desiccation until future use.

Table 9- Sample compositions and molecular weights as determined by GPC analysis and structures for monomers and polythiol crosslinkers used to prepare thiol-ene crosslinked polyurethane shape memory polymers.

Varying TMPAE Series (Varying E_r)	Equiv. TMHDI	Equiv. TMPAE	Equiv. 3-MPD	Equiv. 2x AA	M_n	M_w	PDI
TMPAE-0.05	1.020	0.05	0.950	0.010	15.0	26.9	1.79
TMPAE-0.1	1.020	0.100	0.900	0.010	17.2	30.7	1.79
TMPAE-0.3	1.020	0.300	0.700	0.010	1.9	5.2	2.78
TMPAE-0.5	1.020	0.500	0.500	0.010	1.3	3.7	2.81
TMPAE-0.7	1.020	0.700	0.300	0.010	1.1	3.5	3.01
TMPAE-0.9	1.020	0.900	0.100	0.010	2.8	9.5	2.69

Varying Diol Series (Varying T_g)	Equiv. TMHDI	Equiv. TMPAE	Equiv Diol	Equiv. 2x AA	M_n	M_w	PDI
DEG-0.9	1.020	0.100	0.900	0.010	16.3	38.7	2.37
1,4-BD-0.9	1.020	0.100	0.900	0.010	11.5	28.6	2.49
2-MPD-0.9	1.020	0.100	0.900	0.010	18.7	57.3	3.06
2,2-DMPD-0.9	1.020	0.100	0.900	0.010	17.0	41.4	2.44
CHDM-0.9	1.020	0.100	0.900	0.010	11.9	31.2	2.62

Varying DCHMDI Series (Varying T_g)	Equiv. DCHMDI	Equiv. HDI	Equiv TMPAE	Equiv. 2x AA	Mn	Mw	PDI
DCHMDI-0.0	0.000	1.020	1.000	0.010	21.2	65.4	3.08
DCHMDI-0.1	0.100	0.920	1.000	0.010	10.0	20.6	2.06
DCHMDI-0.5	0.500	0.520	1.000	0.010	5.5	11.0	2.00
DCHMDI-1.0	1.000	0.020	1.000	0.010	5.4	9.7	1.80

Polythiol Crosslinking Agents:

EGBMP   TMPTMP   3-TI   PETMP   DPEHMP

159
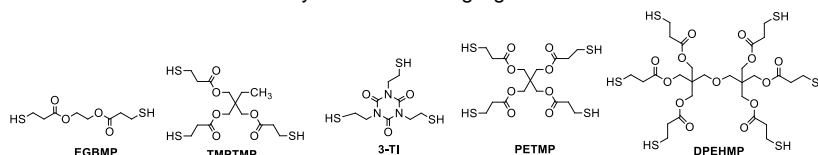
1.2. Characterization of Thermoplastic Molecular Weight by Gel Permeation Chromatography

To determine the molecular weights of all thermoplastic polyurethane formulations, gel permeation chromatography (GPC) experiments were performed on a Waters Chromatography, Inc., 1515 isocratic HPLC pump equipped with an inline degasser, a model PD2020 dual angle (15° and 90°), a model 2414 differential refractometer (Waters, Inc.), and four PLgel polystyrene-co-divinylbenzene gel columns (Polymer Laboratories, Inc.) connected in series: 5 μm Guard (50×7.5 mm), 5 μm MixedC (300×7.5mm), 5 μm 104 (300×7.5mm), and 5 μm 500Å (300×7.5mm) using the Breeze (version 3.30, Waters, Inc.) software. The instrument was operated at 35 °C with THF as eluent (flow rate set to 1.0 mL/min). Data collection was performed with Precision Acquire 32 Acquisition program (Precision Detectors, Inc.) and analyses were carried out using Discovery32 software (Precision Detectors, Inc.). A system calibration curve generated from plotting molecular weight as a function of retention time for a series of broad polydispersity poly(styrene) standards was used to determine the molecular weight values of polycarbonates, and the value was determined using dn/dc values that were calculated for each sample.

1.3. Polythiol and Photoinitiator Solution Blending, Film Casting, and Sample Curing

To prepare thermoplastic PU, polythiol and photoinitiatior blended mixtures for UV curing, approximately 5 g of each thermoplastic PU formulation were dissolved in

THF solutions in 40 mL amber glass vials in 0.13 g/mL concentrations. Polythiol crosslinking agents and photoinitiator were then added to each solution in specified quantities. Unless otherwise stated, a 1:1 C=C:SH stoichiometric ratio, 3.0 wt% DMPA photoinitiator, a post cure time of 24 h, less than 4 wt% THF solvent at cure, and TMPTMP polythiol selection were used. After pouring the mixtures into 10 cm × 5 cm × 5 cm PP containers, the THF was evaporated by placing the PP containers in a vacuum oven at 50°C at ambient pressure using a house air purge for 24 h for all series except for the varying THF series, for which THF evaporation times were varied to afford the specified THF compositions. Percent THF at curing time was determined by taking the masses of the PP containers before and after pouring the blended solutions into them and again after THF evaporation. All thiol-ene blends were irradiated using 365 nm UV light in a UVP CL-1000L crosslinking chamber for 45 min, and after UV curing, all samples were post-cured at 120°C at 1 torr for 24 h, except for samples in the varying post cure time series, for which post cure time was varied as specified. For the varying C=C:SH stoichiometric ratio series, C=C:SH ratios of 4.0:1.0, 2.0:1.0, 1.5:1.0, and 1.0:1.0 were used. For the varying photoinitiator composition series, DMPA compositions of 0.1, 0.5, 1.0, 3.0, and 10.0 wt% were used. For the varying post-cure time series, post cure times of 0 min, 10 min, 1.5 h, 6 h, and 24 h were used. For the varying THF at cure series, THF compositions of 300, 100, 50, 25, and < 4 wt% at cure were used. For the varying polythiol functionality series, EGBMP, TMPTMP, PETMP, and DPHMP were used. For the varying diol co-monomer and varying diisocyanate co-monomer ratio T_g

variation series, 3TI and PETMP polythiol crosslinkers were used, respectively. After

post-curing, all crosslinked films were stored under desiccation until future use.

2. Materials Characterization Methods

2.1. Sol/Gel Analysis

To determine the percent of thermoplastic PU chains and polythiol crosslinking

additives incorporated into each network after UV curing and post curing, sol/gel

analysis experiments were run on select formulations. Dry, ~50 mg samples were

massed in triplicate for each formulation and placed in 20 mL glass vials, after which

THF was added in approximately a 150:1 solvent:polymer mass ratio. The vials were

capped and vortexed at 50 RPM at 50°C for 48 h using a LabConco RapidVap

instrument. After 48 h, the solvent swollen polymer samples were removed from the

THF/sol fraction solutions and placed in new 20 mL glass vials, dried at 80°C for an

additional 48 h at 1 torr, and then re-massed to provide sufficient mass data to determine

the gel fractions of each irradiated sample. Sol/gel analysis results are provided in Table

10.

2.2. Dynamic Mechanical Analysis

To determine key thermomechanical data for each sample, including rubbery

moduli and glass transitions, dynamic mechanical analysis (DMA) experiments were run

on every crosslinked sample synthesized in this study. Rectangular $25.0 \times 4.0 \times 0.4$ mm

specimens were machined using a Gravograph LS100 40 W CO_2 laser machining system using a power setting of 15, a speed setting of 12, and a pass multiplicity of n = 2. Using a TA Instruments Q800 dynamic mechanical analyzer in the DMA Multifrequency/ Strain mode, DMA experiments were run in tension at 1 Hz from -20 to 140°C using a heating rate of 2°C/min, a Preload Force of 0.01 N, a Strain of 0.1%, and a Force Track of 150%. DMA results were recorded using TA Instruments QSeries software and analyzed using TA Instruments Universal Analysis software.

2.3. Shape Memory Characterization

To determine percent recoverable strain and recovery stress for select samples, shape memory characterization experiments were performed using a TA Instruments Q800 DMA on laser machined $25.0 \times 4.0 \times 0.4$ mm rectangular specimens prepared using the same laser machining parameters as those used to prepare the DMA samples in the above paragraph. In the DMA Strain Rate Mode in tension, rectangular specimens were heated to $T_g + 25$°C (glass transitions were determined by the peak of the tangent deltas from the previous DMA results), allowed to equilibrate for 30 min, and then strained to deformations of 25, 50, or 100%. The strained samples were then cooled to 0°C and allowed to equilibrate for an additional 30 min. For constrained recovery experiments, which were used to measure the recovery stress of the materials, the drive force of the DMA instrument was maintained, and the samples were heated to 120°C at 2°C/min. For free strain recovery experiments, which were used to measure the percent recoverable strains of the SMPs, the drive force was set to zero after equilibration at 0°C,

the samples were re-heated to 120°C at 2°C/min, and the amount of recoverable

deformation was recorded using TA Instruments QSeries software and analysized using

TA Instruments Universal Analysis software.

2.4. Tensile Testing

Multi-temperature strain-to-failure experiments were performed to determine

ultimate tensile properties and toughness for select crosslinked samples. ASTM Type V

dog bone samples were machined using a Gravograph LS100 40 W CO2 laser

machining device using a power setting of 15, a speed setting of 12, and a pass

multiplicity of n = 2. All laser machined samples were sanded around the edges using

400, then 800, then 1200 grit sandpaper. Strain-to-failure experiments were conducted

on select samples (n ≥ 5) using an Instron Model 5965 electromechanical, screw driven

test frame, which was equipped with a 500 N load cell, 1 kN high temperature pneumatic

grips, and a temperature chamber that utilizes forced convection heating. An Instron

Advanced Video Extensometer with a 60 mm field-of-view lens was used to optically

measure the deformation of the samples by tracking parallel lines applied at the ends of

the gauge length. The samples were heated to $T = T_{\text{loss modulus peak}} - 10°C$, which

corresponds to a thermal state of high toughness for this polyurethane system as

observed in previous experiments (loss modulus peak temperatures were determined

from previously obtained DMA data). The samples were heated under zero loading,

which was achieved by keeping the bottom grip unclamped during thermal equilibration.

The temperature was held at the target temperature for 30 min to allow for thermal

equilibrium, after which the bottom grip was clamped, and then experiments were started thereafter using a deformation rate of 10 mm/min. Data were recorded using Instron Bluehill 3 software.

2.5. Biocompatibility Testing

      To determine percent cell viability for select crosslinked samples, four $9.0 \times 4.0 \times 0.4$ mm specimens of each sample that would be subject to biocompatibility testing were laser cut using a Gravograph LS100 40 W CO_2 laser machining system using the laser cutting parameters specified in the previous paragraph. After laser machining, all specimens were washed with soap and water, rinsed with isopropanol, and then dried in a vacuum oven at 80°C for 24 and subsequently subjected to EtO sterilization. For the cell culturing protocol, mouse 3T3 fibroblasts were cultured in DMEM containing 10% fetal bovine serum and 1% penicillin/streptomycin at 37°C and 5% CO_2. Polymer samples were then placed in 12 well plates with sterile forceps and covered with 500μL of culture media. The cells were trypsinized, centrifuged, and re-suspended in 500uL solutions of culture media, after which they were placed into each well of the 12 well plate at a density of approximately 66,000 cells/cm^2. At 72 h time points, culture media was aspirated from the wells, and approximately 500μL of Calcein AM stain solution was added to each well before incubation at 37°C and 5% CO_2 for 60 min. Calcein AM is a cell-permeable dye, which fluoresces green upon hydrolysis catalyzed by esterases found in the cytoplasm of living cells. Dead cells do not contain the viable esterases to catalyze this reaction and do not fluoresce green. During incubation, a 5μM BBI stain

solution was prepared by dilution with PBS. BBI was used to evaluate the integrity of the cell membrane, in which only dead cells allow BBI penetration and nuclear staining. In this way, live cells were counted as those fluorescing green, while dead cells were counted as those lacking calcein degradation but displaying nuclear BBI staining (blue). Before imaging, the cells were washed once with PBS, and approximately 500μL of BBI solution was added to each well, after which the wells were covered with aluminum foil when not being imaged to limit light exposure. Three to four replicates of each polymer formulation were imaged and analyzed to comply with ISO 10993 Part 5. Wide field fluorescence images were taken of each well at 10x magnification, and the images were analyzed using ImageJ computer software and its "Cell Counter" plug-in.

3. Microgripper Device Development

3.1. Microgripper Device Fabrication

To prepare Microgrippers, 1g of PU was dissolved in 2g of THF. A portion of the THF added was doped with Epolin. The amount of doped THF added was tailored to achieve the desired wt% of Epolin in the microgrippers. DMPA and 3TI were then added to the dissolved PU solution. Molds consisting of RainX coated silica capillary tubing and Teflon spacers used to center the optical fiber in the gripper were fabricated to achieve our desired geometry. Cleaved optical fiber tips were prepared, inserted into the mold, and dissolved SMP was injected into the distal end of the mold, filling the tube and expelling any bubbles. The microgrippers were then UV crosslinked for 20 minutes

and postcured at 120°C under vacuum overnight. After postcure, the mold was removed and the microgripper was inspected for defects, such as bubbles or improper fiber placement.

To load the coil into the microgripper, the gripper was placed into a capillary tube with an ID slightly larger than the OD of the gripper. The gripper was then heated above its T_g and the ball tip of the wire coil was axially forced into the distal end of the SMP. All of the components were then cooled to room temperature, freezing the SMP in the deformed configuration, locking in the ball tipped coil.

C. Results

This study seeks to present a new shape memory polyurethane system as a platform chemistry for use in medical device applications by (1) providing materials characterization data that show excellent thermomechanical, shape memory and tensile behavior, as well as good biocompatibility and (2) demonstrating the processing advantages of this new SMP system through the fabrication in atmospheric conditions of a laser-activated SMP microgripper device to facilitate the microcather delivery of implantable endovascular devices.

1. Achieving Tailorable Crosslink Density

The SMP system reported herein is synthesized through a post-polymerization crosslinking process in which thermoplastic polyurethanes containing pendant C=C functionalities are first synthesized from (alkene)diol and diisocyanate monomers, as

shown in Scheme 7. After thermoplastic synthesis, crosslinking was achieved by solution blending with polythiol crosslinking agents in atmospheric conditions and was shown to be tailorable by varying a number of synthetic parameters, many of which were at the post-polymerization step. Control over rubbery modulus was achieved over the range of 0.5 to 10.5 MPa to by reacting thermoplastic urethanes comprised of varying TMPAE functionalization with 1:1 equivalents of the trithiol TMPTMP, as shown in the storage modulus data provided in Figure 34(a). Control of rubbery modulus was also demonstrated over the range of 3.0 to 10.5 MPa for a single thermoplastic formulation comprised of 0.9 diol TMPAE fraction by crosslinking this thermoplastic with thiol equivalents ranging from 4.0 C=C :1.0 SH to 1.0 C=C:1.0 SH, as shown in Figure 34(b). Figure 34(c) shows a near-negligible effect of photoinitiator composition on rubbery modulus as DMPA composition is increased over three orders of magnitude, from 0.1 wt% to 10.0 wt%, and Figure 34(d) demonstrates that both glass transition and crosslink density increase slightly over the course of a 24 h post-cure. Figure 34(e) shows that rubbery modulus decreases 10.5 to 3.0 MPa as THF solvent composition is increased from 4% to 300% during curing. Finally, the effects of increasing polythiol crosslinker functionality for a 0.1 TMPAE diol component sample are shown in Figure 34(f). As thiol functionality increases from n=2 to 6, rubbery modulus increases from 0.4 to 4.1 MPa.

Table 10- Sol/Gel analysis data for thiol-ene crosslinked polyurethane shape memory polymers prepared using various synthetic conditions

Series	Sample	Polythiol Crosslinker	% DMPA	% THF	Post Cure @ 120°C	Gel Fract-ion	Error
Varying TMPAE	TMPAE-0.1	TMPTMP	3.00%	< 4.00%	24 h	0.998	± 0.004
	TMPAE-0.5	TMPTMP	3.00%	< 4.00%	24 h	0.967	± 0.005
	TMPAE-0.9	TMPTMP	3.00%	< 4.00%	24 h	0.957	± 0.005
Varying Diol	1,4-BD-0.9	3TI	3.00%	< 4.00%	24 h	0.964	± 0.012
	CHDM-0.9	3TI	3.00%	< 4.00%	24 h	0.893	± 0.015
	DEG-0.9	3TI	3.00%	< 4.00%	24 h	0.932	± 0.010
	2,2-DMPD-0.9	3TI	3.00%	< 4.00%	24 h	0.831	± 0.057
Varying DCHMDI Co-Monomer	DCHMDI-0.0	PETMP	3.00%	< 4.00%	24 h	0.985	± 0.012
	DCHMDI-0.1	PETMP	3.00%	< 4.00%	24 h	0.998	± 0.016
	DCHMDI-0.5	PETMP	3.00%	< 4.00%	24 h	0.981	± 0.011
	DCHMDI-1.0	PETMP	3.00%	< 4.00%	24 h	0.986	± 0.015
Varying % Solvent During Cure	TMPAE-0.9	TMPTMP	3.00%	300%	24 h	0.987	± 0.014
	TMPAE-0.9	TMPTMP	3.00%	100%	24 h	0.992	± 0.007
	TMPAE-0.9	TMPTMP	3.00%	50%	24 h	0.985	± 0.017
	TMPAE-0.9	TMPTMP	3.00%	25%	24 h	0.992	± 0.009
	TMPAE-0.9	TMPTMP	3.00%	10%	24 h	0.997	± 0.008
	TMPAE-0.9	TMPTMP	3.00%	4%	24 h	0.998	± 0.004
Varying Polythiol	TMPAE-0.1	EGBMP	3.00%	< 4.00%	24 h	0.818	± 0.031
	TMPAE-0.1	TMPTMP	3.00%	< 4.00%	24 h	0.946	± 0.006
	TMPAE-0.1	PETMP	3.00%	< 4.00%	24 h	0.997	± 0.007
	TMPAE-0.1	DPEHMP	3.00%	< 4.00%	24 h	0.917	± 0.049
Varying PI	TMPAE-0.9	TMPTMP	0.10%	< 4.00%	24 h	0.981	± 0.021
	TMPAE-0.9	TMPTMP	1.00%	< 4.00%	24 h	0.979	± 0.015
	TMPAE-0.9	TMPTMP	10.00%	< 4.00%	24 h	0.974	± 0.009
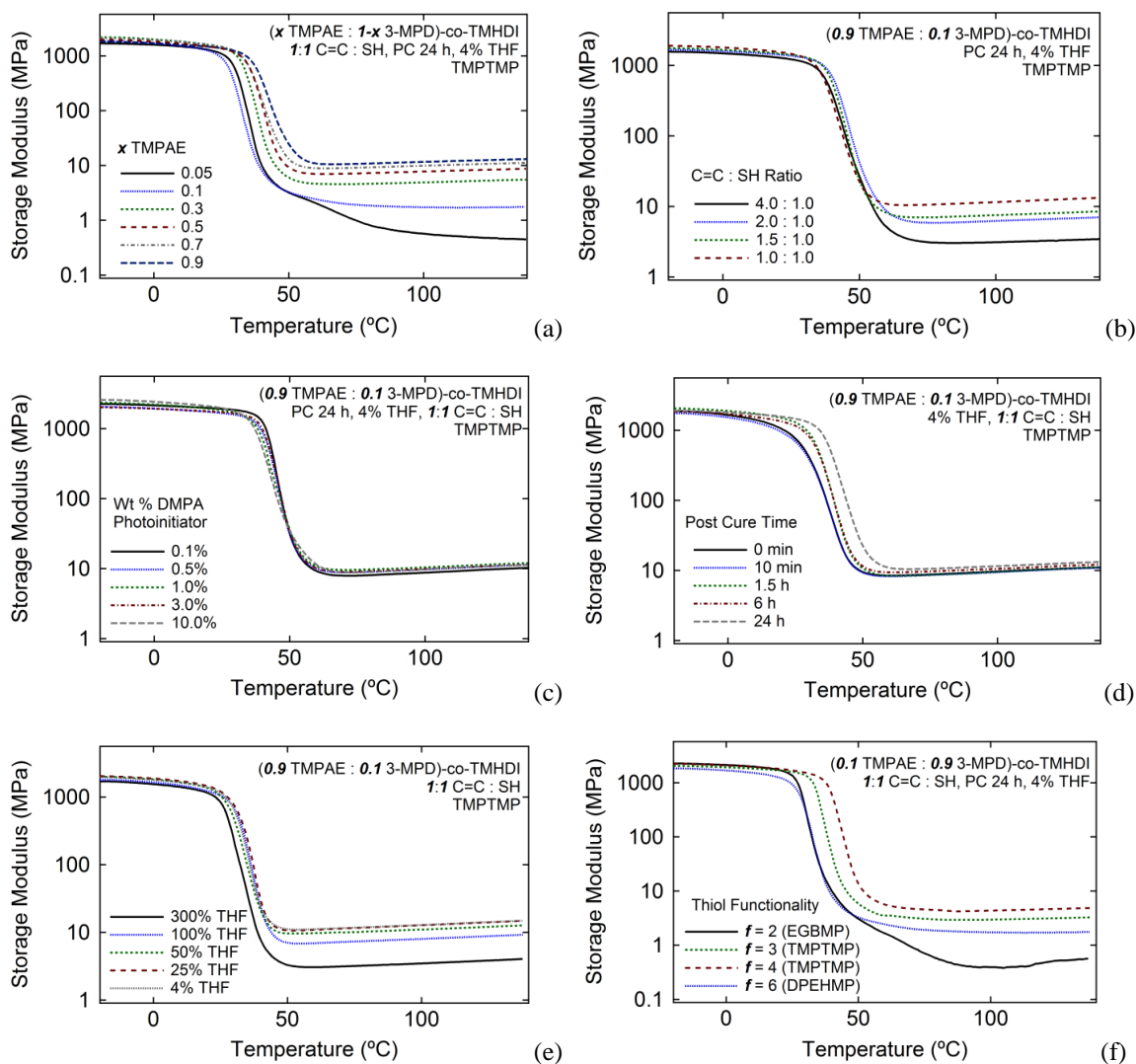
Figure 34- The effects of (a) varying C=C composition, (b) varying C=C : SH ratio, (c) varying DMPA photoinitiator, (d) varying post-cure time at 120°C at 1 torr, (e) varying wt % solvent present during UV curing, and (f) varying thiol crosslinker functionality on crosslink density of PU SMPs prepared from (*x* TMPAE : *1-x* 3-MPD)-co-TMHDI thermoplasticpolyurethanes and polyfunctional thiol crosslinking agents.

2. Achieving Tailorable Glass Transition

To achieve synthetic control over glass transition, two approaches were taken. First, T_g was controlled by varying diol co-monomer composition for thermoplastics comprised of low C=C diol monomer composition (0.10 TMPAE, 0.90 diol), as shown in Table 9. Instead of selecting a "high-T_g and "Low-T_g" diol and moving glass transition by blending such diols in varying ratios, the 0.10 TMPAE : 0.90 diol varying T_g series was formulated to provide increased network homogeneity and more narrow glass transition breadths. Figure 35(a) and (b) show a T_g range of approximately 38 to 70°C and a roughly constant rubbery modulus of approximately 2.1 MPa for all samples, which were prepared from thermoplastics with varying 0.90 diol co-monomer constituents. The 38°C T_g was observed for the diethylene glycol co-monomer, and the 70°C T_g was observed for the cyclohexanedimethanol (CHDM) co-monomer. T_g breadths were very narrow and ranged from 9°C to 12°C (tangent delta full width half maximum, FWHM). This observed sharpness in glass transition breadth indicates that the synthetic strategy of varying T_g by changing the entire diol co-monomer compositions was effective and resulted in high network homogeneity. To provide a second manner of tailoring glass transition, a series of thermoplastics was prepared from 0.9 TMPAE and varying ratios of HDI and DCHMDI diisocyanate co-monomers. As the DMA data in Figure 35(c) and (d) show, as DCHMDI composition is increased from 0.0 to 1.0, T_g increased from 56 to 105°C, and rubbery modulus for this SMP series remained roughly constant, in the range of 16.4 to 17.1 MPa. T_g breadth ranged from

171

16°C to 23°C and was greatest for the 0.5 HDI : 0.5 DCHMDI composition, which was comprised of the most heterogeneous formulation.
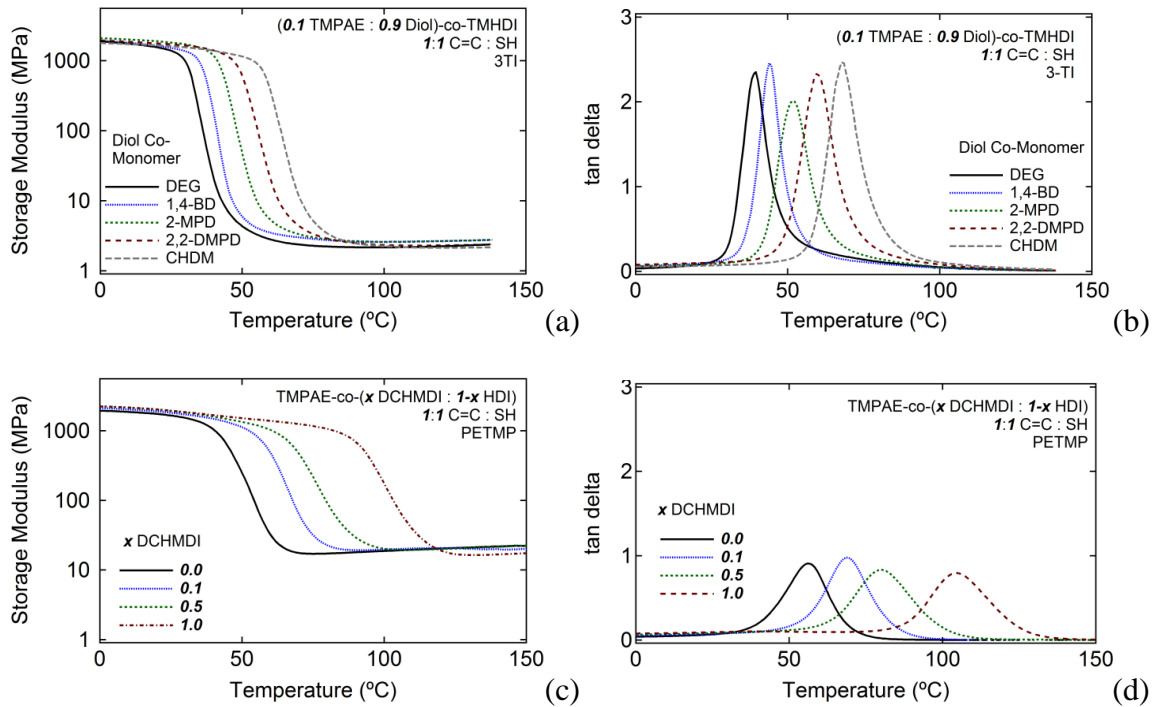
Figure 35- The effects of (a) varying diol co-monomer (diol : TMPAE = 0.9 : 0.1) and (b) varying diisocyanate co-monomer ratio on glass transition temperature.

3. Shape Memory Characterization, Tensile Testing, and Biocompatibility Results

One demonstrated advantage of covalently crosslinked SMP systems is good shape memory behavior, which includes high percent recoverable strains during cyclic testing and recovery stresses that are tunable by varying covalent crosslink density. In Figure 36(a), free strain recovery data showing recoverable strain versus temperature over five straining cycles is shown for the (0.3 TMPAE : 0.7 3-MPD)-*co*-TMHDI SMP crosslinked with TMPTMP, which was subjected to 25% prestrain in each cycle. During

Cycle 1, this SMP exhibits a recoverable strain of 94.5%, and during Cycles 2 to 5, its

recoverable strain approaches 100%. In Figure 36(b), constrained recovery data

showing recoverable stress versus temperature for (x TMPAE : $1-x$ 3-MPD)-co-TMHDI

SMPs crosslinked with TMPTMP are shown. This constrained recovery data is for four

samples subjected to 25% prestrain with TMPAE compositions of 0.1, 0.3, 0.5, and 0.7,

respective rubbery modulus values of 1.7, 4.5, 6.9, and 8.9 MPa, and respective max

recovery stress values of 0.4, 0.9, 1.2, and 1.4 MPa. As predicted, increasing crosslink

results in increasing recovery stress and tailoring crosslink density provides an approach

to tuning recovery stress. Strain-to-failure data run at $T = T_{loss\ modulus}$ - 10°C for (x

TMPAE : $1-x$ 3-MPD)-co-TMHDI samples crosslinked with TMPTMP are provided in

Figure 36(c). TMPAE compositions of 0.05, 0.5, and 0.9, which exhibited rubbery

moduli of 0.5, 6.9, and 10.5 MPa, respectively, were selected for strain to failure testing

at equivalent temperatures relative to each material's loss modulus peak temperature as

determined by DMA. Average toughness was calculated to be > 90.0 MJ/m^3 for the 0.05

TMPAE sample, which did not break in the extension range of the tensile tester, 36.3 ±

3.9 MJ/m^3 for the 0.5 TMPAE sample, and 20.9 ± 2.1 MJ/m^3 for the 0.9 TMPAE

sample. As predicted, toughness was shown to decrease with increasing crosslink

density.

Cell viability data for mouse 3T3 fibroblast cells after exposure for 72 h to (x

TMPAE : $1-x$ 3-MPD)-co-TMHDI samples crosslinked with TMPTMP are provided in

Figure 36(d). Samples with TMPAE compositions of 0.05, 0.3, and 0.7 exhibited

average 72 h percent cell viabilities of 93.5% ± 0.7, 93.8% ± 0.8, and 93.8% ± 1.9, while

the control exhibited a cell viability of 98.8% ± 0.7.
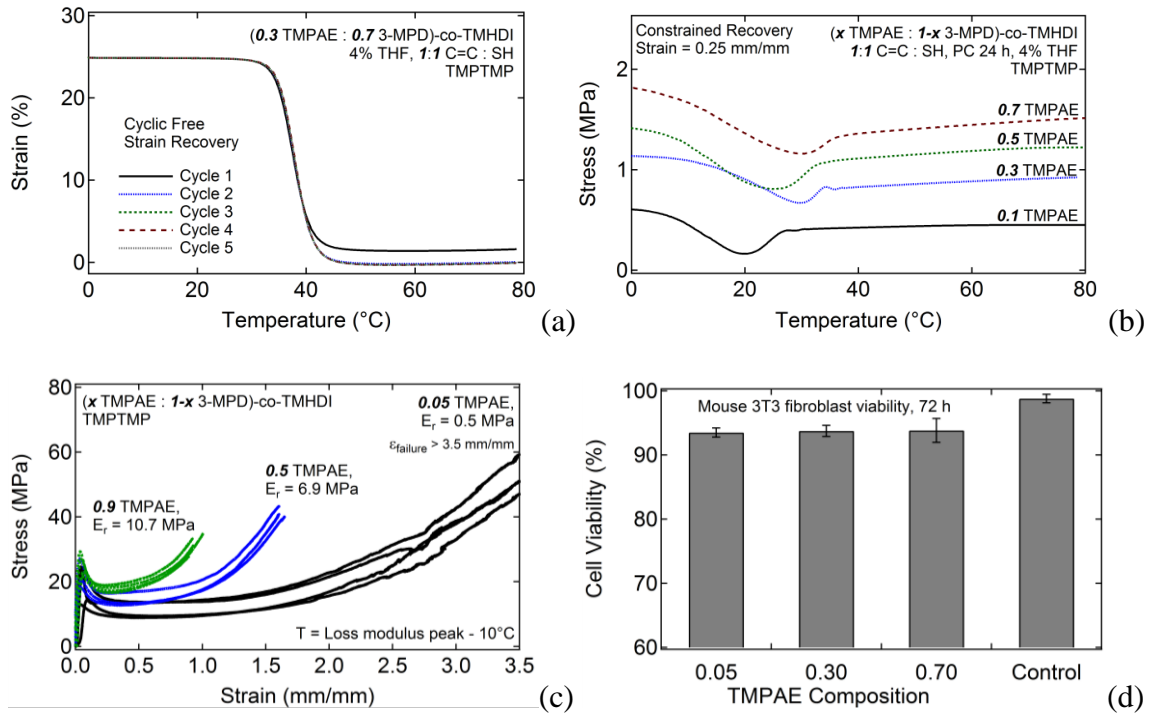
Figure 36- Materials characterization data demonstrating the material advantages of this polymer system. (a) 5-cycle free strain recovery shape memory characterization results for (0.3 TMPAE : 0.7 3-MPD)-co-TMHDI SMP; (b) constrained recovery for samples with increasing TMPAE composition; (c) Strain-to-Failure results for thiol-ene crosslinked PU SMP samples made from TMHDI and varying ratios of TMPAE and 3-MPD (i.e., varying C=C composition); (d) Biocompadability reesults showing mouse 3T3 fibroblast viabilies greater than 93% were observed for TMPAE-0.05, TMPAE-0.3, and TMPAE-0.7 thiol-ene crosslinked polyurethanes for 72 h studies.

4. SMP Microgripper Device Fabrication and Characterization Results

Approximately 6 out 10 devices made were acceptable to use as a microgripper.

The main failure mode of fabrication was an off center optical fiber. If the optical fiber

174

protruded from the SMP cylinder it would result in device failure due to heating when the laser was activated. This problem could be rectified by using a Teflon spacer with an ID equal to the OD of the fiber and an OD equal to the ID of the capillary tube. Our spacers did not have these precise dimensions, leading to variability between samples.

In order to approximate the maximum forces to which the microgripper can be subjected during microcatheter delivery of endovascular devices, a tensile testing experiment to measure device gripping force was set up in an MTS tensile testing system and is pictured in Figure 37(b). Using the immersion chamber of the MTS system, strain-to-failure experiments were carried out on seven devices in water at 37°C. Figure 37(c) shows a table of gripping force at failure values for each of seven devices tested, and the average gripping force was 1.43 ± 0.37 N. Figure 38(a) and (b) show the experimental setup for the PDMS vascular model that was used for *in vitro* microcatheter delivery experiments, and Figure 38(c) shows images of a successful *in vitro* device deployment triggered by laser actuation through a fiber optic cable run through a microcatheter. *In vitro* measurements were carried out within a flow loop held at 35.5°C and flow at 192mL/min. To actuate the gripper, it was irradiated through the optical fiber using an 808nm diode laser (Jenoptik AG, Jena, Germany). A successful device delivery rate of 100% was observed for five microgripper devices laser actuated *in vitro*. Figure 38(d) shows a high-resolution image an a laser actuated device taken under a microscope under immersion conditions at 25°C.

(a)

MTS Tensile Grip

Nitinol wire

37°C Water Immersion Chamber

Thermocouple lead

Crimped SMP Device

Optical Fiber
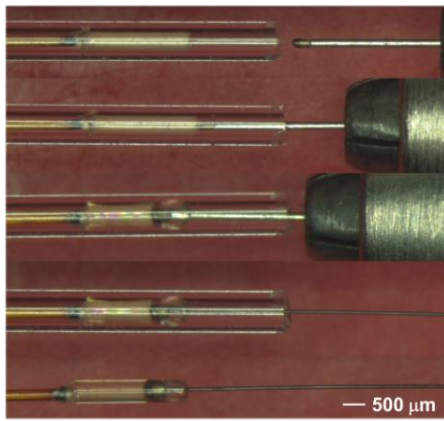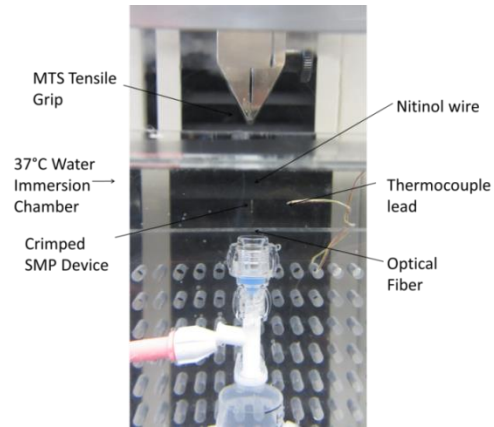
(b)

Device	Max Stress (N)
1	1.75
2	1.86
3	1.30
4	1.75
5	1.34
6	0.90
7	1.10
Average	1.43 ± 0.37

(c)

Figure 37- (a) Crimping process for SMP microgripper device; (b) Tensile testing setup for crimped microgripper devices; (c) maximum and average stresses for seven crimped devices subjeced to strain-to-failure experiments for the devices tested using the setup in (b).

(a)

(b)

(c)

(d)
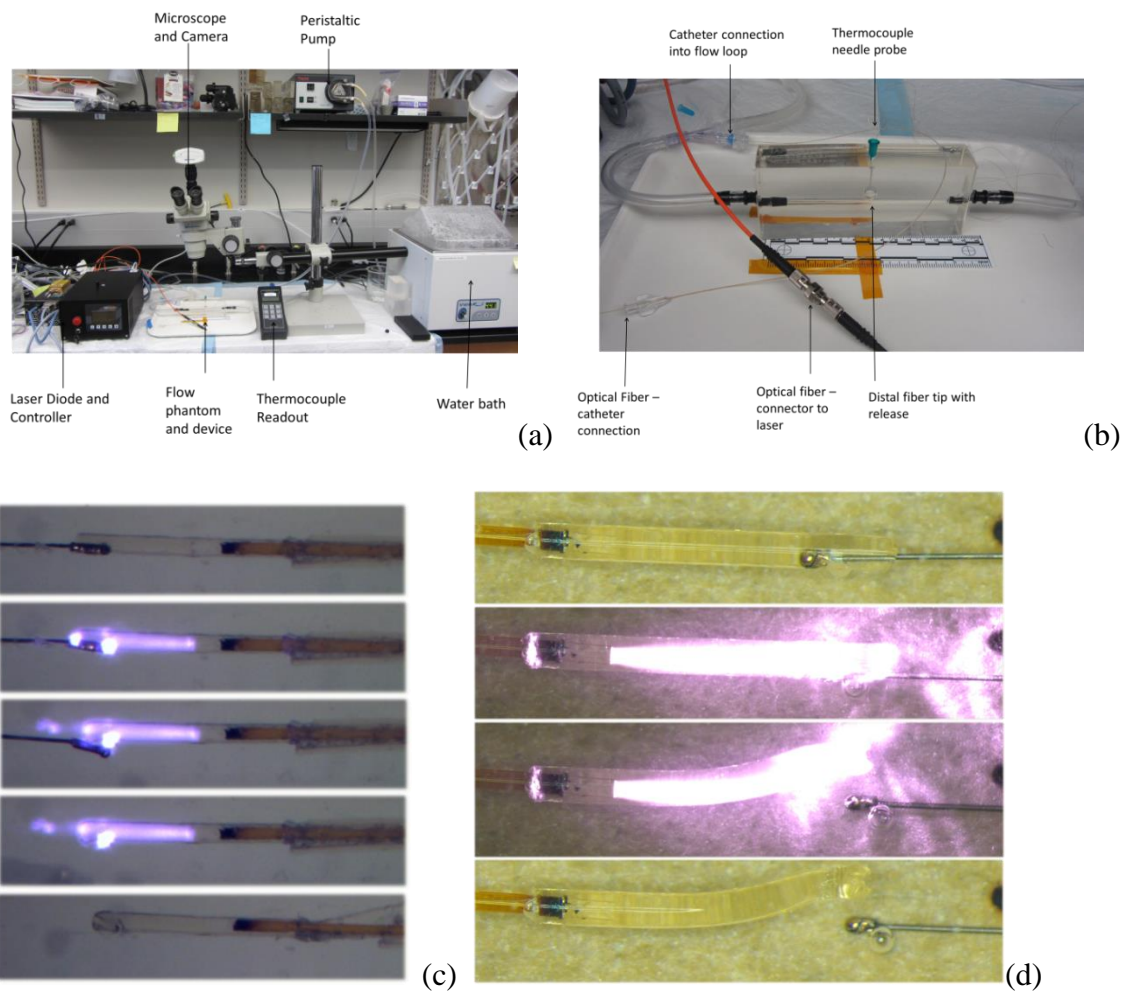
Figure 38- (a) Illustration of setup for *in vitro* microcatheter delivered microgripper deliver experimental setup; (b) photographs of *in vitro* actuation of microcathether delivered device (c) Images of *in vitro* actuation of microgripper device; (d) microscope images of microgripper device

D. Discussion

The ability to achieve a variety of material properties upon crosslinking a single thermoplastic formulation is a synthetic advantage of this material system, as it provides synthetic flexibility at the materials level to the process of medical device fabrication. The ability to control rubbery modulus by varying solvent composition represents an

interesting synthetic concept. Because this decrease in crosslink density with increasing solvent composition most likely occurs because solvent dilution of reactants decreases conversion of reactive species and effectively causes unreacted thiols to remain in the final crosslinked materials, if solvent dilution is to be seriously considered as a means of tailoring mechanical properties, stress-strain and shape memory behavior should be evaluated for these materials, as well as biocompatibility, which may be influenced by the presence of increased residual thiol functionality. The difunctional thiol crosslinker affords what appears to be a very lightly crosslinked network, and rubbery modulus is shown to be tailorable over an order of magnitude in value by varying polythiol crosslinker functionality for a single thermoplastic. Varying polythiol crosslinker functionality thus provides an additional aspect of synthetic flexibility that can enable the fabrication of devices with varying material properties that are controlled completely by synthetic procedures that are carried out at the post-polymerization step.

E. Conclusions

In comparison with the electron beam crosslinked SMP systems reported in Chapters IV to VI, the UV curable thiol-ene crosslinked SMP system possesses advantages in the areas of practical utility and time required for fabrication. Instead of requiring researchers to wait for samples to be irradiated at what is most often and likely an external facility, the thiol-ene crosslinked system allows for synthesis and curing of polymers and devices in a facility that is equipped with the resources generally characteristic of a polymer synthetic research laboratory.

F. Acknowledgements

CHAPTER VIII

GREEN SMP FORMULATIONS: NATUALLY-DERIVED SMPS FOR A

SUSTAINABLE FUTURE*

In accordance with the final design criterion established in this Introduction,

SMP systems built from novel green formulations are reported. The first green SMP

system reported is a poly(thiother-co-carbonate) SMP system derived from the coffee

extract quinic acid, in which glass transition is tunable over the range of 30 to 75°C,

biodegradation rate at physiological conditions is tunable over the range of 10 days to

greater than 60 days, cyclic recoverable strains approaching 100% for samples subjected

to 0.30 mm/mm prestrains were observed, and 72 h mouse 3T3 fibroblast cell viabilities

varying between 80 and 95 % were observed for select formulations subjected to

biocompatibility testing. The second SMP system is prepared using a direct

polymerization of the citrus fruit extract D-limonene and polythiol co-monomers. Upon

addition of recycled polystyrene additives to heated limonene/polythiol monomer

mixtures, homogeneous solutions result, and formation of limonene-*co*-polythiol

networks upon UV curing results in nanocomposite polymers with precipitated PS

microphases, in which modulus at 25°C is tunable from 1 to 600 MPa.

A. Introduction

   As consumer demands drive increased global production of plastic products and waste, the need for innovative strategies for improving environmental sustainability continues to grow. As long as non-environmentally degradable plastics are produced, the development of improved recycling techniques must continue in order to decrease additional material consumption and to reduce non-degradable plastic waste content in landfills.[93] There is hope that progress in polymer science will eventually give rise to alternative plastic materials that may eliminate the need for the production of petroleum-based and other non-degradable plastics altogether, and recent studies have investigated the development of naturally based polymers, such as polycarbonates derived from coffee extracts,[94] terpene-[95] and fatty acid-derived[96] heteropolymers and cellulose-based polymer composites,[97] among others. One drawback that often surrounds sustainable materials development is the seemingly pervasive notion that improving the environmental suitability of materials comes with a sacrifice in material functionality.[98] Studies reporting material selection strategies often weigh material capabilities against environmental sustainability,[99] and recycling processes in general are assumed to bring about some degree of material deterioration.[100] This work is built upon an alternative premise, that the development of new sustainable materials with increased inherent value (i.e., well-engineered, value-driving material properties) is possible through innovative design at the materials engineering level. Two SMP systems are reported. The first SMP system is a poly(thiother-*co*-carbonate) hybrid SMP system that is derived from the coffee extract quinic acid, which exhibits tunable glass transition and biodegradation rate

at physiological conditions. The second SMP system is prepared by the direct polymerization of the terpene citrus fruit extract D-limonene and polythiol co-monomers and combines a breakthrough development in renewable polymer synthesis with a new high-performance recycling solution for petroleum-derived polymeric waste. Upon addition of recycled polystyrene additives to heated limonene/polythiol monomer mixtures, homogeneous solutions result, and formation of limonene-*co*-polythiol networks upon UV curing affords nanocomposite polymers with precipitated PS microphases.

1. A Naturally-Derived SMP System Built from the Coffee Extract Quinic Acid

1.1. Recent Developments in Naturally-Derived Implantable Biomaterials

The development of new biocompatible and degradable polymeric biomaterials provides innovative avenues to achieving advancements in numerous areas of medical research.[101] Recent studies have reported the development of new polymeric systems for tissue engineering applications that have been designed using both naturally occurring polymers such as silk[102] and naturally-occurring monomers such as citric acid[103] and succinic acid.[104] Implantable polymeric systems must exhibit a favorable chemophysiological response upon implantation in the body and must often also exhibit tunability of mechanical and thermomechanical properties in order to meet the material demands of various applications. Two of the most commonly studied orthopedic implantable polymers are poly(lactic acid) (PLA) and poly(glycolic acid) (PGA), which

degrade in physiological environments through hydrolysis of ester linkages[105]. While these polyesters have been shown to be useful in a number of biomedical implant applications,[106] the acidic byproducts that result from hydrolysis in polyesters are believed to have undesirable effects in certain physiological environments. Consequently, polymeric systems that undergo degradation in physiological environments to afford alternative, non-acidic degradation products may be of interest for use in certain biomedical applications.

1.2. Silyl Ether Degradable Linkages

Certain polymeric linkages undergo hydrolytic degradation at significantly more rapid rates than that which is generally observed in polyesters. Polymers that contain labile linkages such as poly(ortho esters)[107] or poly(anhydrides),[108] for example, may undergo degradation on the order of hours to days instead of months, as is often characteristic of polyesters.[109] The hydrolytic degradation behaviors of polymeric systems containing the highly labile silyl ether linkage have also been investigated, and tunable degradation rates have been achieved by synthesizing polymers comprised of varying ratios of highly labile linkages and other less-labile linkages.[110] Silyl ether functionalities are commonly used as protecting groups for alcohols and are readily hydrolyzed to form silanol and alcohol degradation products, which in many cases are not considered to be inherently toxic and do generally not cause significant changes in pH in surrounding environments. To afford rapidly hydrolizable polymeric systems with tunable degradation rates that can be readily cured in a facile manner in bulk to

183

accommodate potential industrial processing requirements, silyl ether linkages have been incorporated into a variety of multifunctional acrylic monomers.[111] More recently, the synthesis of multifunctional thiols containing silyl ether linkages was achieved through the selective condensation of the alcohol group of mercaptoalcohols with chlorosilanes. These monomers may be useful in the synthesis of degradable poly(silyl ethers) that can be readily synthesized through the facile reactions of thiols with alkenes.

1.3. Polycarbonate Degradable Linkages and Quinic Acid

When carbonate linkages undergo hydrolysis in physiological environments, the resulting degradation products are alcohols and carbon dioxide instead of the acids that generally result from hydrolytic degradation of polyesters. The less acidic degradation products of polycarbonates may offer certain advantages over the more acidic degradation products of polyesters, including decreased degradation rate and reduced inflammatory response of native tissue.[112] If synthetic strategies are employed such that polycarbonates are built from naturally-occurring functional precursors, degradation of these polycarbonates can result in the re-formation of the original building block molecules. Consequently, it is possible to design degradable polycarbonates that produce bioactive products upon degradation. One such naturally-occurring building block is quinic acid (QA), a polyhydroxyl compound found coffee beans and other plant products[113] that is metabolized by intestinal microflora to afford tryptophan and nicotinamide[114] and possesses growth promoting properties.[115] In a previous study, the synthesis of poly(quinic acid carbonate)s was investigated by copolymerization of

184

tert-butyldimethylsilyloxy-protected 1,4- and 1,5-diol monomers of quinic acid and

phosgene.[94] Although these thermoplastic polymers exhibited glass transitions greater

than 200°C, they possessed extremely poor mechanical integrity, which likely resulted

from limited molecular weights and incomplete deprotection after polymerization.

1.4. Quinic Acid-Derived Networks with Tunable Thermomechanical Properties and Degradation Rate

To improve the mechanical integrity of the quinic acid-derived polycarbonate

mentioned in 1.3, the synthesis of crosslinked quinic acid-based polycarbonate systems

is reported in this study. A quinic acid lactone was modified to produce the tris(alloc)-

quinic acid (TAQA) alkenyl monomer shown in Scheme 8, and amorphous three-

dimensional networks were achieved by photo-catalyzed thiol-ene chemistry upon

polymerization with the multifunctional thiols also illustrated in Scheme 8.

Scheme 8- Synthetic strategy for quinic acid derived SMP system. Predicted degradation rate is carbonate (red) < ester (blue) << silyl ether (green).
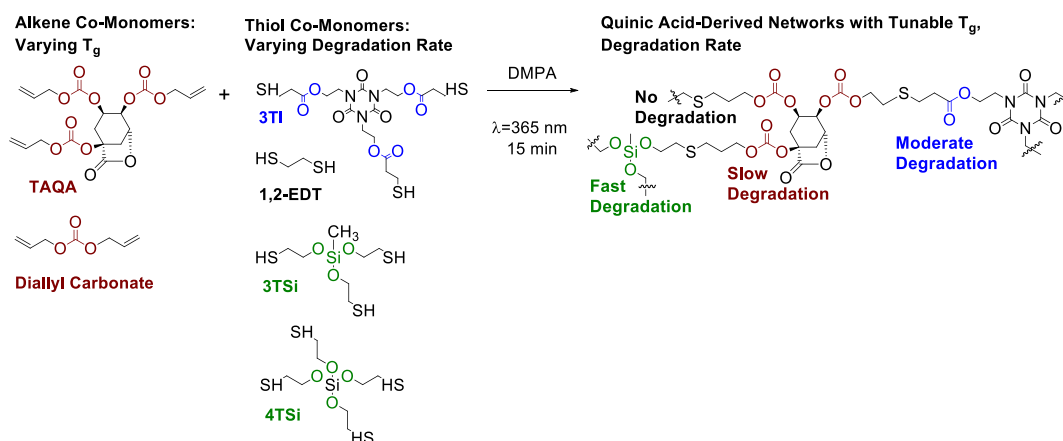
2. A Naturally-Derived SMP System Built from D-Limonene with Utility as a High-Performance Recycling Solution for Polystyrene

We report a novel approach to sustainable materials development that is based upon a new strategy for thermoplastic polymer recycling with a notable advancement in renewable polymer synthesis. By combining petroleum-derived polymers with bio-based monomer feedstocks, biphasic, blended polymer products are produced and are shown to exhibit facile tunability of physical and material properties. This one-pot, solvent-based recycling approach yields neat recycled products without the use of solvent evaporation or solute precipitation, and the functional utility of the resulting polymer blends greatly exceeds that of either homopolymer alone.

2.1. Motivation and Background for Development of a Limonene-Derived Polymer System

Thiol-ene "click" chemistry is a powerful synthetic tool that is being implemented in increasingly diverse areas of polymer science.[116] The reaction between C=C and SH functional groups, which is often UV catalyzed but can also proceed under elevated temperature conditions, is highly efficient, tolerant of many functional groups, and capable of proceeding under mild conditions.[89] A number of network polymers have been prepared from polyfunctional alkene and polythiol monomers and utilized in applications ranging from medical to commodity devices.[82] D-Limonene, shown in Scheme 9, consists of two C=C groups and is, theoretically, capable of functioning as a monomer in thiol-ene polymerization reactions with a co-monomer such as

186

trimethylolpropane tris(3-mercaptopropionate) (TMPTMP). A poly(thioether) network synthesized from D-limonene would thus be, by definition, derived from a naturally-occurring precursor. We observed that at temperatures near 25 °C, D-limonene and TMPTMP mixtures are immiscible, although brief 365 nm UV irradiation and/or heating eventually results in the formation of a homogeneous solution that can be transferred to a mold without further network formation occurring until subsequent exposure to UV irradiation. Previous studies have reported the synthesis of polymers through multi-step processes in which D-limonene is first functionalized and then subjected to various methods of polymerization,[117, 118] and in a recent study, the reactivities of the double bonds in limonene with various thiol groups are reported.[119] However, to our best knowledge, none of these studies has reported the bulk thiol-ene polymerization and thermomechanical characterization of a network polymer consisting solely of D-limonene and a polythiol co-monomer. The ester linkages in TMPTMP also afford the synthesis of a poly(thioether) network that is biodegradable, and Claudino, *et al*. have noted this concept and proposed the use of limonene-*co*-poly(mercaptopropionate) networks as synthetic materials for degradable tissue scaffolds.[119]

Scheme 9- Synthetic approach for the preparation of poly(thioether) networks derived from D-limonene and the polythiol TMPTMP
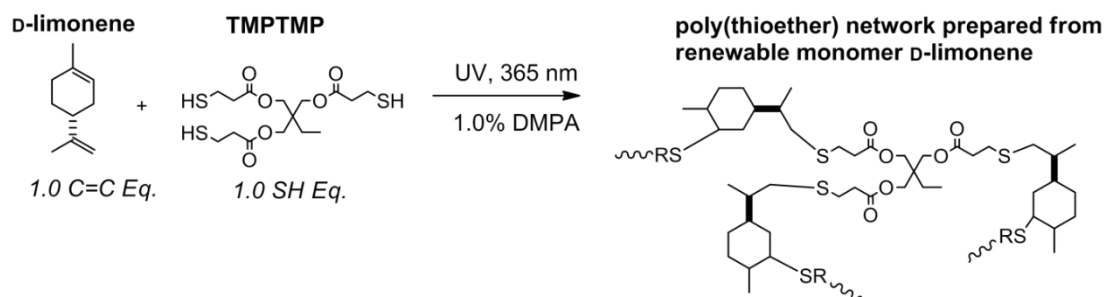
2.2. **Motivation and Background for a High Performance Recycling Solution for**

Polystyrene

Reported herein is a new method for recycling polystyrene (PS), in which special

consideration is given to expanded polystyrene (EPS) waste used in food and beverage

packaging applications. The primary novelty in the present study stems from the idea

that D-limonene can both dissolve polystyrene and can also function as a diene monomer

in thiol-ene reactions to enable a new method of PS reclamation from solution. The

difficulties associated with EPS recycling have been widely publicized. It is estimated

that over 3 million tons of EPS are produced each year globally, with roughly 70% of

EPS products being single-use food and beverage packaging.[120] Because both

transporting low-density EPS waste and cleaning it to remove contaminant residue

greatly increase cost and time required for EPS recycling, an overwhelming majority of

food-contaminated EPS waste is not recycled.[121] EPS recycling is often sub-categorized

using three groups: (1) material recycling, the reduction of EPS volume using

compression or dissolution in solvent; (2) chemical recycling, the breaking of covalent

188

bonds to re-generate monomers or other small molecules; and (3) thermal recycling, the combustion of EPS waste to generate energy.[122] The simplest and most common method of recycling EPS is material recycling by mechanical compaction, and mechanical EPS densifiers are commercially available from multiple sources.[123] Since mechanical densifiers require that EPS be contaminant free before compaction, mechanical densification is not ideal for recycling food or drink contaminated waste items. Solvent-based material recycling has been shown to be tolerant of some contaminated EPS substrates because many contaminants are insoluble in solvents that dissolve EPS and can be removed using coarse filtration after EPS dissolution.[124] The solubility and behavior of EPS in multiple solvents has been previously reported.[125] Polystyrene has been shown to be soluble in aromatic solvents such as toluene, and studies have also reported the solubility of PS in the naturally occurring citrus fruit extract D-limonene,[126] which has a similar dielectric constant to that of toluene.[126, 127] In the late 1990's and early 2000's Sony Corporation instituted a solvent-based recycling effort in Japan, in which D-limonene was used to recycle EPS waste, which was reclaimed from solution by evaporation of D-limonene. Sony's report of this recycling process is extremely in-depth, but this recycling effort appears to have been abandoned sometime between 2004 and 2006.[128] Considering the low inherent value of recycled polystyrene, Sony's apparent decision to cease this recycling effort may have been financially motivated. Other studies have reported limonene-based recycling processes in which PS is reclaimed from solution in limonene using electrospinning[129] or by precipitation by mixing with supercritical carbon dioxide.[130]

Because of the flexible nature of the thioether linkage, many poly(thioether) networks are elastomeric and possess poor mechanical integrity at and above 25 °C.[22] Such elastomeric behavior was predicted for the D-limonene-based network homopolymer whose synthesis is shown in Scheme 9 and was observed upon neat polymer synthesis and handling. The addition of PS additives to this poly(thioether) network was predicted to increase modulus and improve toughness and mechanical strength, and the synthesis of biphasic polymer blends comprised of PS additives dispersed in limonene-co-polythiol networks was therefore attempted both to improve network mechanical integrity and to demonstrate a new method of PS recycling. It is well-known that the functional utility of PS can be increased by the synthesis of PS/rubber blends or co-polymers, and high impact polystyrene (HIPS) can be prepared by dissolving a thermoplastic such as polybutadiene in styrene and curing the solution to produce biphasic materials. These polymers possess improved mechanical strength and toughness in comparison with that of PS.[131] Other studies have reported the synthesis, microstructural imaging, and thermomechanical characterization of other thermoset/thermoplastic heteropolymer blends, including PMMA, PS and polyurethane additives in polyester network matrices[132] and polyetherimide additives in epoxy network matrices.[133] To our best knowledge, a polymer blend comprised of a thermoplastic additive dispersed in poly(thioether) matrix has yet to be reported.

We synthesized blended polymers containing recycled PS additives dispersed in D-limonene-*co*-polythiol network matrices to create a series of polymer blends with greater toughness than either homopolymer exhibits individually. D-Limonene functions

simultaneously as a solvent for dissolving polystyrene (PS) waste and as a monomer that

undergoes UV-catalyzed thiol-ene polymerization reactions with polythiol co-monomers

to afford polymeric products comprised of precipitated PS phases dispersed throughout

elastomeric poly(thioether) networks. By varying PS additive composition, we sought to

achieve tailorability of microstructural morphology, modulus, toughness, tensile strength

and strain capacity in order to demonstrate a broad application range for the new

material system. We believe that this work marks the first instance in which the

successful bulk synthesis and mechanical characterization of network polymers

comprised solely of D-limonene and polythiol co-monomers are reported in the

literature, and the demonstrated synthetic utility of this naturally-derived polymer system

as a new PS recycling strategy provides a unique materials-based avenue to achieving

environmental sustainability, while combining non-renewable and renewable materials

to produce blended networks that exhibit remarkable mechanical properties.

B. Materials and Methods

1. Quinic Acid-Derived SMP System

1.1. Synthetic Strategy, Monomer and Polymer Synthesis

1.1.1 Materials

TAQA was kindly provided by the group of professor Karen L. Wooley in the

Department of Chemistry at Texas A&M University. The silyl ether polythiols whose

synthesis is shown in Scheme 10 were kindly provided by the group of professor David

Son in the Department of Chemistry at Southern Methodist University. The

photoinitiator 2,2-dimethoxy-2-phenylacetophenone, the polythiols 1,2-ethanedithiol and

3TI, and the diene diallyl carbonate were purchased from Sigma Aldrich and used as

received without purther purification.

1.1.2   General Procedure for Fabricating Thiol/TAQA films

Mixtures of multifunctional thiol and TAQA were prepared based on equal molar

functional groups. The amount of photoinitiator, DMPA, was 1 wt% for each mixture.

DMPA was first dissolved in the multifunctional thiol and then TAQA was added and

blended thoroughly. Each mixture was cast between two glass slides separated by a 0.5

mm spacer, and exposed to UV light (365 nm) on a Fusion curing line system (1 m/min,

15 min). The glass slide molds were removed, and the free-standing films were post-

cured at 120 °C for 4 h or as otherwise noted. Formulations are provided in Table 11.

Scheme 10- Synthetic route for custom-synthesized silyl ether-containing polythiol monomers
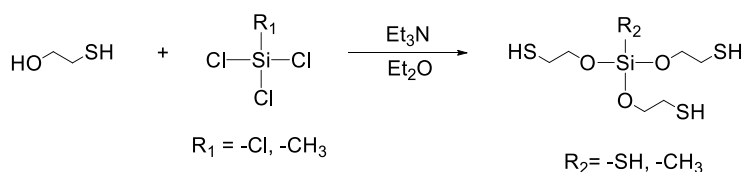
Table 11- Formulations for Quinic Acid-Derived SMPs.

Sample Identity	Eq. TAQA	Eq. DAC	Eq. 1,2-EDT	Eq. Thiol 2
TAQA-1.00	1.000	-	1.000	-
TAQA-0.75	0.750	0.250	1.000	-
TAQA-0.70	0.700	0.400	1.000	-
TAQA-0.50	0.500	0.500	1.000	-
TAQA-0.25	0.250	0.750	1.000	-
TAQA-0.10	0.100	0.900	1.000	-
3TI-1.00	1.000	-	-	1.000
3TSi-1.00	1.000	-	-	1.000
4TSi-1.00	1.000	-	-	1.000

1.1.3 Degradation Measurements

Samples subjected to degradation measurements consisted of ~10 mg laser machined cylinders 3 mm in diameter and 1.2 mm tall. The dry mass of each sample was measured and recorded with a balance with 0.01 mg precision. Equilibrium mass was measured by weight change after Each sample was individually immersed in 2 mL phosphate buffered saline at 37 °C for the recorded amount of time. At each desired time point each sample was removed from the PBS, and the surface of the polymer was gently dried using an absorbent wipe. The equilibrium mass was then recorded. Equilibrium mass change is calculated as the mass change from original mass to swollen/degraded mass normalized to the original mass. Each sample was then dried at 120 °C at a pressure of -635 mTorr on a PTFE sheet to constant mass, approximately 4 hour. Each sample was then re-massed. Mass loss is calculated as the mass change from the original mass to mass after drying normalized to the original mass. The water content in the network is calculated as the difference between equilibrium mass and dried mass

normalized to the original mass. Data reported are the average of 3 samples at each time point. Error bars represent the standard deviation.

2. Limonene-Derived SMP System

2.1. Polymer Synthesis

Functional equivalents totaling 10 g of D-limonene (TCI America, >95%,) trimethylolpropane tris(3-mercaptopropionate), pentaerithritol tetrakis(3-mercaptopropionate) (Sigma Aldrich, >95%), and/or dipentaerithritol hexakis(3-mercaptopropionate) (Wako, >97%) were massed in glass vials, and 1 wt% 2,2'-dimethoxy-2-phenylacetophenone (DMPA) (Sigma Aldrich, >99%) photoinitiator was added. EPS powder, which was ground from EPS cups provided by Chick-fil-A, Inc. (CFA), was added to the monomer mixtures in varying quantities so as to formulate mixtures with polystyrene compositions of 0, 10, 20, and 30% overall weight fraction. The monomer and EPS mixtures were not miscible initially and were heated to 140°C for 2 h, after which the formation of homogeneous solutions occurred. The resulting solutions exhibited viscosity increases with increasing EPS composition. Neat films were cast by injecting the hot solutions inside glass molds pre-heated to 140°C. The injections were carried out inside a vacuum oven heated to 140°C. The hot glass molds were then immediately removed from the oven, placed in a UVP CL-1000L 365 nm UV crosslinking chamber, and exposed to 365 nm UV irradiation for 1 h. Within 10-20 seconds of UV exposure, the clear homogeneous solutions inside the glass molds began

194

to turn white, apparently undergoing polystyrene phase separation brought on by either poly(thioether) network formation, cooling temperatures, or both factors. The resulting films became completely white within 1-2 min. After 1 h, the cured films were post-cured at 130°C at 1 torr for 24 h. Without polystyrene, the poly(thioether) networks were amorphous, optically clear rubbers, and the addition of PS resulted in the formation of opaque materials.

2.2. Polystyrene Molecular Weight Characterization

To determine the average molecular weight of EPS samples taken from EPS CFA cups, gel permeation chromatography (GPC) measurements were conducted using a tetrahydrofuran GPC system equipped with a Waters Chromatography (Milford, MA) model 1515 isocratic pump, a model 2414 differential refractometer, and a three-column set of Polymer Laboratories (Amherst, MA) Styragel columns (PL$_{gel}$ 5 µm Mixed C, 500 Å, and 104 Å, 300 _ 7.5 mm columns). The system was equilibrated at 35 °C in tetrahydrofuran, which served as the polymer solvent and eluent (flow rate set to 1.00 mL/min). Polymer solutions were prepared at a known concentration (ca. 3 mg/mL), filtered with a 0.2 micron PTFE mesh filter, and an injection volume of 200 µL was used. Data collection and analyses were performed with Precision Acquire software and Discovery 32 software (PrecisionDetectors). The differential refractometer was calibrated with standard polystyrene materials (SRM 706 NIST). The average M_n, M_w, and PDI were 150 kDa, 396 kDa, and 2.635, respectively.

2.3. Microstructural imaging by scanning electron microscopy

SEM imaging was used to understand the effects of increasing PS composition on microstructural morphology. SEM samples were prepared by immersion of ~100 mg samples in liquid nitrogen for 30 s, cold fracturing by hand, attempted thermoplastic PS phase extraction by immersion of fractured ~50 mg samples in 100 mL dicholoromethane and light vortexing for 48 h using a LabConco RapidVap apparatus at vortex setting 15 and at ambient temperature and pressure, drying of DCM-swelled samples at 50°C at 1 torr for 48 h, and gold sputtering with a Cressington 108 sputter coater, model 6002-8 (Ted Pella, Inc., Redding, CA) for 60 s at a height of 3 cm, prior to imaging. All samples were imaged on the fractured faces at 25, 500, and 3000x magnification using a Hitachi TM3000 Tabletop Microscope (Hitachi High Technologies America, Inc. Nanotechnology Systems Division, Dallas, TX), with a filament current set to 1750 mA. Software used to acquire the images was Bruker Quantax 70 Microanalysis Software package (Bruker Nano GmbH, Berlin, Germany).

2.4. Atomic Force Microscopy

AFM micrographs of the system were taken with an Asylum 3D-SA atomic force microscope operated in tapping mode at 142 kHz, a nominal drive voltage of 500 mV. A silica nitride probe was used with k = 40 N/m (Vista Probes) and a nominal tip diameter of 10-15 nm as reported by the manufacturer. Sample preparation included a fast rinse of the samples (0%, 10%, 20% and 30% PS) with a 25% by volume aqueous ethanol

solution (<5 seconds) followed immediately by drying under a dry, filtered nitrogen gas flow for *ca.* 10 minutes and fixture to a glass slide.

2.5. Dynamic Mechanical Analysis

DMA experiments were performed on triplicate samples using a TA Instruments Q800 Dynamic Mechanical Analyzer in the DMA Multifrequency/Strain mode in tension using a deformation of 0.1% strain, a frequency of 1 Hz, a force track of 150%, and a preload force of 0.01 N. Each experiment was run from -50 to 150°C using a heating rate of 2°C/min on $4.0 \times 25.0 \times 0.75$ mm rectangular samples, which were machined using a Gravograph LS100 40 W CO_2 laser machining instrument.

2.6. Tensile testing

ASTM Type V dog bone samples were machined using a Gravograph LS100 40 W CO_2 laser machining device. All laser machined samples except for the rubbery 0% PS samples were sanded around the edges using 400, 800 grit sandpaper.   Strain-to-failure experiments were conducted at 25°C in a temperature chamber that utilizes forced convection heating on 0% and 30% samples synthesized in this study and on 100% PS samples (McMaster-Carr, $M_w \sim 350$ kDa) on $n \geq 5$ specimens for each sample. There experiments were conducted using an Instron Model 5965 electromechanical, screw driven test frame equipped with a 500 N load cell and 1 kN high temperature pneumatic grips.   An Instron Advanced Video Extensometer with a 60 mm field-of-view lens optically measured the deformation of the samples by tracking parallel lines

applied at the ends of the gauge length. The samples were heated to 25°C under zero

load (unclamped bottom grip). The temperature was held for 10 min to allow for

thermal equilibrium to be reached, after which the bottom grip was clamped, and then

experiments were started thereafter using a deformation rate of 10 mm/min. Data were

recorded using Instron Bluehill 3 software.

2.7. Cellular Phone Protective Case Prototype Fabrication

A positive mold with geometric dimensions approximately representative of

those of a protective case made to fit an Apple iPhone 4™ cellular device was designed

using SolidWorks software. Using a Stratasys Fortus 360mc 3D printer, positive molds

were printed using the Stratasys base-soluble resin. Each printed positive molds was

then placed in pre-assembled 2"× 6"× 4" acrylic molds and attached to the bottom of the

mold using super glue. Pre-mixed silicone Sylgard 184™ base and curing agent were

then poured over the printed molds and evacuated at 1 torr at 25°C for 5 min, after which

a smooth surface layer was observed. The silicone mold was then cured at 50 C for 4 h.

The printed resin was dissolved out of the silicone mold by etching in 0.1 N NaOH

solution using the Stratasys base bath for 72 h. The resulting silicone mold contained a

negative image of an Apple iPhone 4™ case. This silicone mold and 50 g of functional

equivalents of limonene and TMPTMP with 30 wt% PS additive were pre-heated to

140°C for 2 h. The dissolved PS solution was then poured in the oven into the silicone

mold. The molded solution was then moved into a UVP CL-1000L 365 nm UV

crosslinking chamber, exposed to UV irradiation for 1 h, and post-cured at 130°C at 1 torr for 24 h.

C. Results

1. Quinic Acid Derived SMP Results

1.1. Dynamic Mechanical Analysis Results

Dynamic mechanical analysis results for all QA-derived SMPs indicate that covalent networks formed during UV-catalyzed thiol-ene polymerizations. For the DMA results showing plots of storage modulus and tangent delta versus temperature for the varying diallyl carbonate series shown in Figure 39(a) and (b), glass transition is shown to be tailorable from approximately 35 to 75°C as diallyl carbonate composition is increased from 0.00 to 0.50 mole % alkene co-monomer fraction. For the DMA results showing plots of storage modulus and tangent delta versus temperature for the varying polythiol/varying biodegradability series provided in Figure 39(c) and (d), shear rubbery modulus values varying from 3.1 to 7.9 MPa and glass transition temperatures varying from 41 to 75°C are observed.
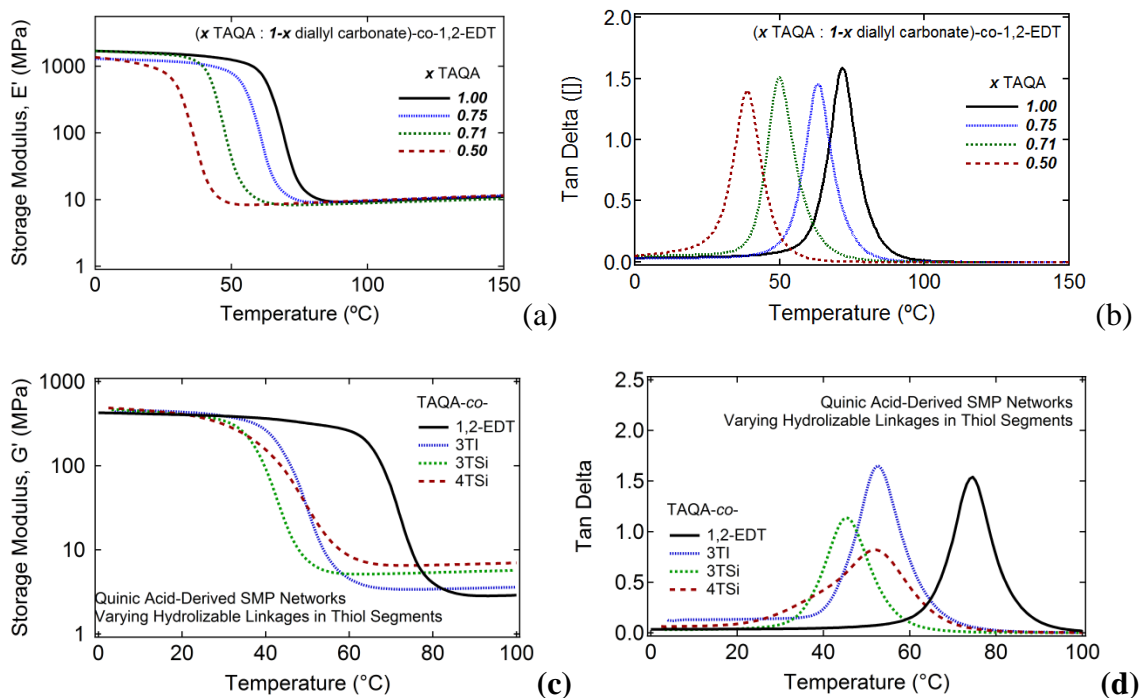
Figure 39- DMA results for Quinic acid-derived SMP system

1.2. Degradation and Water Uptake Results

The degradation and moisture uptake data for the TAQA-co-varying polythiol series whose DMA data are provided in Figure 39(c) and (d) are shown in Figure 40. As shown in Figure 40(a) and (c), over a 40-to-60 day time period, degradation in physiological conditions (37°C PBS) increased as TAQA-co-polythiol monomer composition varied from 1,2-EDT (no hydrolysable internal linkages) to 3TI (ester internal hydrolysable linkages) to 3TSi/4TSi (silyl ether internal hydrolysable linkages). The silyl ether-containing formulations are the only formulations that exhibited full degradation over the course of the 40-to-60 day degradation period. As shown in Figure

40(b) and 40(d), absorbed water content varied from approximately 0.00 to 3.80 g/g with

varying polythiol co-monomer composition.
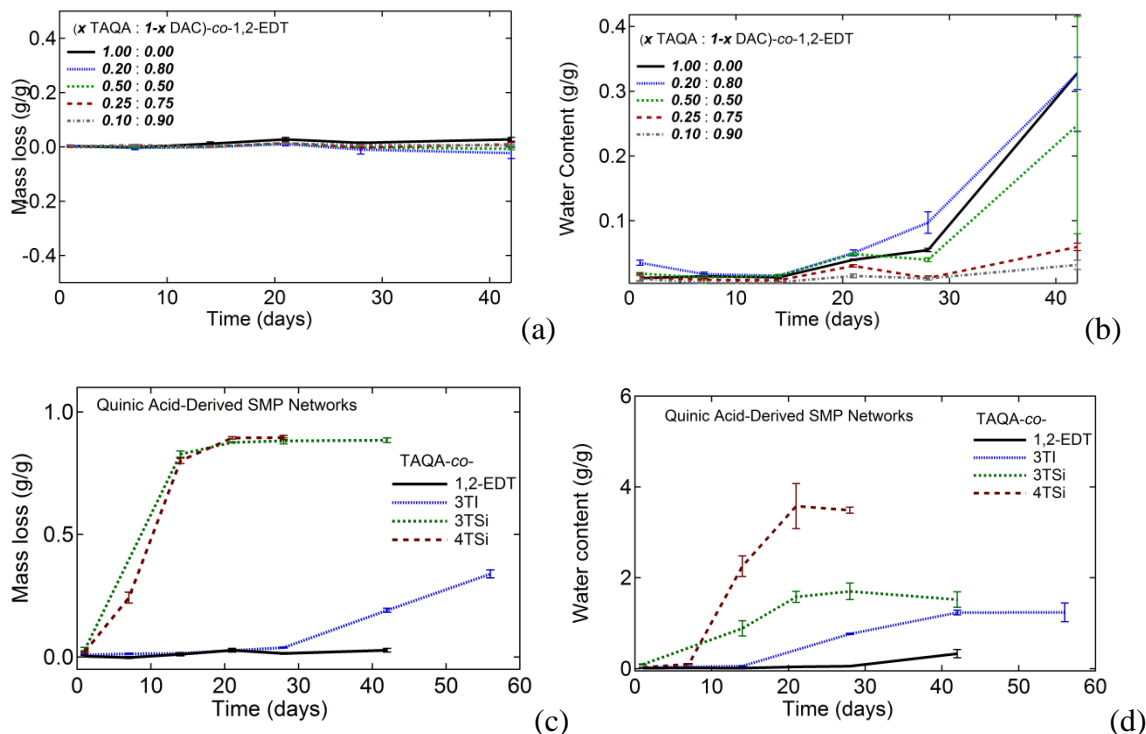
Figure 40- Water uptake and degradation data for varying alkene system and for varying thiol co-monomer series

1.3. Shape Memory Characterization Results

The tunable glass transitions in the materials in Figure 39 indicate that these

materials are expected to have tunable actuation temperatures when subjected to shape

memory characterization. As shown in Figure 41, good tunable and good cyclic shape

memory behavior during free strain recovery characterization is observed for the varying

diallyl carbonate TAQA-based SMP series. Recoverable strains greater than 99% are

observed after Cycle 1 for five-cycle free strain recovery characterization. A recovery

stress is also observed during constrained recovery experiments.
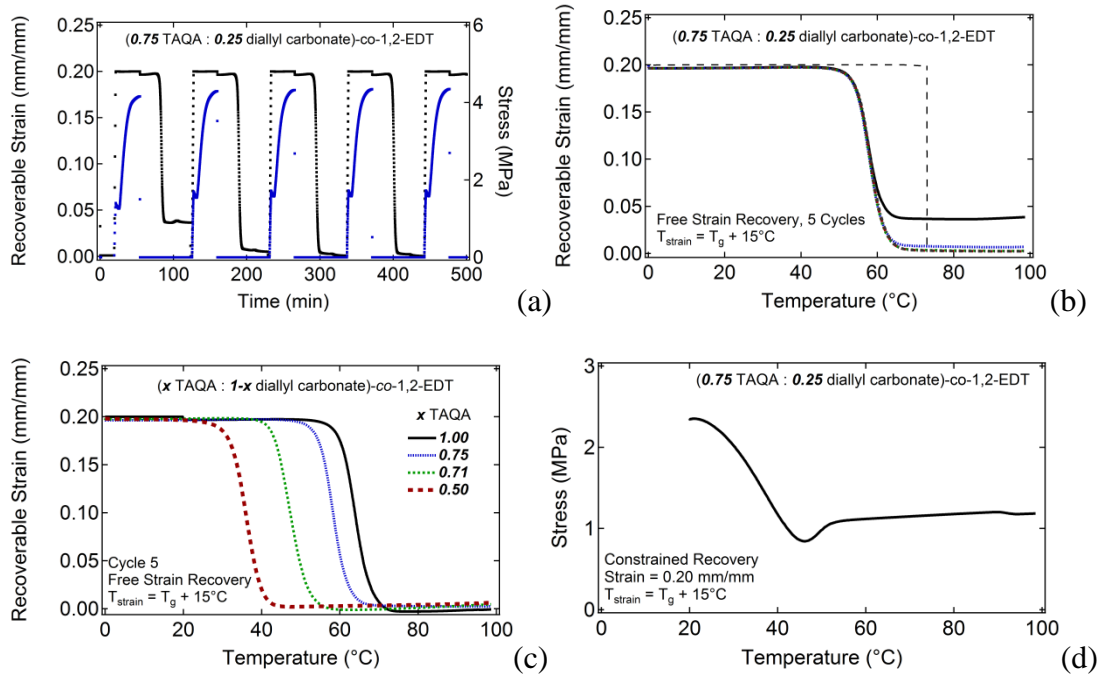
Figure 41- Shape memory characterization data for quinic acid-derived SMP system

1.4. Strain-to-Failure Results

DMA plots of storage modulus, loss modulus, and tangent delta versus

temperature and corresponding stress/strain plots at varying temperatures for TAQA-co-

1,2-EDT SMPs are provided in Figure 42. The tough region of this particular

formulation appears to be near 37°C, and consequently this material may be useful for a

number of engineering biomedical applications that require tough polymeric behavior in

physiological environments.
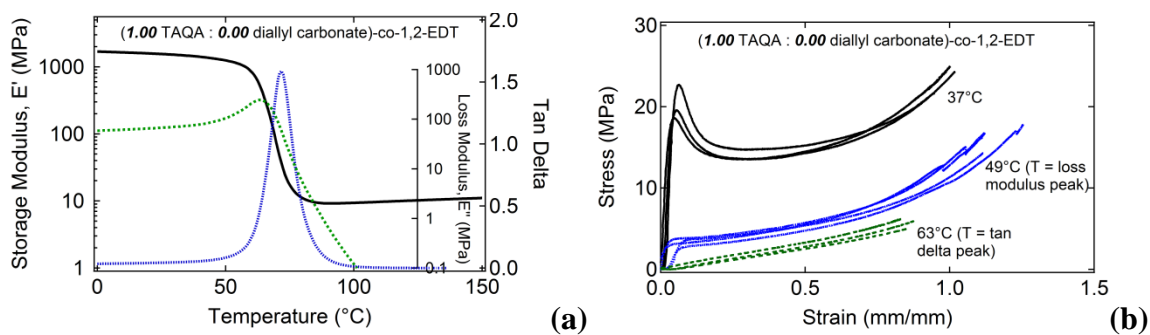
Figure 42- DMA and strain-to-failure results for quinic acid-derived SMP

1.5. Biocompatibility Testing Results

Results for biocompatibility testing for TAQA-based SMPs with varying polythiol co-monomer composition are provided in Figure 43. The biocompatibility data represent 72 h mouse 3T3 fibroblast cell viability testing. Cell viabilities greater than 80% were observed for all formulations subjected to biocompatibility testing.
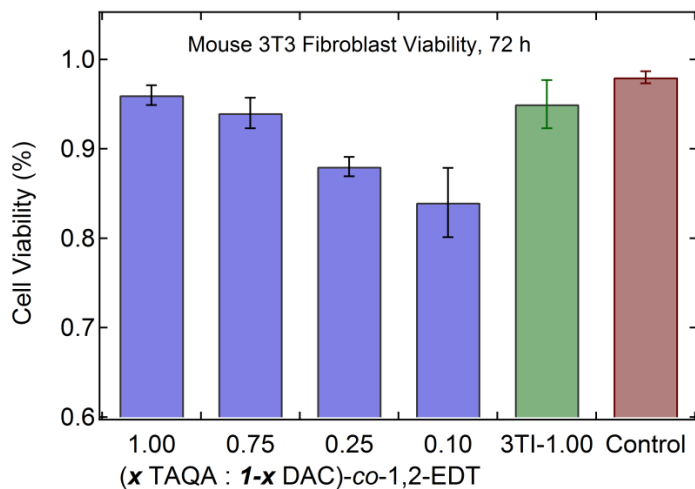
Figure 43- Cell viability data for biocompatibility results for TAQA-based materials

2.1. Purification of Contaminant Waste Results

The novel process reported herein enables the simultaneous densification, purification, and reclamation of food or beverage-contaminated EPS waste. As shown in Figure 44, food or drink-contaminated EPS waste can first be immersed in a reservoir containing D-limonene. After mixing and EPS dissolution in D-limonene, a liquid bilayer forms. In the last image in Figure 44, the bottom layer consists of Coca-Cola™ and the top layer consists of an EPS cup provided by Chick-fil-A, Inc. dissolved in D-limonene (M_w ~ 396 kDa). Through basic extraction, the bottom layer contaminants can be drained, and upon coarse filtration, a purified solution of polystyrene in D-limonene remains.
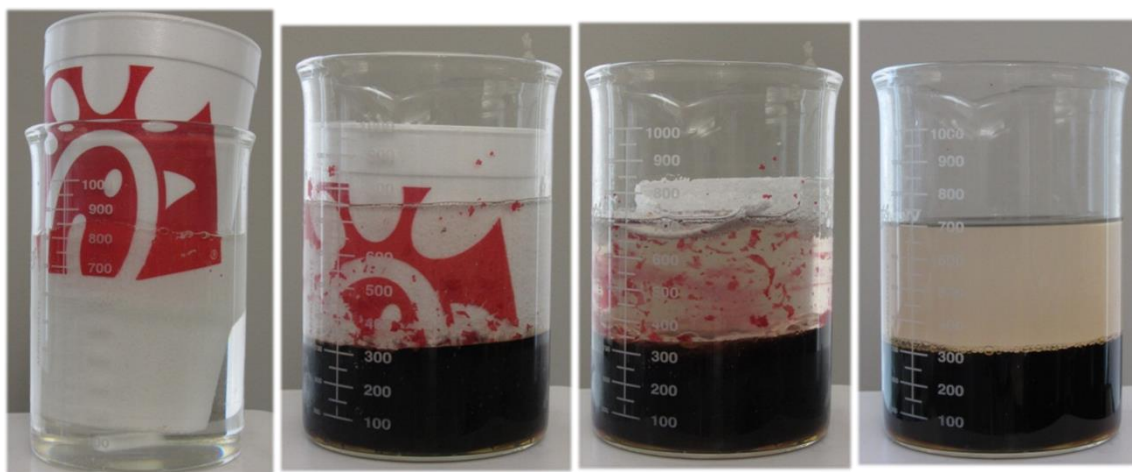
Figure 44- Simultaneous densification and purification of beverage-contaminated EPS waste cup containing 300 mL of Coca-Cola™. The cup completely dissolves in D-limonene, and separation of the Coca-Cola waste contaminant layer from the polystyrene/limonene solution occurs immediately after stirring is stopped

2.2. Qualitative Macroscopic Imaging Results

As shown in Figure 45(a), reclamation of polystyrene is achieved by addition of polythiol co-monomer and photoinitiator and subsequent heating to 140 °C, which results in a homogeneous dissolution of all species. Pouring of this hot solution into a pre-heated mold and subsequent UV irradiation causes the formation of an elastomeric poly(thioether) network, after which phase separation of polystyrene proceeds, producing dispersed polystyrene microphases and/or nanophases throughout the network. Demonstrating the change in optical behavior from transparency to opacity that occurs upon PS heterophase addition to D-limonene-co-polythiol networks, macroscale images of D-limonene-*co*-TMPTMP films containing 0% and 30% PS additives are provided in Figure 45(b). The iPhone 4™ protective case prototype pictured in Figure 45(a) was fabricated to demonstrate the processability of these new materials into a geometry representative of that of a potential industrial application.

Figure 45- Synthetic process for preparing limonene-derived network SMPs with precipitated PS phases

2.3. SEM Results

In order to understand the effects of increasing PS additive composition on microstructural morphology, SEM images of samples containing 0, 10, 20, and 30% overall weight fraction PS were taken and are provided at 3000x magnification in Figure 46. For the SEM images in Figure 46, the samples were prepared by immersion in liquid nitrogen, cold fracturing, attempted thermoplastic PS phase extraction using dichl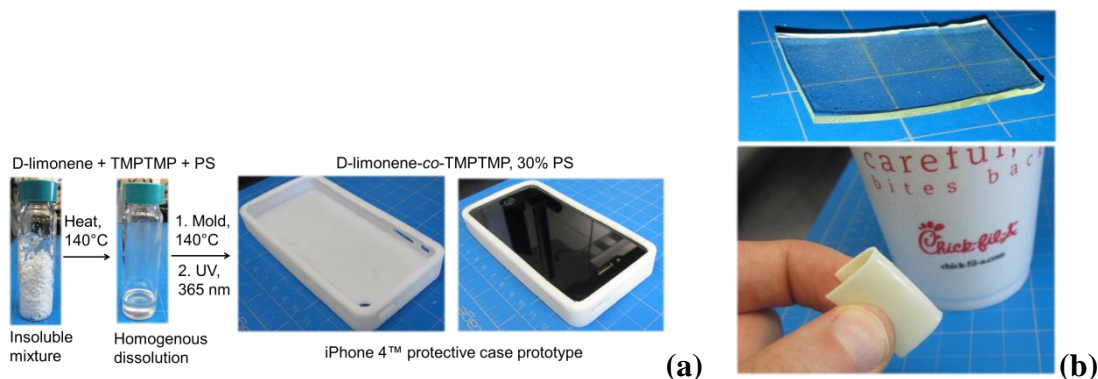oromethane, sample drying, and gold sputtering prior to imaging. Consequently, the more lightly-colored phases in Figure 46 correspond to poly(thioether) networks, and any cavities shown represent empty space that corresponds to extracted thermoplastic PS phases. In general, poly(thioether) network phases appear to decrease in average size with increasing PS composition, although the specific morphologies corresponding to the varying PS phases are notably different in nature. In Figure 46(a), 0% PS shows only a single poly(thioether) phase, and in Figure 46(b), 10% PS shows what appear to be $\sim$3-5 μm sized cavities corresponding to PS phases that were dispersed throughout a network matrix similar to that shown in 46(a). In Figure 46(c), 20% PS appears to have generated a bimodal microstructural morphology with spherical $\sim$3μm network phases and cavities that could correspond to PS microphases of similar size and geometry. In Figure 46(d), the network obtained following extraction of the 30% PS composition appears to exhibit a bimodal microstructure with spherical network and PS phases that are sub-micron in size and of similar homogeneity and distribution to the 20% PS sample in Figure 46(c). Our interpretation of the SEM images is limited to a qualitative assessment to confirm that phase segregation had occurred uniformly throughout the

matrix material, as quantitative interpretation is complicated by potential perturbations to the initial blended networks during the processing steps.

2.4. Atomic Force Microscopy Results

Atomic force microscopy (AFM) of the composite systems at 0, 10, 20 and 30% PS weight fraction were obtained. Topographic maps of the micrographs of the assessed systems are provided at two separate scales, 20 µm × 20 µm and 3 µm × 3 µm and are provided in Figure 46(e). The 3 µm × 3 µm rendering also has phase contrast overlaid to elucidate phase boundaries where present. While generally following the trends observed in SEM, the findings for this series can be summarized as follows: (1) 0% PS displayed a small amount of residual processing residues, exhibited exceptional flatness with shallow pitting (*ca*. 10 nm deep) and had no indication of intrinsic phase boundaries, (2) 10% PS displayed some PS sheeting at the microscale, similar to the gaps observed by SEM and possessed *ca*. 500 nm PS phase domains at smaller scale, (3) 20% PS displayed the largest microscale heterogeneity, exhibited the roughest surface morphology of the samples observed, had pitting and protrusions consistent with the scale of the features observed in the solvent etched PS SEM figures, and displayed microscale phase separation wherein the PS domain expressed smaller sub-domains on scales similar to that observed in the 10% PS system, and (4) the 30% PS sample presented an overall more homogeneous surface on the microscale with periodic large protrusions which appeared to be surface buckling; in the homogeneous regions, fully isolated PS nanodomains (<200 nm) saturated the landscape.
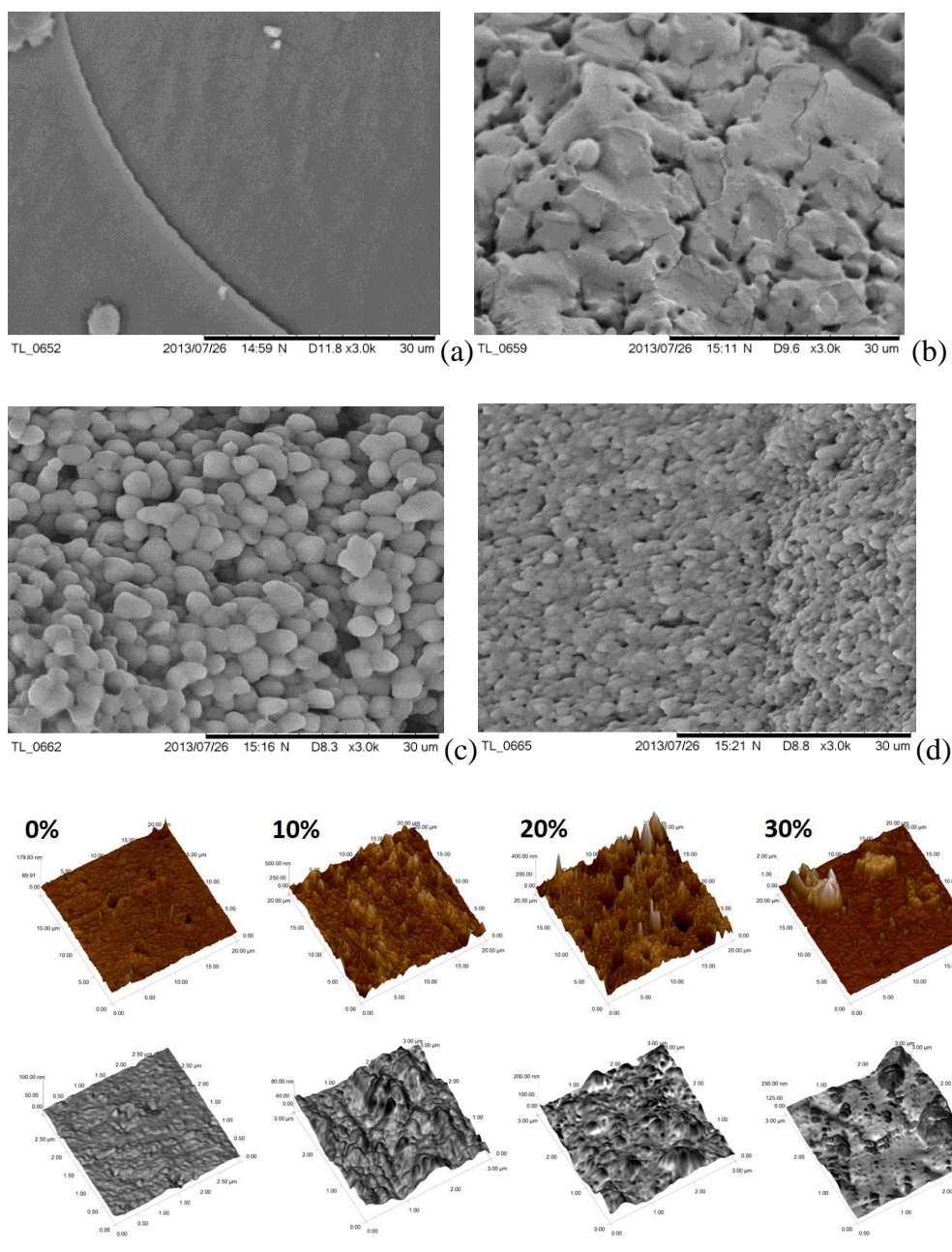
Figure 46- **(a-d) SEM images taken at 3000x magnification showing microstructures of D-limonene-co-TMPTMP networks containing PS weight fractions of (a) 0%; (b) 10%; (c) 20%; (d) 30%. All scale bars are 30 □m. Prior to SEM imaging, samples were immersed in liquid nitrogen and fractured, immersed in dichloromethane to extract the PS phases, dried, and gold sputtered; (e) AFM Micrographs of 0-30% PS wt/wt D-limonene-co-TMPTMP networks. Top: 3D topography for a 20 μm × 20 μm area. Bottom: 3 μm × 3 μm area with topography (3D) overlaid with a grey scale rendering of the phase contrast image (range ±5o in all images).**

208

2.5. Dynamic Mechanical Analysis and Tensile Testing Results

To determine the effects of increasing polystyrene composition on the thermomechanical behavior of the D-limonene-*co*-TMPTMP networks imaged in Figure 46, dynamic mechanical analysis (DMA) experiments were run in tension on 0, 10, 20, and 30 wt% PS samples. Figure 47(a) shows plots of storage modulus *versus* temperature for D-limonene-*co*-TMPTMP, -PETMP, and -DPEHMP networks. The increase in rubbery modulus from TMPTMP to PETMP-based networks as polythiol functionality increases from 3 to 4 is expected and indicates an increase in crosslink density with increased monomer functionality. The lack of an increase in rubbery modulus from PETMP to DPEHMP as functionality increases from 4 to 6 is most likely the result of poor monomer miscibility and high DPEHMP viscosity, which could prevent the reaction of functional groups and prevent network formation. Figure 47(b), 47(c) and 47(d) show DMA characterization data for D-limonene-*co*-TMPTMP networks containing varying PS additive compositions. Plots of (b) storage modulus, E', (c) loss modulus, E'', and (d) tangent delta *versus* temperature for each PS composition are shown, and each PS-containing rubber whose DMA is shown in Figure 47(b-d) exhibits a thermal transition below -10 °C that is consistent with the glass transition of the D-limonene-*co*-TMPTMP poly(thioether) network and also exhibits a thermal transition near 100 °C that is consistent with the glass transition of polystyrene. As polystyrene composition increases, the storage and loss modulus of each sample increase with a clear trend at temperatures between the glass transition of the rubber network and the glass transition of polystyrene. Figure 47(e) shows that both E' and E'' increase

roughly two orders of magnitude at 25 °C as PS composition is increased from 0 to 40%.

The toughening effect that arises from creating a material with combined glassy and

rubbery phases is demonstrated in Figure 47(f), which shows average strain-to-failure

data for 0%, 30% and 100% PS D-limonene-*co*-TMPTMP samples at 25 °C. While the

100% PS material exhibits brittle behavior at 25°C and fails at 1.8% strain and the 0%

PS material exhibits weak elastomeric failure and fails at a stress of 1.2 MPa, the 30%

PS material exhibits a more ductile behavior and fails at 55% strain while also exhibiting

a failure stress greater than 12 MPa. While the average toughness of the 100% PS

sample at 25 °C was 0.34 ± 0.06 MJ/m^3 and that of the 0% PS sample was 0.13 ± 0.02

MJ/m^3, that of the 30% PS sample was 5.03 ± 0.82 MJ/m^3. This increase in toughness at

25°C of more than an order of magnitude in comparison with that of either

homopolymer is promising, and a toughness of ~5 MJ/m^3, while lower than that of

poly(acrylonitrile-*co*-butadiene-co-styrene (ABS) and some other high-performance

HIPS resins reported in the literature, actually exceeds reported toughness values for a

number of HIPS materials.[134] The thermomechanical behavior as a function of PS

fraction, taken in conjunction with the micro- and nano-domain features observed for the

PS phase in this series by SEM and AFM, indicate that the observed toughening for the

30% PS material can be explained by the existence of a high number of nanodomains,

which allow expression of a large surface to volume ratio for the PS fraction.
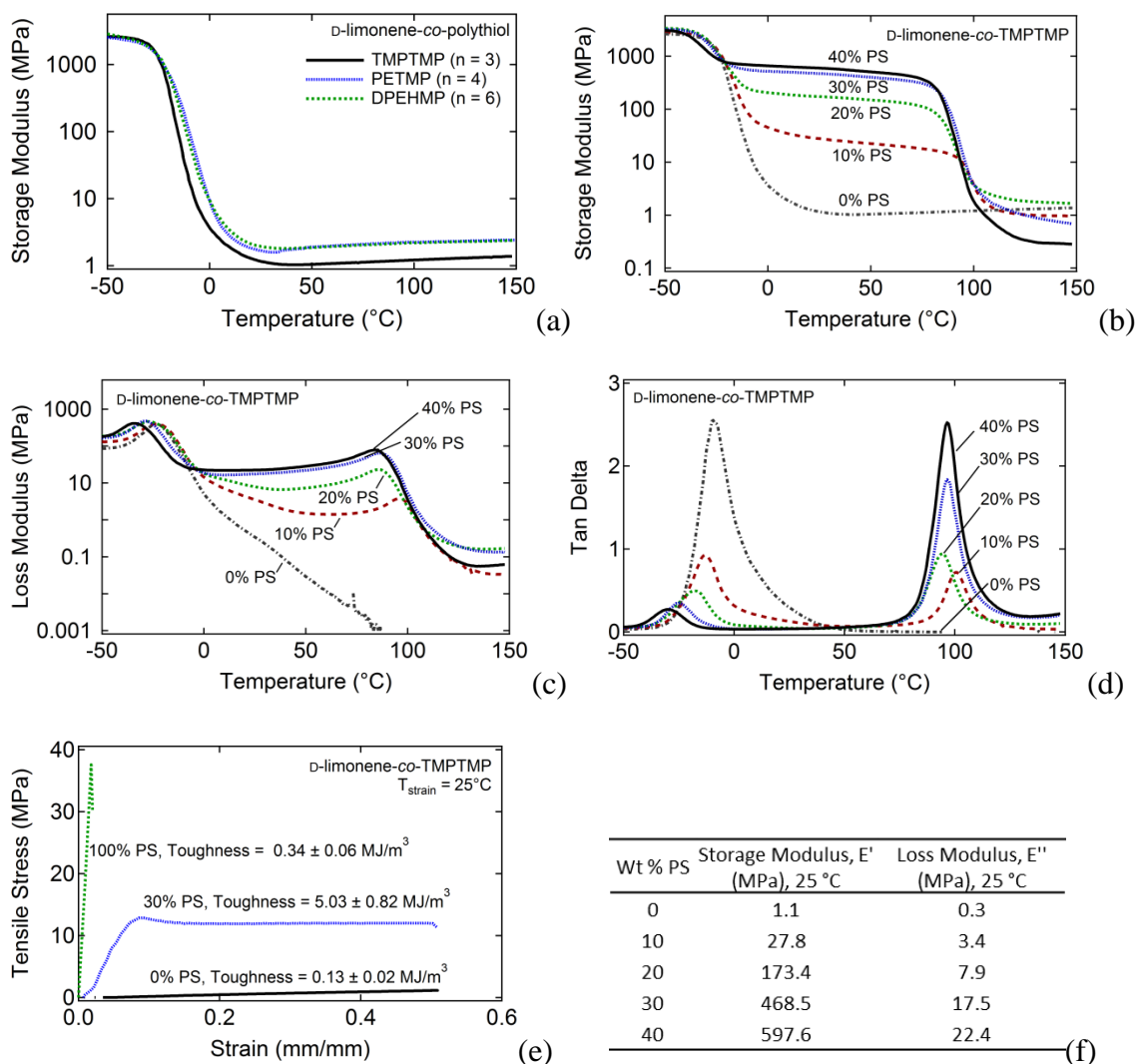
Figure 47- **(a) DMA data showing plots of storage modulus versus temperature for D-limonene-co- TMPTMP, PETMP, and DPEHMP network polymers indicate network thermomechanical behavior for all three samples; DMA data showing (b) storage modulus, E', (c) loss modulus, E'', and (d) tangent delta for samples containing 0, 10, 20, and 30%; (e) strain-to-failure data showing an order of magnitude higher toughness for 30% PS blends in comparison with that of 0% and 100% neat polystyrene; (f) table showing effect of increased PS composition on storage modulus, E', and loss modulus, E'', at 25°C**

211

2.6. Shape Memory Characterization

The tunable moduli in the materials in Figure 47 indicate that these materials may have a commercial value that exceeds that of a traditional recycled material. An even greater increase in the commercial value of the recycled materials could occur if the materials are determined to have advanced material capabilities and marketed as such. The DMA results in Figure 47 show that the PS-containing blends exhibit a drop in modulus across the T_g of the poly(thioether) network and a drop in modulus that is associated with the glass transition of polystyrene, which is approximately 100°C. If a significant change in modulus (usually 2-3 orders of magnitude) occurs during a thermal transition, and if this change occurs over a fairly narrow temperature range, then such a thermal transition is often well-suited for shape memory behavior. As shown in Figure 48, good cyclic shape memory behavior during free strain recovery and a recovery stress was observed during constrained recovery at approximately 0°C for a limonene-co-TMPTMP sample across the glass transition of the poly(thioether) network. Recoverable strains greater than 99% were observed after Cycle 1 for five-cycle free strain recovery characterization. As shown in Figure 49(a), multi-cycle shape memory behavior was also observed at approximately 100°C across the glass transition of the precipitated PS microphases. Recoverable strains greater than 95% were observed after Cycle 2 for 25% prestrain. As pictured in Figure 49(b), a flat strip of the 30% PS sample was heated to 115°C, deformed to the geometry shown in Figure 49(b) at t = 0 s, cooled to 25°C, and subsequently unloaded. The secondary geometry was successfully maintained. Re-heating to 125°C resulted in shape recovery in 8 s. This demonstration

of the shape memory effect in P6P-recycled materials opens the door to a number of investigative studies in this area, and shape memory will continue to be investigated in attempt to maximize commercial value.
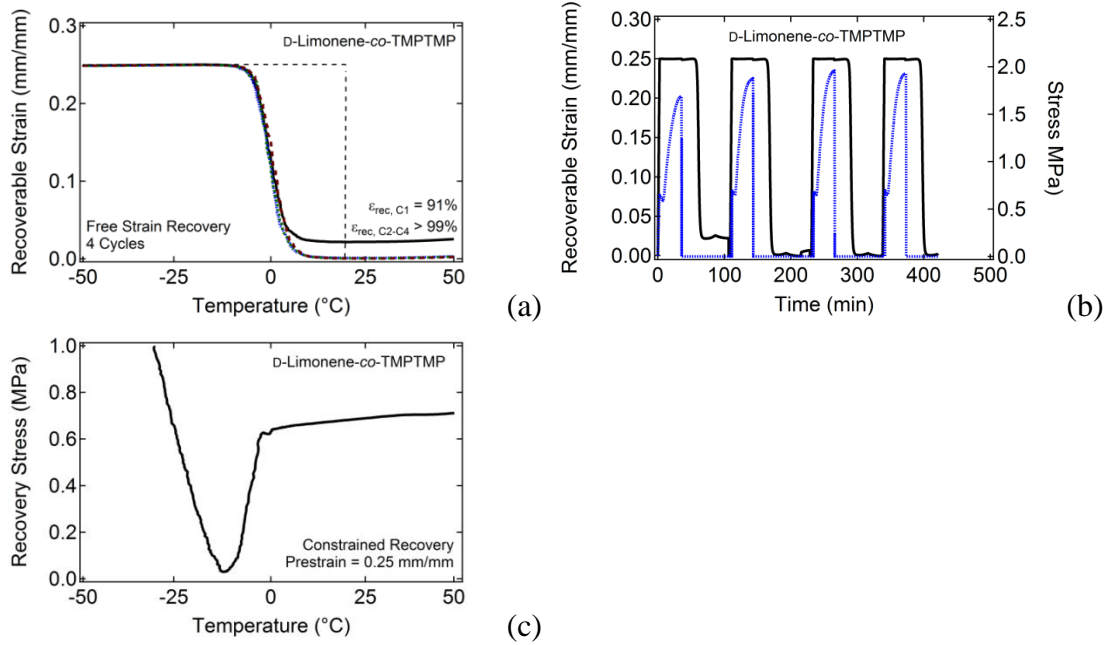
Figure 48- Shape memory characterization data for D-limonene-co-TMPTMP homopolymer, in which the glass transition of the limonene-derived rubber is utilized as a switching segment: (a) 4-cycle plots of recoverable strain and stress versus time; (b) 4-cycle plots of recoverable strain versus temperature; (c) 1-cycle plot of recovery stress versus temperature

(a)

(b)
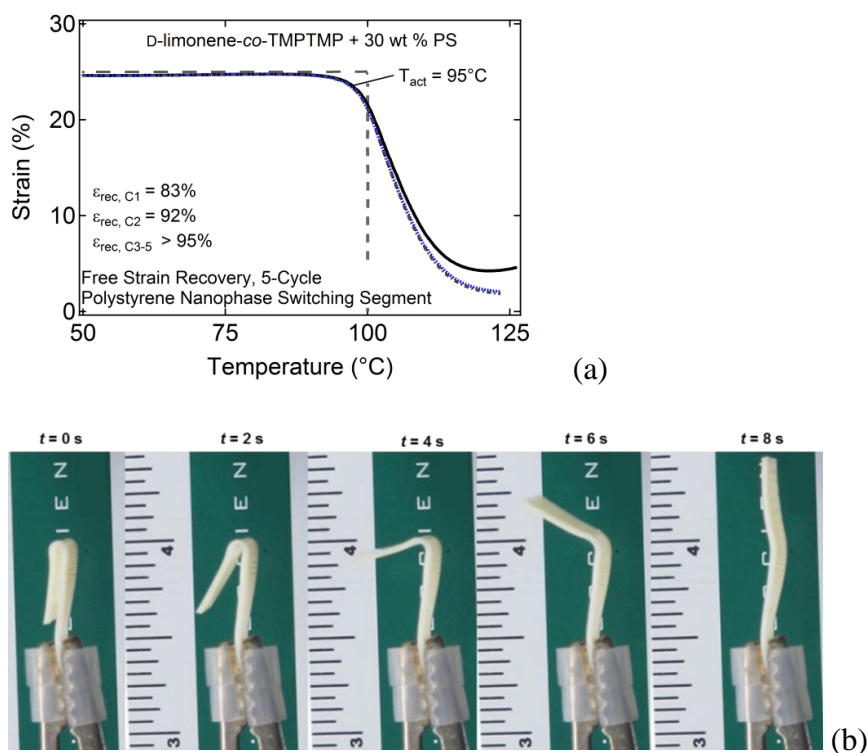
Figure 49- **Shape recovery images for D-limonene-co-TMPTMP with 10% PS additive, in which the glass transition of the PS is utilized as a switching segment.**

D. Summary and Conclusions

In this work, we report a multicomponent process for sustainable materials development that combines an innovative polystyrene recycling technique with a breakthrough achievement in renewable polymers synthesis to afford a new polymer system with tunable physical and material properties. Through a well-engineered material design strategy, blended polymeric materials comprised partly of recycled thermoplastic PS components and partly of D-limonene-derived poly(thioether) network components exhibit mechanical integrity that greatly exceeds that exhibited by either

component alone. By varying PS composition between 0 and 30 wt %, storage modulus at 25°C can be tuned over the range of 1 to nearly 600 MPa, and these materials consequently may be suitable for use in a diverse array of polymeric applications. One set of applications that appears promising is that of impact resistant polymers, and the fabrication of a cellular phone protective case prototype was demonstrated in this work to provide an example of one potentially well-suited industrial application. Future studies will investigate the effects of various synthetic conditions on the microstructures of the biphasic materials to provide a basis for determining structure-property relationships, and further characterization of thermomechanical properties, tensile behavior, and impact strength will then be used to identify trends relating material structures to mechanical properties.

Concerning the significance of this work with respect to the broader scope of renewable materials development, this work demonstrates that environmental suitability in new polymers can be achieved without sacrificing functional utility. If innovative material design were to become a staple component of sustainable materials development, the scientific community could produce new classes of materials that excel from both environmental stewardship and material functionality standpoints. Concerning the significance of the specific process for preparing naturally-derived polymers from D-limonene that is reported, a number of studies have stated the potential significance of such naturally inspired network polymers for use in soft polymer applications[118] (and in implantable tissue applications in the case of D-limonene-*co*-poly(mercaptopropionate) networks).[119] While previous studies have provided

excellent groundwork for limonene-based poly(thioether) synthesis using a "ground-up chemistry-based approach," we have chosen to address terpene-derived polymer synthesis instead from a "top-down materials synthesis approach," in which bulk materials are first synthesized, mechanically characterized and evaluated on material grounds for potential industrial relevance. This work should complement previous chemistry-focused works very well and should provide a unique perspective on terpene-derived polymer synthesis.

E. Acknowledgements

CHAPTER IX

SUMMARY, CONCLUSIONS AND FUTURE DIRECTIONS

The primary motivation behind the studies reported herein is to establish one or more new SMP systems in the literature as potential platform systems for the design of medical devices and other applications. Despite the fact that improving processing capability is an objective of this work, careful efforts were implemented in order to ensure that accomplishing this objective was not done at the expense of controlling or maintaining hight integrity of mechanical behavior. The materials that this work introduces, when fully optimized, are completely processable by thermoplastic processing techniques, exhibit tunable glass transitions between approximately 40 and 80°C and tunable rubbery moduli between 1 and 30 MPa, exhibit toughnesses between 50 and 100 MJ/m^3, exhibit good biocompatibility, and can be fabricated into medical devices to demonstrate their viability as candidate materials for medical device design. Additionally, the development of polymerization crosslinkable SMP systems through green synthetic processes and/or from naturally-derived precursors was demonstrated in order to demonstrate the importance of including environmental sustainability initiatives in the design objectives of materials engineering studies moving forward.

A. Summary and Conclusions

In Chapter III, a thermally crosslinkable aliphatic polyurethane SMP system is reported that undergoes post-polymerization crosslinking upon exposure to elevated

218

temperatures under evacuated environmental conditions. A tunable glass transition range from approximately 40 to 78°C, a toughness greater than 50 MJ/M^3 at T = T$_g$ for a select formulation, and cyclic recoverable strains approaching 100% for a sample subjected to 0.50 mm/mm prestrain were observed. However, control of crosslink density was limited to a rubbery shear modulus range of 1 to 2.5 MPa, and the industrial viability of this thermally crosslinkable SMP system may also be limited because of the requirement of a mold and evacuated atmospheric conditions during high-temperature post-polymerization curing processes.

In Chapters IV, V, and VI, the focus in this work shifts to the development of electron beam crosslinkable polyurethane shape memory polymer systems. Materials in these systems can be molded into complex geometries and subjected to crosslinking by electron beam irradiation at a later time at ambient temperature so as to maintain molded geometries. To achieve electron beam crosslinking in thermoplastic polymers over a desirable range, a new synthetic strategy is employed that is based on a hypothesis that certain structural moieties enable enhanced thermoplastic susceptibility to e-beam crosslinking. In Chapter IV, crosslink density is tuned over a corresponding rubbery modulus range of 1 to 40 MPa by solution blending acrylic radiation sensitizer additives with thermoplastic polyurethanes prior to e-beam irradiation, and cyclic recoverable strains approaching 100% are observed for sample subject to 0.25 mm/mm prestrain. While this crosslink density range is acceptable in accordance with the material design objectives of this work, the acrylic sensitizer additives present potential problems because of thermal instability during elevated temperature processing. In Chapter V, the

219

thermal stabilization effects of the addition of varying quantities of the free radical

inhibitor 1,4-benzoquinone are investigated for the sensitizer-based e-beam crosslinkable

PU SMP system reported in Chapter IV, and increased elevated temperature working

times of up to 24 h are demonstrated by the addition of select free radical inhibitor

compositions. In Chapter VI, new formulations for a sensitizer-free e-beam

crosslinkable SMP system are reported. This new SMP system exhibits tunable rubbery

moduli from 0.1 to 55 MPa, tunable glass transitions from 40 to 80°C, toughness values

greater than 90 MJ/m^3 for select compositions, cyclic recoverable strains approaching

100% for samples subject to 0.25, 0.50 and 1.00 mm/mm prestrains, and 72 h mouse

3T3 fibroblast cell viabilities greater than 90% for select formulations subjected to

biocompatibility testing. The sensitizer-free SMP system reported in Chapter VI

represents the final, optimized version of the e-beam crosslinkable SMP systems

reported in this dissertation.

In Chapter VII, a thermoplastic PU SMP system that can by crosslinked by

solution blending with polyfunctional thiol additives and subsequent subjection to UV

light to afford UV catalyzed thiol-ene free radical addition crosslinking is reported. This

thiol-ene crosslinkable PU SMP system was developed to provide an "all-in-house"

alternative system to the e-beam crosslinkable SMP system reported in Chapter VI,

which requires e-beam irradiations that generally must take place at external facilities.

The thiol-ene crosslinkable PU SMP system reported in Chapter VII exhibits tunable

rubbery moduli from 0.1 to 25 MPa, tunable glass transitions from 35 to 105 °C,

toughness values greater than 90 MJ/m^3 for select formulations, cyclic recoverable

strains approaching 100% for samples subject to 0.25, 0.50 and 1.00 mm/mm prestrains and 72 h mouse 3T3 fibroblast cell viabilities greater than 91% for select formulations subjected to biocompatibility testing.

In Chapter VIII, in accordance with the final design criterion established in the Introduction in Chapter I, SMP systems built from novel green formulations are reported. UV catalyzed thiol-ene "click" chemistry is utilized as the polymerization mechanism for these SMP systems. The first green SMP system reported is a poly(thiother-co-carbonate) SMP system derived from the coffee extract quinic acid, in which glass transition is tunable over the range of 30 to 75°C, biodegradation rate at physiological conditions is tunable over the range of 10 days to greater than 60 days, cyclic recoverable strains approaching 100% for samples subjected to 0.30 mm/mm prestrains were observed, and 72 h mouse 3T3 fibroblast cell viabilities varying between 80 and 95 % were observed for select formulations subjected to biocompatibility testing. The second SMP system reported in Chapter VIII is prepared using a direct polymerization of the citrus fruit extract D-limonene and polythiol co-monomers, and 72 h mouse 3T3 fibroblast cell viabilities greater than 93% were observed for select formulations subjected to biocompatibility testing. Upon addition of recycled polystyrene additives to heated limonene/polythiol monomer mixtures, homogeneous solutions result, and formation of limonene-*co*-polythiol networks upon UV curing results in nanocomposite polymers with precipitated PS microphases, in which modulus at 25°C is tunable from 1 to 600 MPa as recycled polystyrene composition increases from 0 to 40 weight fraction. Cyclic free strain recovery showed 5-cycle recoverable

strains approaching 100% across the glass transitions of both the polythioether (~0°C) and polystyrene (~100°C) phases.

B. Future Directions

Concerning future directions for the work presented in this dissertation, the development of biodegradable analogs of the materials reported herein is a natural area of progression. Multiple paths to formulating biodegradable analogs are provided in Scheme 11. The formulation of polyurethanes from ester-containing diols such as neopentyl glycol mono(hydroxypivalate) (NGMHP) that contain hydrolysable segments is one potential synthetic strategy, shown in 11(a). NGMHP is an inexpensive, commercially available monomer. Diol esters would be co-polymerized with alkene diol monomers to enable post-polymerization crosslinking. The NGMHP monomer is predicted to drive up glass transition, so HDI and a low-T_g diol comonomer may be necessary counteract this rise in T_g. For high crosslink densities to be achieved, polymers should contain as many double bonds as possible in their repeat units. However, increasing alkene diol monomer composition will simultaneously decrease ester diol monomer composition and consequently decrease degradation rate. Ideally, biodegradation rate should be controllable independently of crosslink density; however, an SMP system based solely on the above monomers would exhibit a tradeoff between control over crosslink density and control over biodegradation rate. To address this problem, the alkene functionality in the diol monomers could be increased so that less NGMHP would need to be sacrificed to achieve desired crosslink densities. As shown in

222

Scheme 11(b), The 1,5-hexadiene-3,4-diol monomer, pictured below, is commercially available, and custom monomers could also be synthesized in one-step reactions similar to the one used for DEA-diol synthesis. Alternatively, alkyne-diol monomers could be purchased or synthesized for thiol-yne crosslinking, in which one alkyne group reacts with two thiol groups, effectively doubling crosslink density.

To enable complete independent control over biodegradation rate and crosslink density, a custom diol monomer containing both an ester linkage and an alkene group could be synthesized, as shown in Scheme 11(c). Substituting such a monomer with either an ester diol or an alkene diol would allow crosslinking or degradation to be controlled independently. One proposed synthesis is the Michael Addition of allylamine to 2-hydroxyethyl methacrylate, shown below. Both of these starting materials are commercially available and inexpensive. It should also be noted that the use of all acrylate sensitizers and certain polythiol crosslinkers such as PETMP will result in the formation of biodegradable crosslinks, which would be significant factors in determining degradation rate.

Less conventional methods of making polyurethanes could also be explored, such as the amine-chloroformate reaction shown in Scheme 11(d), which would allow diamine and dichloroformate chemistries to be incorporated into the polyurethane backbone. As shown in Scheme 11(e), the moisture-sensitive urethane polymerization could be bypassed altogether by building polymer chains from difunctional monomers that contain carbamate linkages, such as the commercially available diurethane dimethacrylate monomer, which acts as an A-A step growth monomer in Michael Addition polymerizations.

Scheme 11- Suggested synthetic route #1 for the development of a post-polymerization crosslinkable, biodegradable polyurethane SMP.

(a)

(b)

(c)

(d)

(e)

224
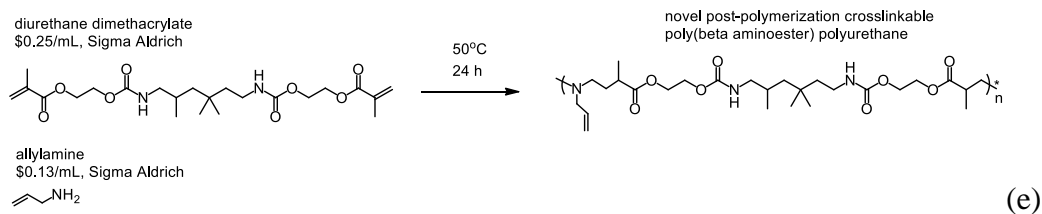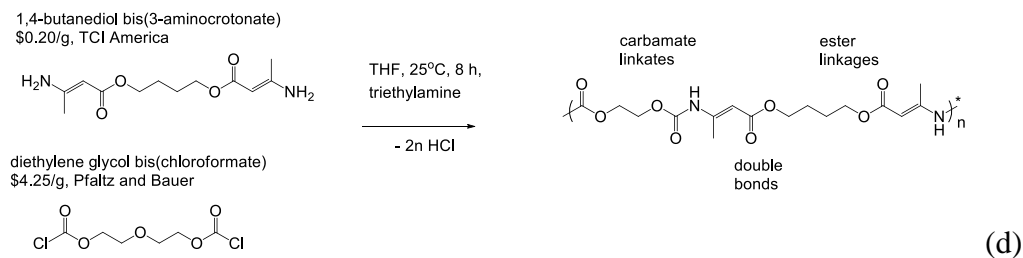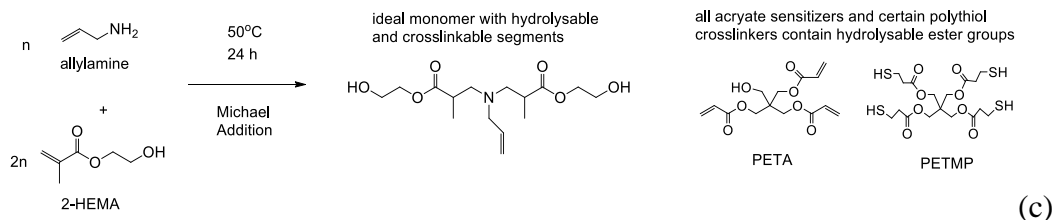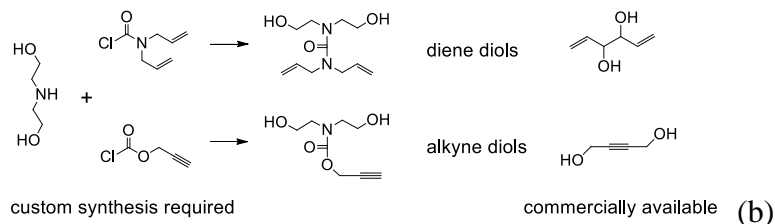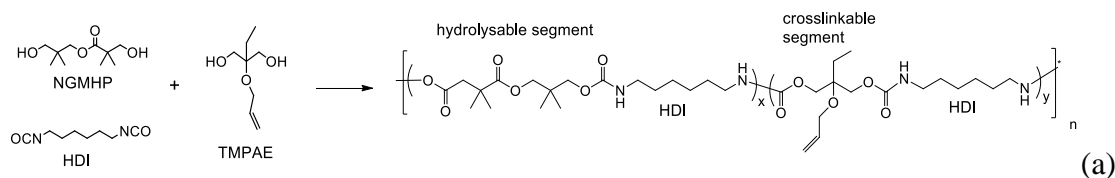
REFERENCES

[1]   I. V. W. Small, P. Singhal, T. S. Wilson, D. J. Maitland, *Journal of Materials Chemistry* **2010**, *20*, 3356.

[2]   A. Lendlein, R. Langer, *Science* **2002**, *296*, 1673.

[3]   A. Lendlein, S. Kelch, *Angewwandte Chemie International Edition* **2002**, *41*, 2035.

[4]   C. Liu, H. Qin, P. T. Mather, *Journal of Materials Chemistry* **2007**, *17*, 1543.

[5]   C. Yakacki, K. Gall, in *Advances in Polymer Science* **2010**, 226, 147-75.

[6]   T. Sanderson, K. Gall, *Raytheon Technology Today* **2007**, *10*, 10.

[7]   G. J. Monkman, *Mechatronics* **2000**, *10*, 489.

[8]   FDA, in *FDA Medical Devices*, (Ed: U. S. D. o. H. a. H. Services), 2009.

[9]   H. Tobushi, H. Hara, E. Yamada, S. Hayashi, *Smart Materials and Structures* **1996**, *5*, 483.

[10]   C. Liu, S. B. Chun, P. T. Mather, L. Zheng, E. H. Haley, E. B. Coughlin, *Macromolecules* **2002**, *35*, 9868.

[11]   B. Yang, W. M. Huang, C. Li, L. Li, *Polymer* **2006**, *47*, 1348.

[12]   J. Li, J. A. Viveros, M. H. Wrue, M. Anthamatten, *Advanced Materials* **2007**, *19*, 2851.

[13]   T. Xie, *Nature* **2010**, *464*, 267.

[14]   A. Lendlein, H. Jiang, O. Junger, R. Langer, *Nature* **2005**, *434*, 879.

[15]   J. L. Hu, F. L. Ji, Y. W. Wong, *Polymer International* **2005**, *54*, 600.

[16]   J. Hu, Z. Yang, L. Yeung, F. Ji, Y. Liu, *Polymer International* **2005**, *54*, 854.

[17]   T. Xie, I. A. Rousseau, *Polymer* **2009**, *50*, 1852.

[18]   K. Gall, C. M. Yakacki, Y. Liu, R. Shandas, N. Willett, K. S. Anseth, *Journal of Biomedical Materials Research Part A* **2005**, *73A*, 339.

[19]   A. Lendlein, A. M. Schmidt, M. Schroeter, R. Langer, *Journal of Polymer Science Part A: Polymer Chemistry* **2005**, *43*, 1369.

[20]   Y.-J. Yu, K. Hearon, T. S. Wilson, D. J. Maitland, *Smart Materials and Structures* **2011**, *20*, art. no. 085010.

[21]   C. A. Schoener, C. B. Weyand, R. Murthy, M. A. Grunlan, *Journal of Materials Chemistry* **2010**, *20*, 1787.

[22]   S. E. Kasprzak, B. Martin, T. Raj, K. Gall, *Polymer* **2009**, *50*, 5549.

[23]   S. Zhang, Z. Yu, T. Govender, H. Luo, B. Li, *Polymer* **2008**, *49*, 3205.

[24]   W. Small, T. S. Wilson, D. J. Maitland, *Optics Express* **2005**, *13*.

[25]   T. S. Wilson, J. P. Bearinger, J. L. Herberg, J. E. M. III, W. J. Wright, C. L. Evans, D. J. Maitland, *Journal of Applied Polymer Science* **2007**, *106*, 540.

[26]   L. D. Loan, *Radiation Physics and Chemistry (1977)* **1977**, *9*, 253.

[27]   M. Heckele, W. K. Schomburg, *Journal of Micromechanics and Microengineering* **2004**, *14*, R1.

[28]   W. E. Biles, in *Handbook of Materials Selection*, John Wiley & Sons, Inc., 2007, 969.

[29]   D. Hosler, S. L. Burkett, M. J. Tarkanian, *Science* **1999**, *284*, 1988.

[30]   P. M. B. Le Roy, Pattein, Jacky P. (Etrechy, FR), *United States Patent*, *4366301A*, 1982.

[31]   W. L. Goyert, (Leverkusen, DE) Winkler, Jurgen (Leverkusen, DE), Perrey, Hermann (Krefeld, DE), Heidingsfeld, Herbert (Frechen, DE), *United States Patent 0334186A3*, 1988.

[32]   D. C. T. Bezuidenhout, ZA), Theron, Jacobus P. (Stellenbosch, ZA), Higham, Lawrence J. (Durbanville, ZA), Zilla, Peter P. (Cape Town, ZA), *United States Patent 7538163*, 2009.

[33]   W. Voit, T. Ware, K. Gall, *Polymer* **2010**, *51*, 3551.

[34]   D. P. Nair, N. B. Cramer, J. C. Gaipa, M. K. McBride, E. M. Matherly, R. R. McLeod, R. Shandas, C. N. Bowman, *Advanced Functional Materials* **2012**, *22*, 1502.

[35]   S. H. Park, J. W. Kim, S. H. Lee, B. K. Kim, *Journal of Macromolecular Science, Part B: Physics* **2005**, *43*, 447

[36]   Y. Liu, K. Gall, M. L. Dunn, A. R. Greenberg, J. Diani, *International Journal of Plasticity* **2006**, *22*, 279.

[37]   U. Schulze, P. S. Majumder, G. Heinrich, M. Stephan, U. Gohs, *Macromolecular Materials and Engineering* **2008**, *293*, 692.

[38]   C. Giovedi, E. S. Pino, M. R. Rossi, L. D. B. Machado, *Nuclear Instruments and Methods in Physics Research Section B: Beam Interactions with Materials and Atoms* **2007**, *265*, 256.

[39]   M. Frounchi, S. Dadbin, F. Panahinia, *Nuclear Instruments and Methods in Physics Research Section B: Beam Interactions with Materials and Atoms* **2006**, *243*, 354.

[40]   G. Sui, Z.-G. Zhang, C.-Q. Chen, W.-H. Zhong, *Materials Chemistry and Physics* **2003**, *78*, 349.

[41]   P. Bracco, V. Brunella, M. P. Luda, M. Zanetti, L. Costa, *Polymer* **2005**, *46*, 10648.

[42]   D. J. Dijkstra, W. Hoogsteen, A. J. Pennings, *Polymer* **1989**, *30*, 866.

[43]   G. Odian, B. S. Bernstein, *Journal of Polymer Science Part A* **1964**, *2*, 2835.

[44]   P. S. Majumder, A. K. Bhowmick, A. B. Majali, V. K. Tikku, *Journal of Applied Polymer Science* **2000**, *75*, 784.

[45]   G. L. Batch, C. W. Macosko, *Thermochimica Acta* **1990**, *166*, 185.

[46]   C. Patacz, X. Coqueret, C. Decker, *Radiation Physics and Chemistry* **2001**, *62*, 403.

[47]   W. Burlant, J. Hinsch, C. Taylor, *Journal of Polymer Science Part A: General Papers* **1964**, *2*, 57.

[48]   A. Charlesby, S. H. Pinner, *Proceedings of the Royal Society of London. Series A. Mathematical and Physical Sciences* **1959**, *249*, 367.

[49]   L. A. Wall, *Journal of Polymer Science* **1955**, *17*, 141.

[50]   D. J. T. Hill, J. H. O'Donnell, M. C. S. Perera, P. J. Pomery, P. Smetsers, *Journal of Applied Polymer Science* **1995**, *57*, 1155.

[51]   A. R. Shultz, F. A. Bovey, *Journal of Polymer Science* **1956**, *XXII*, 485.

[52]   F. A. Bovey, I. M. Kolthoff, *Chemical Reviews* **1948**, *42*, 491.

[53]   G. N. Babu, A. Narula, S. L. Hsu, J. C. W. Chien, *Macromolecules* **1984**, *17*, 2749.

[54]   G. M. Zhu, Q. Y. Xu, G. Z. Liang, H. F. Zhou, *Journal of Applied Polymer Science* **2005**, *95*, 634.

[55]   G. Zhu, G. Liang, Q. Xu, Q. Yu, *Journal of Applied Polymer Science* **2003**, *90*, 1589.

[56]   T. Ware, W. Voit, K. Gall, *Radiation Physics and Chemistry* **2010**, *79*, 446.

[57]   V. Vijayabaskar, S. Bhattacharya, V. K. Tikku, A. K. Bhowmick, *Radiation Physics and Chemistry* **2004**, *71*, 1045.

[58]   D. Grosso, *Journal of Materials Chemistry* **2011**, *21*, 17033.

[59]   G. M. Baer, T. S. Wilson, W. Small, J. Hartman, W. J. Benett, D. L. Matthews, D. J. Maitland, *Journal of Biomedical Materials Research Part B: Applied Biomaterials* **2009**, *90B*, 421.

[60]   Z. He, W. Blank, M. Picci, *Journal of Coatings Technology* **2002**, *74*, 31.

[61]   J. Hu, Y. Zhu, H. Huang, J. Lu, *Progress in Polymer Science* **2012**.

[62]   A. M. Ortega, C. M. Yakacki, S. A. Dixon, R. Likos, A. R. Greenberg, K. Gall, *Soft Matter* **2012**, *8*, 3381.

[63]   M. C. Clochard, J. Bègue, A. Lafon, D. Caldemaison, C. Bittencourt, J. J. Pireaux, N. Betz, *Polymer* **2004**, *45*, 8683.

[64]   D. L. Safranski, in *Materials Science & Engineering*, Vol. Masters, Georgia Institute of Technology, Atlanta 2008, 80.

[65]   K. Hearon, K. Gall, T. Ware, D. J. Maitland, J. P. Bearinger, T. S. Wilson, *Journal of Applied Polymer Science* **2011**, *121*, 144.

[66]   A. Dannoux, S. Esnouf, J. Begue, B. Amekraz, C. Moulin, *Nuclear Instruments and Methods in Physics Research Section B: Beam Interactions with Materials and Atoms* **2005**, *236*, 488.

[67]   C. M. Yakacki, R. Shandas, D. Safranski, A. M. Ortega, K. Sassaman, K. Gall, *Advanced Functional Materials* **2008**, *18*, 2428.

[68]   W. Voit, T. Ware, R. R. Dasari, P. Smith, L. Danz, D. Simon, S. Barlow, S. R. Marder, K. Gall, *Advanced Functional Materials* **2010**, *20*, 162.

[69]   H. Wang, M. Wang, X. Ge, *Radiation Physics and Chemistry* **2009**, *78*, 112.

[70]   A. Citterio, A. Arnoldi, F. Minisci, *The Journal of Organic Chemistry* **1979**, *44*, 2674.

[71]   S. B. Smith, *United States Patent 5,863,997*, 1999.

[72]   I. Banik, S. K. Dutta, T. K. Chaki, A. K. Bhowmick, *Polymer* **1999**, *40*, 447.

[73]   J. Y. Lee, H. K. Choi, M. J. Shim, S. W. Kim, *Thermochimica Acta* **2000**, *343*, 111.

[74]   K. Hearon, L. D. Nash, B. L. Volk, T. Ware, J. P. Lewicki, W. E. Voit, T. S.Wilson, D. J.Maitland, *Macromolecular Chemistry and Physics* **2012**, *10.1002/macp.201200348*.

[75]   D. L. Safranski, K. Gall, *Polymer* **2008**, *49*, 4446.

[76]   James, *The Journal of chemical physics* **1943**, *11*, 455.

[77]   H. M. James, E. Guth, *The Journal of Chemical Physics* **1947**, *15*, 669.

[78]   J. L. Hedrick, D. K. Mohanty, B. C. Johnson, R. Viswanathan, J. A. Hinkley, J. E. McGrath, *Journal of Polymer Science Part A: Polymer Chemistry* **1986**, *24*, 287.

[79]   Flory, P. J., *Principles of polymer chemistry*, Cornell University Press, 1953.

[80]   K. K. Julich-Gruner, C. Löwenberg, A. T. Neffe, M. Behl, A. Lendlein, *Macromolecular Chemistry and Physics* **2013**, *214*, 527.

[81]   D. L. Safranski, K. E. Smith, K. Gall, *Polymer Reviews* **2013**, *53*, 76.

[82]   T. Ware, D. Simon, K. Hearon, C. Liu, S. Shah, J. Reeder, N. Khodaparast, M. P. Kilgard, D. J. Maitland, R. L. Rennaker, W. E. Voit, *Macromolecular Materials and Engineering* **2012**, *297*, 1193.

[83]   K. Hearon, L. D. Nash, B. L. Volk, T. Ware, J. P. Lewicki, W. E. Voit, T. S. Wilson, D. J. Maitland, *Macromolecular Chemistry and Physics* **2013**, *214*, 1258.

[84]   K. Hearon, S. E. Smith, C. A. Maher, T. S. Wilson, D. J. Maitland, *Radiation Physics and Chemistry* **2013**, *83*, 111.

[85]   Q. Li, H. Zhou, D. A. Wicks, C. E. Hoyle, D. H. Magers, H. R. McAlexander, *Macromolecules* **2009**, *42*, 1824.

[86]   J. N. Rodriguez, F. J. Clubb, T. S. Wilson, M. W. Miller, T. W. Fossum, J. Hartman, E. Tuzun, P. Singhal, D. J. Maitland, *Journal of Biomedical Materials Research Part A* **2013**, *10.1002/jbm.a.34782*.

[87]   U. D. Harkal, A. J. Muehlberg, D. C. Webster, *Progress in Organic Coatings* **2012**, *73*, 19.

[88]   C. E. Hoyle, A. B. Lowe, C. N. Bowman, *Chemical Society Reviews* **2010**, *39*, 1355.

[89]   D. P. Nair, N. B. Cramer, T. F. Scott, C. N. Bowman, R. Shandas, *Polymer* **2010**, *51*, 4383.

[90]   S. Beigi, H. Yeganeh, M. Atai, *Dental Materials* **2013**, *29*, 777.

[91]   Z. Yang, D. A. Wicks, C. E. Hoyle, H. Pu, J. Yuan, D. Wan, Y. Liu, *Polymer* **2009**, *50*, 1717; D. B. Otts, E. Heidenreich, M. W. Urban, *Polymer* **2005**, *46*, 8162.

[92]   D. J. Maitland, M. F. Metzger, D. Schumann, A. Lee, T. S. Wilson, *Lasers in Surgery and Medicine* **2002**, *30*, 1.

[93]   W. Mueller, *Waste Management* **2013**, *33*, 508.

[94]   C. J. Besset, A. T. Lonnecker, J. M. Streff, K. L. Wooley, *Biomacromolecules* **2011**, *12*, 2512.

[95]   P. A. Wilbon, F. Chu, C. Tang, *Macromolecular Rapid Communications* **2013**, *34*, 8.

[96]   K. Yao, C. Tang, *Macromolecules* **2013**, *46*, 1689.

[97]   T. M. Mututuvari, A. L. Harkins, C. D. Tran, *Journal of Biomedical Materials Research Part A* **2013**, n/a.

[98]   H. Lewis, in *Packaging for Sustainability*, (Eds: K. Verghese, H. Lewis, L. Fitzpatrick), Springer London, 2012, 41.

[99]   T. Tambouratzis, D. Karalekas, N. Moustakas, *Journal of Industrial Ecology* **2013**, n/a.

[100]   S. Rajendran, L. Scelsi, A. Hodzic, C. Soutis, M. A. Al-Maadeed, *Resources, Conservation and Recycling* **2012**, *60*, 131.

[101]   S. Mecking, *Angewandte Chemie International Edition* **2004**, *43*, 1078.

[102]   N. Kuboyama, H. Kiba, K. Arai, R. Uchida, Y. Tanimoto, U. K. Bhawal, Y. Abiko, S. Miyamoto, D. Knight, T. Asakura, N. Nishiyama, *Journal of Biomedical Materials Research Part B: Applied Biomaterials* **2013**, *101B*, 295.

[103]   H. Qiu, J. Yang, P. Kodali, J. Koh, G. A. Ameer, *Biomaterials* **2006**, *27*, 5845; Y. Chandorkar, G. Madras, B. Basu, *Journal of Materials Chemistry B* **2013**, *1*, 865.

[104]   I. Bechthold, K. Bretz, S. Kabasci, R. Kopitzky, A. Springer, *Chemical Engineering & Technology* **2008**, *31*, 647.

[105]   Y. Tokiwa, B. P. Calabia, *Journal of Polymers and the Environment* **2007**, *15*, 259.

[106]   C. K. Williams, *Chemical Society Reviews* **2007**, *36*, 1573.

[107]   J. Heller, J. Barr, S. Y. Ng, H. R. Shen, K. Schwach-Abdellaoui, S. Emmahl, A. Rothen-Weinhold, R. Gurny, *European Journal of Pharmaceutics and Biopharmaceutics* **2000**, *50*, 121.

[108]   L. Erdmann, B. Macedo, K. E. Uhrich, *Biomaterials* **2000**, *21*, 2507.

[109]   S. Li, *Journal of Biomedical Materials Research* **1999**, *48*, 342.

[110]   M. Wang, Q. Zhang, K. L. Wooley, *Biomacromolecules* **2001**, *2*, 1206.

[111]   M. C. Parrott, J. C. Luft, J. D. Byrne, J. H. Fain, M. E. Napier, J. M. DeSimone, *Journal of the American Chemical Society* **2010**, *132*, 17928.

[112]   T. Artham, M. Doble, *Macromolecular bioscience* **2008**, *8*, 14.

[113]   Y. Sato, S. Itagaki, T. Kurokawa, J. Ogura, M. Kobayashi, T. Hirano, M. Sugawara, K. Iseki, *International journal of pharmaceutics* **2011**, *403*, 136.

[114]   C. Åkesson, H. Lindgren, R. W. Pero, T. Leanderson, F. Ivars, *International immunopharmacology* **2005**, *5*, 219.

[115]   M. Gordon, F. A. Haskins, H. K. Mitchell, *Proceedings of the National Academy of Sciences of the United States of America* **1950**, *36*, 427.

[116]   M. J. Kade, D. J. Burke, C. J. Hawker, *Journal of Polymer Science Part A: Polymer Chemistry* **2010**, *48*, 743.

[117]   O. Türünç, M. A. R. Meier, *European Journal of Lipid Science and Technology* **2013**, *115*, 41.

[118]   M. Firdaus, L. Montero de Espinosa, M. A. R. Meier, *Macromolecules* **2011**, *44*, 7253.

[119]   M. Claudino, M. Jonsson, M. Johansson, *RSC Advances* **2013**.

[120]   J. A. Bhatti, Columbia University, 2010.

[121]   M. Boatwright, S. Leonard, M. McDanel, K. Raleigh, E. Wright, L. Barlow, **2010**; S. M. Al-Salem, P. Lettieri, J. Baeyens, *Waste Management* **2009**, *29*, 2625.

[122]   A. Kan, R. Demirboğa, *Journal of Materials Processing Technology* **2009**, *209*, 2994.

[123]   Wastecare Corporation., http://www.wastecare.com/Products-Services/Densifiers/Densifiers-Guide.htm, 2013.

[124]   J. M. Seo, B. B. Hwang, "A Reappraisal of Various Compacting Processes for Wasted Expandable Polystyrene (EPS) Foam", presented at *Materials Science Forum*, 2006.

[125]   M. T. García, I. Gracia, G. Duque, A. d. Lucas, J. F. Rodríguez, *Waste Management* **2009**, *29*, 1814.

[126]   R. T. Mathers, K. C. McMahon, K. Damodaran, C. J. Retarides, D. J. Kelley, *Macromolecules* **2006**, *39*, 8982.

[127]   G. A. Thomas, J. E. Hawkins, *Journal of the American Chemical Society* **1954**, *76*, 4856.

[128]   T. Noguchi, M. Miyashita, Y. Inagaki, H. Watanabe, *Packaging Technology and Science* **1998**, *11*, 19.

[129]   C. Shin, G. G. Chase, *Polymer Bulletin* **2005**, *55*, 209.

[130]   C. Gutiérrez, M. García, I. Gracia, A. Lucas, J. Rodríguez, *J Mater Cycles Waste Manag* **2012**, *14*, 308.

[131]   R. S. Coelho, C. Cunico, S. Zawadzki, L. Akcelrud, *Journal of Applied Polymer Science* **2001**, *82*, 2098.

[132]   Y.-J. Huang, J. C. Horng, *Polymer* **1998**, *39*, 3683.

[133]   Y. Liu, X. Zhong, G. Zhan, Y. Yu, J. Jin, *The Journal of Physical Chemistry B* **2012**, *116*, 3671.

[134]   B. Chen, J. R. G. Evans, *Journal of Polymer Science Part B: Polymer Physics* **2011**, *49*, 443.